2024

INSULIN AND DMA SUPPRESS THE INNATE IMMUNE RESPONSE AGAINST AAV

Tianxiang Qi
Saint John's University, Jamaica New York

INSULIN AND DMA SUPPRESS THE INNATE IMMUNE RESPONSE AGAINST AAV

A dissertation submitted in partial fulfillment
of the requirements for the degree of

DOCTOR OF PHILOSOPHY

to the faculty of the

DEPARTMENT OF PHARMACEUTICAL SCIENCE

of

COLLEGE OF PHARMACY AND HEALTH SCIENCE

at

ST. JOHN'S UNIVERSITY
New York
by
Tianxiang Qi

Date Submitted 3/15/2024 Date Approved 3/20/2024

Tianxiang Qi

Dr. Ashely Thomas Martino

ABSTRACT

INSULIN AND DMA SUPPRESS THE INNATE IMMUNE RESPONSE AGAINST AAV

Tianxiang Qi

Adeno-Associated Virus (AAV) is extensively utilized in various clinical trials and approved gene therapies. Despite its widespread use, the immune response to AAV vectors remains a significant limitation. Extensive research has been conducted to mitigate adaptive immune challenges, such as pre-existing antibodies and inhibiting the adaptive immune response. This study, however, centers on the innate immune response elicited by AAV, exploring the modulatory effects of insulin and DMA.

Initially, we examined the impact of DMA and insulin on the human liver cell line Hep3B and the human macrophage cell line U937 by culturing together in transwell inserts. Following stimulation with AAV1 and a TLR9 agonist for 2 hours, Hep3B cells exhibited increased levels of TNF-α, IL-6, and IL-12, while U937 cells showed heightened IL-1β, IL-6, and INF-β. These elevations were effectively mitigated by either DMA or insulin. At subsequent 6-hour and 24-hour intervals, neither U937 nor Hep3B cells responded to AAV and TLR9 agonist stimulation.

We further extended our analysis *in vivo* using C57BL/6 mice. AAV and TLR9 agonists were administered intramuscularly, while insulin and DMA were delivered intraperitoneally. At 2 hours post-administration, there was a notable increase in IL-6 expression in vivo, accompanied by approximately 2.5-fold increases in interferon-α and

interferon-β. These increases were significantly attenuated by the administration of insulin or DMA. By the 6-hour mark, gene expression levels stimulated by AAV and TLR9 agonists had normalized, and no additional suppressive effects were observed from insulin and DMA. Concurrently, immunohistochemical analysis was conducted to assess CD11b positive macrophage recruitment. At 2 hours, no groups exhibited M1/70 positive macrophage recruitment. However, at 6 hours, the group stimulated with AAV and TLR9 agonists showed macrophage recruitment, whereas groups co-administered with insulin or DMA did not, suggesting a potential blockade or delay in recruitment by these agents.

In summary, our findings indicate that insulin and DMA can effectively suppress the innate immune response triggered by AAV. This suppression could provide a strategy to prevent the activation of adaptive immunity. However, further investigation is required to fully elucidate the underlying mechanisms of this suppression.

ACKNOWLEDGEMENTS

There are many individuals and groups who have helped guide me through my thesis work at Saint John's University. I would first like to thank my mentor, Dr. Ashley T. Martino. His guidance on experiment handling and research direction throughout the program was the most important in my graduate life. Thanks for his patient guidance, enthusiastic encouragement, and useful critiques of this research work in the lab every day. I am also grateful for my fellow lab mates- Sean Carrig, Igor Ban, and Thy Nguyen exchanging ideas and technical advice with them has been extremely helpful with my work. Thank you to my committee members, Dr. Chen, Dr. Low, Dr. Perron, and Dr. Reznik for their time and support. My grateful thanks are also extended to Dr. Trombetta, Dr. Low for their help in sharing their lab resources. I am thankful to the Pharmaceutical Sciences Department for funding Dr. Martino's lab as well as awarding me as teaching assistant. I also appreciate the work of the administration in the Pharmaceutical Sciences Department and the Dean's Office for helping make my study at Saint John's run smoothly. Last and not least, I would like to thank my friends and family for their unyielding emotional support.

TABLE OF CONTENTS

LIST OF TABLES

LIST OF FIGURES

LIST OF ABBREVIATIONS

AAV	Adeno-associated viruses
CFTR	Cystic fibrosis transmembrane conductance regulator
CRISPR/Cas9	Clustered Regularly Interspaced Short Palindromic Repeats and CRISPR-associated protein 9
DMA	N, N-Dimethylacetamide
DMEM	Dulbecco's Modified Eagle Medium
ELISA	Enzyme-linked immunosorbent assay
ERK	Extracellular Signal-Regulated Kinase
INF	Interferon
ITR	Inverted terminal repeat
IL	Interleukin
MOI	Multiplicity of Infection
NK	Natural killer
NAB	Neutralizing antibody
NF-κB	Nuclear factor kappa-light-chain-enhancer of activated B cells
PRR	Pattern recognition receptors
PAMP	Pathogen-associated molecular pattern
PI3K	Phosphoinositide 3-Kinase

PMA	Phorbol 12-myristate 13-acetate
PEI	Polyethyleneimine
qPCR	Quantitative real-time polymerase chain reaction
SCID	Severe combined immunodeficiency
TLR	Toll-like receptor
TNF	Tumor necrosis factor

CHAPTER 1 INTRODUCTION

1.1 Genetic Disorders and Gene Therapy

Genetic diseases are disorders caused by DNA abnormalities, ranging from single-gene mutations, as seen in cystic fibrosis and Huntington's disease, to chromosomal abnormalities like Down syndrome.(McNeill, 2023) They can also include multifactorial disorders, influenced by multiple genes and environmental factors, such as heart disease and diabetes, and mitochondrial disorders, often inherited maternally. (Jackson et al., 2018) Diagnoses are typically made through genetic or chromosomal testing. Treatments vary widely, from managing symptoms to advanced approaches like gene therapy, depending on the specific disorder.(Chen et al., 2023)

Gene therapy is a revolutionary medical technique that involves modifying or manipulating genes to treat or prevent disease. Instead of using drugs or surgery, gene therapy works by introducing, removing, or altering genetic material within a person's cells to restore normal function or to enhance the body's ability to fight disease.(Mulligan, 1993) This can be achieved through various methods, such as replacing a disease-causing gene with a healthy copy, inactivating a malfunctioning gene, or introducing a new or modified gene to help treat a condition. Gene therapy holds immense potential for treating a range of diseases, including inherited disorders, some types of cancer, and certain viral infections. The approach is still largely experimental but has seen significant advancements and successes in recent years, particularly in treating genetic disorders like spinal muscular atrophy and certain forms of inherited blindness. (Danaeifar, 2022) Despite its promise, gene therapy faces challenges such as delivery methods, immune responses, and ensuring

precise and safe gene editing.

The history of gene therapy clinical trials is a testament to the evolving field of genetic medicine, beginning in the late 1980s with the first human trials and experiencing a significant milestone in 1990 with the successful treatment of a child with severe combined immunodeficiency (SCID).(Fischer et al., 2002) However, the journey has not been without setbacks, including safety concerns highlighted by the tragic death of Jesse Gelsinger in 1999 and instances of leukemia in treated SCID patients, which prompted stricter regulations and a reevaluation of therapy protocols.(Grilley & Gee, 2003) Despite these challenges, the 2000s and 2010s saw remarkable advancements, including improved vector designs, the introduction of genome editing technologies like CRISPR/Cas9, and the first FDA approvals of gene therapies for inherited diseases and certain cancers.(Zhang et al., 2018) This progress has solidified gene therapy's role as a groundbreaking and viable treatment option for a range of genetic disorders.

1.2 Gene Therapy Vehicles

Gene therapy involves introducing genetic material into a patient's cells to treat or prevent disease, typically achieved using vectors – vehicles that deliver therapeutic genes into the cells. The most common vectors are viruses, which have evolved to efficiently insert their genetic material into host cells. These viruses are modified to be safe, removing their ability to cause disease while retaining their delivery capabilities. Adenoviruses, adeno-associated viruses (AAV), lentiviruses, and retroviruses are among the most used viral vectors.(Jiang et al., 2023) Besides viral vectors, non-viral methods, such as lipid nanoparticles and naked DNA, are also explored for their safety and simplicity, though they generally offer lower efficiency compared to viral methods.(Jin et al., 2022)

Comparing the four common types of viral vectors used in gene therapy, each of them has their own advantages and disadvantages. Adenoviruses are highly efficient in a wide range of cell types and can carry large DNA payloads (up to 7.5kb), but their use is often limited by strong immune responses and transient gene expression.(Trivedi et al., 2023) Lentiviruses can integrate into the host genome, ensuring long-term expression, and infect both dividing and non-dividing cells, but this integration raises concerns about insertional mutagenesis.(Perry & Rayat, 2021) Retroviruses, also integrating vectors, are limited to infecting dividing cells and carry similar risks of insertional mutagenesis, which has led to a decline in their use compared to other vectors.(Li et al., 2023) AAV, with its restricted genetic material capacity of up to 4.3kb, stands as the most widely employed viral vector in clinical trials due to its non-pathogenic nature, which minimizes safety concerns. It can infect both dividing and non-dividing cells, making them suitable for a variety of applications.(Sant'Anna & Araujo, 2022)

1.3 AAV biology

AAV belongs to the Parvoviridae family and is a small, non-enveloped virus characterized by its simplicity.(Naso et al., 2017) It possesses a single-stranded DNA genome of approximately 4.7 kilobases, enclosed within a protective protein shell.(Asaad et al., 2023) Within its genome, AAV houses two crucial genes, rep (replication) and cap (capsid), flanked by inverted terminal repeats (ITRs) necessary for replication and packaging. What sets AAV apart is its unique reliance on helper viruses, such as adenovirus or herpesvirus, to complete its life cycle. In the absence of a helper virus, AAV can either integrate into the host genome or persist episomally. Additionally, AAV exhibits a broad tropism, allowing it to infect various cell types, and is relatively less immunogenic

compared to other viral vectors, making it a favorable choice for gene therapy applications.(Oliveira, 2010)

The history of AAV is a remarkable journey from its serendipitous discovery in the 1960s as a contaminant in adenovirus preparations to its pivotal role in gene therapy.(Carter, 2004) Initially mistaken as a variant of adenovirus, further research revealed its distinct nature. While primarily of interest to virologists studying its interactions with helper viruses in its early years, AAV's potential in gene therapy became evident in the 1980s(Hermonat & Muzyczka, 1984) and 1990s(Ohi et al., 1990). Its ability to infect both dividing and non-dividing cells, coupled with its low pathogenicity and immunogenicity, made it an attractive candidate for gene therapy. The turning point came in the early 2000s when clinical trials using AAV vectors began, leading to a significant breakthrough with the FDA approval of Luxturna in 2017, an AAV-based therapy for inherited blindness.(Dias et al., 2018) This marked a transformative moment in the field of gene therapy, and today, AAV stands as one of the most widely used vectors in this field, with numerous ongoing clinical trials targeting various diseases, underscoring its journey from laboratory curiosity to a cornerstone of modern medicine.

Figure 1.1 Genome of wild type AAV.

Cap and Rep gene are flanked by ITR region.

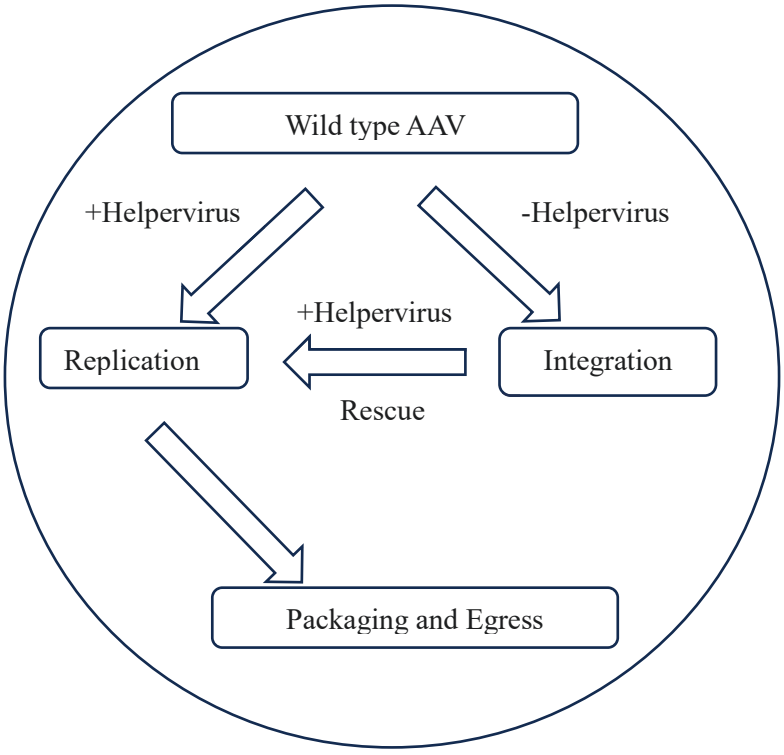

Figure 1.2 AAV life cycle and integration.

1.4 AAV Laboratory production

Laboratory production of AAV has undergone significant advancements for both research and therapeutic applications, driven by technological progress and a deeper understanding of the virus's biology. Discovered in the 1960s as an incidental finding in adenovirus samples, AAV initially garnered interest among virologists for its unique biological properties.(Hoggan et al., 1966) By the 1980s, the emergence of gene therapy highlighted AAV's potential as a vector, attributed to its broad infectivity across various cell types and low immunogenicity. Early AAV production methods in labs relied on co-infecting cell cultures with a helper virus, typically an adenovirus, reflecting AAV's natural requirement for a helper virus for replication. This approach, however, faced challenges in yield and purity.(Rolling & Samulski, 1995) Addressing these issues, researchers later developed helper virus-free systems, utilizing plasmids in a transfection method to supply the necessary AAV Rep and Cap proteins, along with the helper functions initially provided by the helper virus.(D. Wang et al., 2019)

Modern AAV production typically involves the transfection of a producer cell line, such as HEK293 cells, with multiple plasmids. One plasmid carries the AAV vector genome, encompassing the gene of interest flanked by AAV ITRs, while another plasmid contains the Rep and Cap genes. A third plasmid provides the necessary helper functions.(Kimura et al., 2019) This approach is widely favored for its efficiency and safety benefits. Notably, it eliminates the need for a helper virus, thereby reducing the risk of contamination with wild-type viruses and enhancing the purity of the AAV product. Moreover, a recent innovation in AAV production has introduced a two-plasmid system,

consolidating the Rep and Cap genes with the adenoviral helper gene into a single plasmid.(Tang et al., 2020) This streamlined system has demonstrated superior efficiency and convenience compared to the conventional three-plasmid setup. Advancements in cell culture and purification techniques have further enabled the scalable production of AAV vectors. Purification methods, including ultracentrifugation, chromatography, and filtration, are employed to refine and purify the AAV particles.(Lam et al., 2023)

The production of AAV in the laboratory has transitioned from a helper virus-dependent process to a sophisticated, helper-free system. This evolution reflects a deeper understanding of AAV biology and meets the need of gene therapy, leading to more efficient, scalable, and safer AAV vector production methods.

1.5 AAV serotypes

AAV serotypes are distinct variations of the AAV virus, each characterized by its unique capsid protein structure.(Wu et al., 2006) These serotypes are naturally occurring variants that have been isolated from various sources over time. The differences in their capsid proteins confer distinct tissue tropisms, transduction efficiencies, and immunogenic profiles, making each serotype suitable for different therapeutic applications in gene therapy.

Over a dozen AAV serotypes have been identified (e.g., AAV1, AAV2, AAV5, AAV8, AAV9 etc.), each with unique properties.(Wu et al., 2006) They were discovered through both isolation from human and non-human tissues and through molecular engineering. One of the most critical features distinguishing AAV serotypes is their tissue tropism – the ability to target and transduce specific cell types. For example, AAV1 is efficient in transducing muscle cells, AAV2 is often used for targeting the central nervous system and

retina, while AAV8 and AAV9 are known for their ability to transduce liver and heart cells, respectively. Different serotypes vary in their ability to transduce cells efficiently.(Wu et al., 2006) This efficiency is influenced by the serotype's ability to bind to specific receptors on the target cell surface and by its subsequent ability to transport the genetic material into the cell nucleus.

The diversity of AAV serotypes and their unique characteristics offer a versatile toolkit for gene therapy, allowing for tailored approaches to treat a wide range of genetic disorders. As research progresses, the understanding and utilization of different AAV serotypes continue to evolve, enhancing the precision and effectiveness of gene therapy strategies.

Table 1.1 Serotypes of AAV in Gene Therapy and Targeting Tissue

Serotypes	Targeting Tissue
AAV1	Skeletal muscle, CNS
AAV2	Kidney
AAV4	CNS, Eyes
AAV5	CNS, Eyes
AAV6	Skeletal muscle
AAV7	Skeletal muscle
AAV8	Skeletal muscle, Liver, Heart, Pancreas
AAV9	Skeletal muscle, Liver, Lung

1.6 AAV Mediated Gene Therapy Clinical Trial

The history of clinical trials involving AAV spans several decades. The first disease to be investigated in order to assess the effectiveness of AAV as a gene therapy platform was cystic fibrosis. Cystic fibrosis is primarily caused by mutations in both copies of the Cystic fibrosis transmembrane conductance regulator gene (CFTR), resulting in its improper function.(Taylor-Cousar et al., 2023) In these clinical trials, Recombinant AAV vectors were modified to carry the CFTR gene. The introduction of the normal CFTR gene had the potential to restore chloride transport and reduce the abnormal proinflammatory cytokines associated with cystic fibrosis. However, the efficiency of CFTR gene correction using AAV was limited due to the challenging environment in the cystic fibrosis lungs, which includes a high number of white blood cells, mucus, and lytic enzymes. Additionally, the episomal proviral DNA introduced by AAV in lung epithelial cells did not integrate, and the rapid turnover of these cells prevented long-term correction. This trial proved that AAV gene delivery was safe.

Hemophilia B became the second target of AAV-based gene therapy.(Leebeek & Miesbach, 2021) Hemophilia B, an X-linked disorder primarily affecting males, is characterized by coagulation impairment due to mutations in the factor IX gene. The relatively small size of the factor IX gene at 1.3 kbps made it a suitable target for AAV gene therapy. A clinical trial based on AAV2 achieved a 10% increase in factor IX levels.(Manno et al., 2003) However, the therapeutic effect was hampered by the host's immune response. Subsequently, another clinical trial for hemophilia B utilized self-complementary AAV8-hFIX and demonstrated a therapeutic effect that was still vulnerable to host immune system attacks.(Nathwani et al., 2011) They also found that immune suppressors like prednisone

could mitigate the immune response against the AAV-transgene cells.

The first AAV-based gene therapy approved by the FDA was Luxturna, developed to treat an inherited retinal dystrophy caused by mutations in the RPE65 gene.(Rodrigues et al., 2019) The relative isolation of the immune system within the eyeball made it a more favorable environment for overcoming host immune system challenges associated with AAV. Another FDA-approved AAV-based gene therapy was Roctavian, designed to treat severe hemophilia A (factor VIII deficiency) in individuals without detectable antibodies to AAV5, absence of a pre-existing immune response against AAV.(Dougherty & Dougherty, 2023)

Immune response limited the effect of AAV based gene therapy, which makes it the main difficulty in clinical trials.

1.7 Immune Response Against AAV

The immune response against AAV vectors is a critical factor in gene therapy. The immune system can react to AAV vectors through both innate and adaptive responses.(Gardin & Ronzitti, 2023) The innate immune response is the first line of defense and is non-specific, whereas the adaptive immune response involves specific recognition of the AAV vectors. The adaptive immune response against AAV can involve both cellular immunity (T cells) and humoral immunity (B cells and antibodies). T cells may recognize and destroy cells transduced by the AAV vector, while B cells can produce antibodies against AAV capsid proteins, neutralizing the vectors and preventing gene transfer.(Boutin et al., 2010) The presence of pre-existing immunity to AAV in many individuals is very common among populations, due to natural exposure to AAV. This pre-existing immunity, especially in the form of neutralizing antibodies, can significantly impact the effectiveness

of AAV-based gene therapy.(Dai et al., 2023)

The immune response to AAV vectors is a major challenge in clinical applications of gene therapy. It can limit the efficacy of the therapy, cause adverse reactions, and prevent repeated administration of the vector. Understanding and managing this immune response is crucial for the success of AAV-mediated gene therapies. Researchers are exploring various strategies to circumvent the immune response to AAV vectors. These include using alternative serotypes of AAV to which the population has less pre-existing immunity,(Hadi et al., 2024) modifying the AAV capsid to evade immune detection, using immunosuppressive drugs, (Nathwani et al., 2011) and developing transient or localized delivery methods(Blanc et al., 2022) to reduce immune activation.

1.8 Innate Immune Response Against AAV

The innate immune system, which is the body's first line of defense against pathogens, can recognize AAV vectors as foreign entities. This recognition is typically mediated by pattern recognition receptors (PRRs) that detect pathogen-associated molecular patterns (PAMPs) present on the AAV capsid or the viral DNA. TLRs (Toll-like Receptor) are a type of PRR that play a significant role in the innate immune response to AAV.(Rogers et al., 2011) For instance, TLR9 can recognize unmethylated CpG motifs in the AAV genome, leading to an immune response.

Upon recognition of AAV, innate immune cells like macrophages, dendritic cells, and natural killer (NK) cells can be activated. These cells can phagocytose viral particles and produce various cytokines and chemokines, leading to an inflammatory response. Pro-inflammatory cytokines such as interleukins (e.g., IL-6), tumor necrosis factor (TNF), and interferons was elevated.(Martino & Markusic, 2020) These cytokines help in mobilizing

and activating other immune cells but can also contribute to inflammation and potential toxicity. Interferon response, particularly type I interferons, could also be induced by AAV. This response can inhibit viral replication and spread and activate other immune cells.

It is well established that the initial innate immune responses to recombinant AAV viruses are linked to TLR-2 and TLR-9, which activate pro-inflammatory gene expression through MyD88 intracellular signaling. Dr. Martino was notably the first to report that TLR-9 activation via the viral vector genome triggers innate immune responses, potentially eliciting both humoral and cellular adaptive immunity. This early finding has since been corroborated and expanded upon by subsequent research. We now understand with greater certainty that TLR-2 is involved in recognizing viral capsid proteins, whereas TLR-9 activation occurs through the viral vector genome. Further investigations have revealed that TLR-9 plays a key role in developing adaptive immune responses.(Rogers et al., 2015) This was evidenced by knockout mouse experiments showing significantly reduced neutralizing antibody (NAB) levels in MyD88-/- and TLR9-/- mice, but not in TLR2-/- mice. Additionally, pro-inflammatory cytokine levels significantly changed in both MyD88-/- and TLR9-/- mice. Given that MyD88 is a downstream component of TLR2 and TLR9 signaling, these results highlight distinct functions of TLR9 and MyD88 in responding to the AAV virus. The innate immune response was found to be mediated through the TLR9-MyD88 dependent pathway. Moreover, when the TLR9-MyD88 complex is stimulated, MyD88 can recruit either the nuclear factor kappa-light-chain-enhancer of activated B cells (NF- κB) or the IRF7 pathway.(Rogers et al., 2011)

The innate immune response to AAV can impact the efficiency of gene transfer and the overall success of AAV-mediated gene therapy. A strong innate immune response can

lead to the rapid clearance of the viral vectors, reducing the duration and effectiveness of gene expression. To improve the efficacy of AAV-based gene therapies, strategies are being developed to evade or modulate the innate immune response. These include engineering AAV capsids to reduce recognition by immune cells, using pharmacological agents to suppress the immune response, and modifying the AAV genome to avoid activation of immune responses.

1.9 Toll-like Receptor 9

TLR9 is a type of pattern recognition receptor that is primarily located within endosomal compartments of immune cells like B cells and plasmacytoid dendritic cells. It is not typically found on the cell surface, unlike some other TLRs. TLR9 is specialized in recognizing unmethylated CpG dinucleotides, which are common in bacterial and viral DNA but are rare and usually methylated in mammalian DNA. This allows TLR9 to distinguish between pathogenic and self-DNA. Upon recognizing CpG motifs, TLR9 triggers a signaling cascade that leads to the activation of NF-κB and the production of type I interferons and other pro-inflammatory cytokines.(Kumagai et al., 2008) This response is crucial for the initiation of an effective immune response against pathogens. Through the production of cytokines and interferons, TLR9 plays a vital role in the activation and regulation of both innate and adaptive immune responses. It stimulates the innate immune system and also helps in shaping adaptive immunity by influencing the activation and maturation of B cells and T cells.(Zhu et al., 2009)

When AAV enters a cell, it is typically endocytosed and trafficked to the endosome. In the endosome, the AAV capsid was removed, and its DNA exposed. The unmethylated CpG motifs in the AAV DNA can be recognized by TLR9 in the endosome. This recognition is

specific to the pattern of these motifs, which are distinct in viral DNA. In the realm of gene therapy employing AAV vectors, the detection of AAV by TLR9 presents both benefits and drawbacks. On one hand, it can lead to an immune response against the vector, potentially reducing its efficacy. Conversely, the identification of AAV confirms its non-pathogenic nature, thereby assuring the safety of AAV use. Investigation in this interaction can help in designing better vectors that evade immune detection or modulate the immune response for therapeutic benefit.

1.10 Macrophages

Macrophages are a type of immune cell known as phagocytes. Their main function is to phagocytose (engulf and digest) cellular debris, foreign substances, microbes, cancer cells, and anything else that does not have the types of proteins specific to healthy body cells on its surface, in a process called phagocytosis. They are also involved in antigen presentation, a critical step in the activation of the adaptive immune system.(Ovchinnikov, 2008)

Macrophages develop from monocytes. These macrophages originate from bone marrow stem cells. In this process, bone marrow stem cells are stimulated by granulocyte-macrophage colony-stimulating factor and interleukin-3 (IL-3). This stimulation prompts the stem cells to partially differentiate into bone marrow precursor cells, which typically remain in the bone marrow for less than 24 hours. During this period, they mature into undifferentiated monocytes, acquiring specific membrane receptors that are essential for activating cytokine gene expression.(Mosser & Edwards, 2008)

Once matured, monocytes travel through the bloodstream and eventually migrate into various tissues of the body. It's in these tissues that they complete their transformation into

macrophages. Depending on their location within the body, these macrophages can differ in type. For example, alveolar macrophages are found in the lungs, while Kupffer cells are in the liver.(Lendeckel et al., 2022) Each type of macrophage plays a role tailored to its specific environment and function.

As part of the innate immune system, macrophages are among the first cells to respond to a pathogen invasion. They are important in the initiation and regulation of inflammation. Macrophages are involved in wound healing and tissue repair. Macrophage release cytokines, which are signaling molecules that mediate and regulate immunity, inflammation, and hematopoiesis.

1.11 Pro-inflammatory Cytokines

Pro-inflammatory cytokines are pivotal signaling molecules within the immune system, playing a key role in initiating and promoting inflammation. They are essential in the body's defense against infections, injuries, and various immune challenges. These cytokines are produced by immune cells such as macrophages, dendritic cells, and T cells, in response to pathogens, tissue damage, or other inflammatory triggers.(Zlotnik & Yoshie, 2012)

Their primary function is to stimulate and attract additional immune cells to the site of infection or injury, thereby enhancing the overall immune response. Generally, these mediators can change vascular permeability and summon successive waves of inflammatory cells to specific infection sites, largely driven by resident macrophages in tissue or luminal spaces.(Frew et al., 2018) In addition to their local impact, some pro-inflammatory cytokines can also have systemic effects. When secreted in appropriate amounts, these cytokines are beneficial for the host, aiding in effective immune responses. However, excessive production of these cytokines can lead to fatal side effects, potentially

causing severe consequences for the individual.(Qudus et al., 2023)

The production of pro-inflammatory cytokines mainly involves PRR Pathways within the immune system. Especially, in the infection of AAV virus, the expression of pro-inflammatory cytokines was induced by TLR9-NF- κB pathway.(Rogers et al., 2011)

1.12 Type I Interferons

Type I interferons (IFNs) are a significant group of polypeptides crucial in the body's defense against viral infections, primarily functioning within the innate immune system. These interferons, including the well-known interferon-alpha (IFN-α) and interferon-beta (IFN-β), are secreted by white blood cells and other cell types in response to pathogenic challenges, particularly intercellular pathogens like viruses. Upon viral infection, type I interferons could induce an antiviral state in both infected and neighboring cells, thereby limiting the replication of viruses.(Schultz, 2004) This function is critical in suppressing viral production while the adaptive immune system is being primed.

Type I interferons activate a signaling cascade that enhances the expression of interferon-stimulated genes. These genes encode proteins that interfere with viral replication and spread. Additionally, type I interferons inhibit protein synthesis and cellular proliferation in infected cells and increase the expression of receptors needed for recognition by cytotoxic T-cells and NK cells. The activation of TLR9 can increase the expression of type I interferons through the MyD88-IRF7 pathway.(Ji et al., 2022)

1.13 Insulin

Insulin is a vital hormone that plays a central role in regulating glucose metabolism in the body. Insulin is produced by beta cells in the pancreas. Its release is primarily stimulated by an increase in blood glucose levels, typically after eating. Insulin secretion is a tightly

regulated process, responding to the body's fluctuating metabolic needs. It promotes fat storage by inhibiting the breakdown of fat (lipolysis) and supports protein synthesis in various tissues.(Sonksen & Sonksen, 2000) This anabolic role of insulin is essential for growth and repair processes in the body.

Insulin exerts its effects by binding to insulin receptors on the surface of cells. This liganded receptor will be internalized through dynamin clathrin-coated endocytosis. After insulin receptor phosphorylation occurs, the insulin pathway will be triggered.(Ward & Lawrence, 2009) This activates a cascade of signaling pathways that lead to the various metabolic effects of insulin, including increased glucose uptake, enhanced synthesis of glycogen, fats, and proteins, and decreased breakdown of these molecules.

In recent research, insulin exhibits acute anti-inflammatory properties. Insulin has been shown to suppress the production of pro-inflammatory cytokines, such as tumor TNF-α and IL-6.(Petersen & Shulman, 2018) This action can help mitigate systemic inflammation, which is a common feature in conditions like obesity and type 2 diabetes. Insulin exhibits anti-inflammatory effect through blunting the expression of NF-κB in the nucleus and stimulates IkappaB kinase.

Insulin is also recognized as a regulator of the immune system, including different immune cells.(Makhijani et al., 2023) This regulatory effect was believed to involve in the uptake and utilization of glucose, which is vital for the energy needs of these cells. Metabolic control is essential for the proper functioning of immune cells, including their growth, differentiation, and response to pathogens. Different immune cells could display different responses upon insulin challenge. In dendritic cells, insulin drives increased scavenger receptor expression via Extracellular Signal-Regulated Kinase signaling (ERK)

with and without TLR activation.(Lu et al., 2015) In T-cell and T-regulatory cells, insulin increased IL-2 responsiveness and chemotaxis, improved glycolytic and mitochondrial metabolism and drives reduction of IL-10 production.(Han et al., 2014) Bone marrow derived macrophages (laboratory generated) exhibit an increase in cytokine production upon insulin stimulation. However, in tissue-specific macrophages like alveolar and peritoneal macrophages, insulin displayed a suppression against cytokines.(Tessaro et al., 2017)

Insulin's role in inflammation is an important aspect of its physiological effects, extending beyond its metabolic actions. This dual role makes insulin a molecule of significant interest not only in the context of metabolic disorders but also in a broader range of inflammatory diseases.

1.14 Insulin Improves Transduction to Skeleton Muscle and Liver

Previous studies conducted by our lab have demonstrated that co-administering insulin with AAV significantly enhances gene transfer in murine skeletal muscle, liver, and similar in cultured cells.(Carrig et al., 2016) When insulin is activated, it triggers the Phosphoinositide 3-Kinase (PI3K) pathway, leading to various metabolic functions, such as increased glucose uptake in skeletal muscles and adipose tissue and stimulating glycogenesis in the liver. This pathway also promotes the synthesis of triglycerides. Crucially, heightened PI3K activity boosts Dynamin-mediated clathrin-coated endocytosis, a mechanism utilized by AAV for cellular entry. Our laboratory has demonstrated that the improved AAV gene transfer to the liver and skeletal muscle following acute insulin co-administration is primarily due to an increased entry of the vector into cells. This is based on the observation that the co-administration of insulin was brief (lasting 2 to 4 hours),

suggesting that the enhanced viral vector uptake was the primary response mechanism.

When comparing the outcomes of *in vivo* and *in vitro* studies regarding insulin's role in enhancing AAV transduction, it is evident that the *in vivo* studies demonstrate a more pronounced increase. *In vitro* studies have confirmed that insulin promotes endocytosis, leading to enhanced transduction efficiency. Based on these findings, it is reasonable to infer that insulin *in vivo* may have additional effects beyond just facilitating endocytosis.

1.15 N, N-Dimethylacetamide (DMA)

Dimethylacetamide (DMA), with the chemical formula $CH_3C(O)N(CH_3)_2$, is a colorless, high boiling, polar aprotic solvent with a slight ammonia odor. It is miscible with water, benzene, alcohols, ethers, and chlorinated solvents.

DMA is an excellent solvent for a wide range of organic and inorganic compounds. Its high solvency power makes it particularly useful in the pharmaceutical, textile, plastic, and coating industries. DMA's ability to dissolve a wide range of organic compounds makes it valuable in the pharmaceutical industry for solubilizing drugs that are poorly soluble in water or other common solvents. This property can enhance the bioavailability of certain medications. DMA was shown to be related to toxic hepatitis upon long term exposure in several factories that utilize DMA as solvent.(J. Wang & Chen, 2020)

In recent years, there has been growing interest in the pharmacological effects of DMA. Initially, DMA demonstrated its anti-inflammatory properties by rescuing timed pregnant mice from pre-term birth induced by lipopolysaccharide exposure.(Gorasiya et al., 2018) Subsequently, its anti-inflammatory potential was subsequently confirmed in the context of inflammatory bowel disease, where DMA effectively reduced the release of cytokines and chemokines both *in vivo* and *in vitro*.(B Koya et al., 2022) Moreover, DMA exhibited

the ability to inhibit amyloid-β-induced inflammation in Alzheimer's disease models, both *in vitro* and *ex vivo*.(Wei et al., 2023)

While the comprehensive impact of DMA and its associated pathways are still subjects of ongoing research, DMA holds promise as a potential anti-inflammatory agent. Furthermore, it may have the potential to mitigate the innate immune response against AAV.

1.16 Transwell Co-culture

Transwell is essentially permeable culture insert that consist of a plastic housing with a porous membrane at the bottom. These devices were designed to allow the study of cellular processes such as cell migration, invasion, and interaction between cells in a controlled laboratory environment.(Yuan et al., 2020) They enable researchers to create a barrier or separation between two compartments while still allowing for the exchange of soluble factors, cells, or molecules between them. This makes them valuable tools for studying processes like chemotaxis, barrier function, drug transport, and cell signaling.

In our earlier research, we examined how individual cell lines react to AAV in terms of cytokine response. We found that neither macrophage cells nor liver cells showed a response when exposed to AAV. This observation led us to consider the complexity of *in vivo* environments, where immune cells and normal cells interact to trigger an immune response. We recognized that single cell lines, when isolated *in vitro*, may not effectively replicate this complex immune response. To address this, we implemented a transwell co-culture system. This system enabled us to culture both macrophages and normal cells within the same environment, better simulating the natural interactions of the immune system. The transwell approach provided a more representative model for studying the immune response to AAV.

1.17 Goal of Study

1.17.1 Hypothesis

The innate immune response includes cytokine expression and macrophage migration can be blocked by insulin and DMA acute administration.

1.17.2 Special Aims

Aim 1: Use insulin or DMA to blunt the innate immune response against AAV1 and TLR9 in co-cultured human macrophage and liver cell lines. The cytokine expressions were measured at 2h, 6h and 24h.

Aim 2: Use insulin or DMA to blunt the innate immune response against AAV1 and TLR9 in C57BL/6 mice skeleton muscle at 2h and 6h.

CHAPTER 2 MATERIALS AND METHODS

2.1 Primer Design

All primers were designed by the primer-blast (https://www.ncbi.nlm.nih.gov/tools/primer-blast/index.cgi) provided by NCBI.(Ye et al., 2012) All primers were chosen to follow this requirements: PCR product bps between 75-250, Melting point between 58.5-61.5℃, Primer self-complimentary less than 3. See Table 2.1 for the list of primers that were generated for this study.

Gene	Primers for Human (5'-3')	Primers for Mouse (5'-3')
TNF-α	F: CACAGTGAAGTGCTGGC AAC R: GATCAAAGCTGTAGGCC CCA	F: GCCGATGGGTTGTACCTTGT R: ATAGCAAATCGGCTGACGGT
IL-1-β	F: CAGAAGTACCTGAGCTC GCC R: AGATTCGTAGCTGGATGC CG	F: CCACCTTTTGACAGTGATGAG R: GACAGCCCAGGTCAAAGGTT
IL-6	F: CAATATTAGAGTCTCAAC CCCCA R: TTCTCTTTCGTTCCCGGT GG	F: ACATTCCTCACTGTGGTCAG AA R: TCTTCGTAGAGAACAACATA AGTCA
IL-12	F: TTGAGGTCATGGTGGATG CC R: CCTGGACCTGAACGCAGA AT	F: AGACCCTGCCCATTGAACTG R: CAGGAGTCAGGGTACTCCC A
INF-γ	F: AGGCTTTATCTCAGGGGC CA R: AGCACTGGCTCAGATTGC AG	F: GACAATCAGGCCATCAGCA AC R: CTCATTGAATGCTTGGCG CT
INF-α	F: TCGCCCTTTGCTTTACT GAT R: GGGTCTCAGGGAGATCA CAG	F: CTACTGGCCAACCTGCTCTC R: CTGCGGGAATCCAAAGTCCT

INF-β	F: AACTCATGAGCAGTCTGC AC R: AGGAGATCTTCAGTTTC GGAGG	F: ATCAACCTCACCTACAGGGC R: ATCTCTTGGATGGCAAAGG CA
GAPDH	F: GGATTTGGTCGTATTGGG R: GGAAGATGGTGATGGGATT	F: GTTGTCTCCTGCGACTTCA R: ATGTCACGCACGATTTCC
ITR	F: GGAACCCCTAGTGATGGA GTT R: CGGCCTCAGTGAGCGA	

Table 2.1 Primers List for quantitative PCR.

F: Forward Primer, R: Reverse Primer.

2.2 U937 Cell Culture and Differentiation

U-937 was a cell line exhibiting monocyte morphology derived from histiocytic lymphoma. U937 cells are purchased from ATCC (ATCC® CRL-1593.2™) and cultured in modified RPMI-1640. This medium contained 10% FBS, 25 mM Hepes, 1% P/S antibiotic, 1.5 g/L $NaHCO_3$, RPMI-1640 with L-glutamine (Corning). Cells were initially cultured in T-75 flask at 37℃ supplied with 5% CO_2 in humidified incubator to prepare for experiments. When the cells reached 1×10^7/mL, U937 cells were seeded into 24-well plate at 2×10^5 cell density. To induce U937 differentiation, 10μM phorbol 12-myristate 13-acetate (PMA) (Thermo Scientific Chemicals) was added for 24h. After 24h the PMA was removed, and the differentiated cells were cultured for another 48h before the experiment, fresh medium were replaced every 24h. All experiments are conducted on cells under passage 20.

2.3 Hep3B Cell Culture

Hep3B cells were purchased from ATCC (ATCC® HB-8064™) and cultured in modified Dulbecco's Modified Eagle Medium (DMEM). This medium contains 10% FBS, 25mmHepes, 1% P/S antibiotic, DMEM with L-glutamine(Corning). Cells were initially cultured in T-75 flask at 37℃ supplied with 5% CO^2 in humidified incubator to prepare for experiments. When the cells reached 75% confluence, Hep3B cells were seeded into 6.5mm diameter and transwell inserts (Corning) at 4×10^4 cell density. The cells were allowed to grow for 24h before the experiment, fresh medium were replaced 2h before experiment. All experiments are conducted on cells under passage 20.

2.4 cDNA Samples Preparation

Cultured cells collected from former studies were centrifuged at 1000×g for 5minitues to pellet the cells. mRNA was then isolated from samples are using a Thermo GeneJet™ RNA purification kit. mRNA was then converted into cDNA by RevertAid™ First Strand cDNA synthesis Kit. cDNA concentration was measured by an Thermo Scientific NanoDrop One UV/VIS Spectrophotometer and diluted to 1000µg/mL.

A total of 10-30mg muscle tissue was sliced and sonicated at 25% amplitude. The homogenized sample was performed following former cultured cell procedure.

2.5 Quantitative PCR Amplification

cDNA was amplified using a StepOne™ Real-Time PCR System. A total of 500ng template cDNA was used per well, performed in duplicate. Power SYBR® Green PCR Master Mix (applied biosystems) was used in the quantitative PCR. Due to amplification following an exponential function, the Ct value or threshold cycle was used for analysis. When a sample crossed the predetermined threshold, the cycle number was recorded. A housekeeping gene's Ct was used to normalize the results by subtracting from the gene of interest's Ct to give ΔCt. The ΔΔCt value was calculated by subtracting the ΔCt control groups from the ΔCt experimental groups. ΔΔCt was then converted into mRNA fold-change by using $2^{--\Delta\Delta Ct}$.

Virus titration was conducted using the pSC-CMV-GFP plasmid as a reference standard. To create a reference solution, 10 µL of the pSC-CMV-GFP plasmid, containing 10^{10} copies, was prepared using a sample obtained from plasmid production. This solution underwent a series of 1:10 serial dilutions, continuing until the concentration was diluted down to 10^5 copies. For quantification, qPCR amplification was carried out

using the StepOne™ Real-Time PCR System, specifically utilizing its standard curve feature.

2.6 Plasmid Production

Three plasmids were generated from their respective glycerol stocks for virus production. DH5α E. coli K12 harboring each plasmid were initially revived in 5 mL of LB broth supplemented with 1 μg/mL ampicillin. This culture was incubated at 37°C for approximately 18-20 hours, with constant shaking at 200 rpm in a MAXQ 4000 shaking incubator. The following day, the 5 mL starter culture was transferred to 1 L of LB broth, also containing 1 μg/mL ampicillin, and incubated overnight for the same duration. Subsequently, the LB broth cultures were centrifuged at 6000×g for 15 minutes, facilitating the pelleting of the bacterial cells. The pITR2-CMV-hFIX plasmid was isolated using the Thermo Scientific GeneJET Plasmid Maxiprep Kit, processed with 1 L of the corresponding LB broth. In parallel, the pDP-1 plasmid was purified utilizing the Invitrogen PureLink™ Expi Endotoxin-Free Giga Plasmid Purification Kit, with an increased volume of 4 L of the corresponding LB broth. The pSC-CMV-GFP plasmid was purified using Thermo Scientific GeneJET Plasmid Miniprep Kit, with 5ml of corresponding LB broth. The concentration of plasmid was tested by Thermo Scientific NanoDrop One UV/VIS Spectrophotometer.

2.7 AAV1-CMV-schFIX Production

AAV1-CMV-schFIX (adeno-associated virus 1- Cytomegalovirus-self complementary human Factor IX) viral vector was produced by a two-plasmid system in HEK293T cells. pDP-1 plasmid and pITR2-CMV-schFIX plasmid were the property of Dr. Martino.

2.7.1 Viral Factory

The experimental protocol utilized 293T cells beyond passage 15 to establish a viral production system. Modified DMEM (10% FBS, 25mmHepes, 100µg/ml gentamycin, DMEM with L-glutamine) was used. Cells were initially cultured in T-75 flask at 37°C supplied with 5% CO^2 in humidified incubator. The cells were cultured in a T-75 flask until they reached over 80% confluence. Subsequently, they were distributed into three T-175 flasks and allowed to proliferate for two days until they achieved approximately 75% confluence. Following this, the cells underwent a passage into ten T-175 flasks. Once these flasks attained 80% confluence, the cells were detached and subsequently seeded into forty 150mm dishes. This setup was then maintained until the cells reached 50% confluence, at which point they were prepared for transfection.

2.7.2 Plasmid Transfection

Before transfection, the medium in the 293T cells cultured in 150mm dishes was replaced with 8 mL of a specialized transfection medium, composed of DMEM with L-glutamine, enriched with 5% FBS and 25 mM HEPES. This medium was introduced two hours prior to the transfection procedure. For the transfection mix, 1800 µg of pDP-1 plasmid and 450 µg of pITR2-CMV-hFIX plasmid were combined in 72 mL of fresh DMEM at room temperature. Subsequently, 8 mL of 1mg/ml polyethyleneimine (PEI) with a molecular weight of 40,000 was gradually added to the DMEM-plasmid solution. The mixture was gently homogenized by inverting the container. This mixture was then left to incubate at room temperature for 12 minutes, allowing for adequate interaction between the plasmids and PEI.

Following the incubation period, 2 mL of the transfection mixture was carefully

dispensed into each 150mm dish. These dishes were then incubated overnight, approximately 16 hours. The next day, each dish received an additional 10 mL of fresh modified DMEM to support continued cell growth. The cells were then cultured for an additional 24 hours. At the end of this period, both the cells and the medium were collected for subsequent processing.

2.7.3 Virus Extraction

A 250 mL solution of PEG-8000 was prepared by dissolving 100g of PEG-8000 and 58.5g of NaCl. The collected medium was then combined with this PEG-8000 solution in a 4:1 ratio. This mixture was incubated on ice for 2 hours to facilitate precipitation. Following the incubation, the mixture underwent centrifugation. After centrifugation, the supernatant was carefully discarded, leaving the pellet behind. This pellet will subsequently be dissolved in citrate buffer for further processing.

Cell pellets obtained from the viral production process were reconstituted in 15 mL of citrate buffer. The resuspended cell pellet undergone sonication three times, each session lasting 1 minute and 30 seconds at 25% amplitude, with 3-minute intervals on ice to prevent overheating. Following sonication, benzonase is added to the mixture to achieve a final concentration of 50 units/mL. Simultaneously, sodium deoxycholate is introduced to reach a final concentration of 0.35%. The solution is then incubated at 37°C for 20 minutes. Post-incubation, the solution's pH is adjusted with 1M HCl to 5, followed by centrifugation at 2000×g. The supernatant is carefully collected after this step. To the remaining precipitate, 10 mL of fresh citrate buffer containing 0.35% sodium deoxycholate is added for resuspension. This extraction step is repeated twice more, following the same protocol. After completing the extraction cycles, all collected supernatants are combined for

subsequent processing steps. This consolidation ensures the maximal recovery of viral particles from the cell lysates.

2.7.4 Iodixanol Gradient Ultracentrifugation and Buffer Exchange

In the ultracentrifugation process, four distinct concentrations of iodixanol were employed: 15% w/v, 25% w/v, 40% w/v, and 60% w/v. The 15% w/v iodixanol solution was prepared by diluting 60% w/v iodixanol with PBS-MK containing 1M NaCl. The 40% w/v and 25% w/v solutions were similarly diluted from 60% w/v iodixanol using PBS-MK. To enhance visibility, one drop of phenol red was added to both the 25% w/v and 60% w/v iodixanol solutions. The supernatant obtained from the previous step, ranging from 15 to 20 mL, was first placed into a 39-mL OptiSeal Polypropylene tube (Beckman Coulter, NJ). To create a gradient of iodixanol concentrations, 4 mL of 15% w/v, 8 mL of 25% w/v, 8 mL of 40% w/v, and 4 mL of 60% w/v iodixanol were carefully layered into the tube. This was done sequentially from the lowest to the highest concentration, using a 16-gauge syringe. The tubes were then centrifuged using a Type 70 Ti Fixed-Angle Titanium Rotor (Beckman Coulter, NJ) installed in an Optima XE-90 ultracentrifuge (Beckman Coulter, NJ). The centrifugation was conducted at 63,100 rpm for 1 hour and 45 minutes at 16 °C. Following centrifugation, the OptiSeal tube was punctured at the interface between the 40% w/v and 60% w/v layers using a 16-gauge needle. The 40% w/v iodixanol layer, which contained the target fraction, was carefully extracted for the next step in the process.

A tube filtration system, Spectrum MicroKros Hollow Fiber Filter Moudule C02-E300-10-N, was employed for buffer exchange, incorporating 1% Triton X-100 into both the 40% w/v fraction and the PBS used for the exchange. This system featured two peristaltic pumps: one to pump out the original solution into the filtering tube and the other

to introduce PBS into the solution. Operating under airtight conditions, the flow rates of the two pumps were adjusted to achieve equilibrium. For the buffer exchange process, 250 mL of PBS was utilized for a 10 mL sample of the 40% w/v fraction. The exchange continued until the volume of the solution was reduced to approximately 0.5mL. This remaining solution was then carefully pipetted out. To ensure thorough recovery, the tube was flushed with an additional 0.5 mL of PBS. All collected solutions were combined and subsequently stored at -20°C for preservation.

2.8 Transwell Co-culture

When the Hep3B cells in the transwell inserts and the U937 cells were prepared, the co-culture and stimulation experiment commenced. Two hours before the experiment, the medium in each well was replaced. To initiate the stimulation, 1 μg/mL of the TLR9 agonist ODN2395 (InvivoGen), 10,000 M.O.I of AAV1-CMV-schFIX, and 10 μg/mL of insulin were added to the respective wells. The specific group assignments for this experiment are detailed in Table 2.2. Each group underwent the experimental procedure at three distinct time points: 2 hours, 6 hours, and 24 hours, to allow for the assessment of cellular responses over time. Cells are collected and mRNA was extracted as described before.

	Control	Co-Culture w/o stimulation	AAV1-CMV-schFIX+TLR9 agonist	AAV1-CMV-schFIX+TLR9 agonist + Insulin	AAV1-CMV-schFIX+TLR9 agonist + DMA
Co-culture	No	Yes	Yes	Yes	Yes
TLR9 agonist	No	No	Yes	Yes	Yes
AAV virus	No	No	Yes	Yes	Yes
Insulin	No	No	No	Yes	No
DMA	No	No	No	No	Yes

Table 2.2 Group Assignment of in vitro Co-culture and stimulation used.

2.9 Animal Experiment Overview

C57BL/6 mice were utilized to investigate the effects of insulin and DMA on the innate immune response elicited by AAV1. To induce a robust innate immune reaction to recombinant AAV (rAAV), the TLR-9 agonist ODN 2395 was co-injected with rAAV into the upper skeletal muscle of the lower left limb (vastus lateralis), distributed across three injection sites. The experimental design involved administering a combination of AAV and TLR-9 agonist to stimulate the innate immune response, followed by either insulin or DMA to potentially mitigate this response.

Insulin was administered intraperitoneally (I.P.) at four time points: 15 minutes before, 15 minutes after, and 45 minutes after the AAV/TLR9 injection. In contrast, DMA was given as a single intraperitoneal (I.P.) dose 15 minutes prior to the AAV/TLR9 injection. The mice were sacrificed at either 2 hours or 6 hours post-injection of AAV/TLR9 to assess immune responses.

Comprehensive controls were included in the study for robust comparison. Post-sacrifice, blood samples were collected then centrifuge at 14,000g, serum samples were stored in -80°C and the skeletal muscle around the injection sites were obtained to evaluate markers of inflammation.

The Detailed group assignments were shown in Table 2.3.

Group	Intramuscular Injection	Intraperitoneal Injection
Insulin Control	PBS	PBS
Insulin Positive Control	AAV1-cmv-schFIX+TLR9 agonist	PBS
Insulin Experimental	AAV1-cmv-schFIX+TLR9 agonist	Insulin
DMA Control	PBS	PBS
DMA Positive Control	AAV1-cmv-schFIX+TLR9 agonist	PBS
DMA Experimental	AAV1-cmv-schFIX+TLR9 agonist	DMA

Table 2.3 Animal Study Group Assignment.

Each group had 2h and 6h subgroup, each sub-group had 8 animals.

2.9.1 Insulin Treatment Groups

The study comprises three groups of mice. Group 1, the control group, received only vehicle injections (200 µL of PBS) without insulin, AAV, or TLR9. Additionally, to mimic the AAV/TLR9 injection, these mice received 100 µL of PBS vehicle in the *vastus lateralis* muscle of the lower left leg, spread over three sites. Group 2, the positive control group, was expected to exhibit maximum innate immunity. These mice were given insulin vehicle injections (200 µL of PBS) at the same intervals as Group 1 but also receive the AAV/TLR9 mixture to stimulate the innate immune response. The AAV/TLR9 injection consisted of 1.0×10^{11} viral particles of AAV and 100 µg of TLR9 agonists in 100 µL of PBS, delivered into the vastus lateralis muscle over three sites. Group 3, the second experimental group, was anticipated to show a reduced innate immune response. These mice receive both insulin (0.6 U/kg in 200 µL of PBS) and the AAV/TLR9 mixture. Insulin injections were given at the same three intervals as in the other groups. The AAV/TLR9 administration was identical to Group 2. Tail bleeding was performed 15 mins after each PBS/insulin injection, blood glucose was tested by glucose strips. When the blood glucose decreased to lower than 30mg/dl, the mice were injected with 200µL 20% glucose in PBS. The blood glucose were measured again 30 minutes after glucose injection and the mice were monitored for other signs of hypoglycemia. If after 30 minutes the blood glucose did not recover, mice were prematurely euthanized. Observations were made at 2 hours and 6 hours post-AAV/TLR9 agonist injection, after which the mice were euthanized. Post-euthanasia, blood samples were collected, and injected skeletal muscle were collected to assess the immune response.

The injection timetable was shown in Table 2.4.

2.9.2 DMA Treatment Group

The study was structured into three groups. Group 1, the control group, received only vehicle injections and no DMA, AAV, or TLR9. These mice were administered 100 μL of PBS intraperitoneally as a control for DMA administration 15 minutes before the AAV/TLR9 vehicle control, and 100 μL of PBS vehicle control for AAV/TLR9 was injected into the vastus lateralis muscle of the lower left leg. Group 2, the positive control group, was expected to show maximum innate immunity. These mice received DMA vehicle administration (100 μL of PBS via intraperitoneal injection) and the AAV/TLR9 mixture. The AAV/TLR9 injection consisted of 1.0×10^{11} viral particles and 100 μg of TLR9 agonists in 100 μL, delivered into the vastus lateralis muscle. Group 3, another experimental group, was anticipated to exhibit reduced innate immunity. These mice received DMA (100 μL of a 50% DMA solution via intraperitoneal injection) and the AAV/TLR9 mixture, which was identical to that of Group 2. Observations were made at 2 hours and 6 hours post-injection, with 24 mice in each time group, totaling 48 mice. Following euthanasia, terminal bleeding was performed, serum was collected via centrifugation, and skeletal muscle were taken.

-15min	First Insulin/PBS Injection
0h	AAV+TLR9/PBS Injection, First Glucose Test
15min	Second Insulin/PBS Injection
30min	Second Glucose Test
45min	Third Insulin Injection
1h	Third Glucose Test, Rescue Glucose Injection(optional)
1h30min	Glucose Test for Rescue Injection (Optional)
2h	Euthanize for 2h
6h	Euthanize for 6h

Table 2.4 Animal Insulin Treatment Group Timetable.

2.10 Interlukin-6 Serum Level Detection

The serum level of IL-6 was quantified utilizing the enzyme-linked immunosorbent assay (ELISA) kit, specifically the Thermo Fisher Scientific Invitrogen Mouse IL-6 Uncoated ELISA Kit. For the assay, 25 µL of mouse serum was employed in duplicate, adhering strictly to the kit's instructions. Absorbance readings of the plates were conducted using a BioTek ELx800 plate reader at a wavelength of 540 nm.

2.11 Immunohistochemistry

Immunohistochemical analysis was conducted on preserved muscle biopsy samples. Initially, the muscle tissues were fixed in 4% paraformaldehyde in PBS for an overnight period (approximately 18 hours) at 4°C. The subsequent day the samples were rinsed four times with 2 mL of PBS, followed by preservation in 70% ethanol at 4°C. The dehydration process for these samples was carried out in a sequential manner: immersion in 85% ethanol for 2 hours, 95% ethanol for 2 hours, 100% ethanol for 2 hours, a 50% xylene/ethanol mixture for 2 hours, and finally 100% xylene for 1 hour. Post-dehydration, each sample, within its cassette, was submerged in paraffin at 65°C for 3 hours. The samples were then embedded into paraffin blocks. These blocks were stored at 4°C until they were ready to be sectioned and stained.

The paraffin-embedded blocks were precisely sectioned using an Accu-Cut® SRM™ 200 Rotary Microtome. Sections, each measuring 6 µm in thickness, were carefully extended in a 50°C water bath to ensure optimal spread. Following this, the sections were mounted onto Fisherbrand Economy Plain Glass Microscope Slides. To guarantee a firm adherence of the tissue sections to the slides, they were left to dry for two days on an open heater at 30°C.

The dried slides underwent a process of rehydration and deparaffinization in a sequential manner: initially, the slides were immersed in 100% xylene for 3 minutes, repeated once more for another 3 minutes, followed by a 3-minute immersion in a 50% ethanol/xylene mixture. This was done by a 3-minute dip in 100% ethanol, then 3 minutes in an 80% ethanol/water solution, and finally, two consecutive 3-minute immersions in a 50% ethanol/water solution. Subsequently, the slides were immersed in PBS. Following the rehydration and deparaffinization, the slides underwent a crucial heat-induced antigen retrieval step. They were immersed in a Tris-EDTA buffer (comprising 10 mM Tris base, 1 mM EDTA solution, and 0.05% Tween 20, with a pH of 9.0) and heated in a 95°C water bath for 15 minutes. After this period, the slides were allowed to gradually cool down to room temperature.

Immediately following the heat-induced antigen retrieval, staining was performed. Excess water was gently removed from the slides by tapping them on absorbent paper. The primary antibody, CD11b Monoclonal Antibody M1/70, (eBioscience), was diluted to a 1:100 ratio and carefully applied directly onto the tissue sections on the slides. This primary antibody incubation lasted for 1 hour. After the primary antibody binding step, the slides were blocked using a 1% bovine serum albumin (BSA) solution in TBST (comprising 0.24g Tris base, 0.88g NaCl in 100ml, adjusted to pH 7.6, with 10 µl Tween-20 added) for 15 minutes. This was followed by an additional blocking step using a 0.5% H_2O_2 solution for 10 minutes. The secondary antibody, Goat anti-Mouse IgG (H+L) Secondary Antibody, HRP (ThermoFisher), was then applied to the slides for 30 minutes. After the secondary antibody application, the slides were treated with the ImmPACT DAB EqV Substrate Kit (Peroxidase) (Vector Laboratories) for visualization, following the kit's instructions.

Subsequently, a 1:5 dilution of Gill's hematoxylin #3 was used for counterstaining. Between each of these steps, the slides were washed with PBS to ensure the complete removal of residues from the previous step.

Following the staining procedure, the slides underwent a systematic dehydration process using a series of solutions. This sequence began with a 3-minute immersion in a 50% ethanol/water solution, followed by 3 minutes in an 80% ethanol/water mixture, then 3 minutes in 100% ethanol. Subsequently, the slides were treated for 3 minutes in a 50% ethanol/xylene mixture, followed by two consecutive 3-minute immersions in 100% xylene. After the final xylene step, while the xylene was still not completely evaporated, each slide was carefully treated with a drop of Permount (Fisher Scientific). Cover slips were then promptly applied to encompass the entire tissue section on each slide. The slides were left to dry thoroughly before any observation or photography was undertaken.

CHAPTER 3 RESULTS

3.1 Gene Expression Change in Human Cell Line Upon Co-Culture for 2h

3.1.1 Gene Expression Change in Hep3B Cells

To determine the profile of cytokine responses to AAV1 and TLR9 agonist stimulation, cytokine expression was measured in Hep3B cells stimulated with the agonists alone or in combination with Insulin or DMA for 2 hr. The gene expression profile was shown in Figure 3.1. Details for each cytokine and interferon were shown in Figure 3.2-3.8. A threshold line at 2.5-fold highlights significant alterations. Notably, TNF-α expression escalated by 2.64-fold upon AAV1 and TLR9 agonist stimulation, a surge mitigated by insulin and DMA treatment. In contrast, IL-1β levels remained unchanged across all experimental conditions. IL-6, similar to TNF-α, experienced a 3.22-fold increase following stimulation, with this rise being attenuated by concurrent insulin and DMA exposure. IL-12 exhibited a notable 3.9-fold augmentation in the AAV1 and TLR9 agonist-stimulated group but reverted to baseline in the presence of insulin and DMA. INF-γ levels remained generally stable, except in the co-culture without stimulation group, where a significant deviation was observed. Intriguingly, this group exhibited substantial elevations in most targeted cytokines and interferons, barring IL-1β: TNF-α spiked by 6.6-fold, IL-6 by 8.7-fold, IL-12 by 12-fold, INF-α by 8.4-fold, INF-β by 7.4-fold, and INF-γ by 7-fold. At the 2-hour mark, both the insulin and DMA groups exhibited a marked reduction in pro-inflammatory cytokines and type I interferons relative to the group stimulated with AAV1 and TLR9 agonists. This observation substantiates the efficacy of insulin and DMA in mitigating the innate immune response triggered by AAV. The

unexpected surge in cytokine levels within the co-culture group lacking stimulation remains enigmatic. However, parallel findings in human macrophage cells (U937) suggest a potential link to *in vitro*-induced macrophages. Prior studies have highlighted those macrophages cultivated *in vitro* exhibit distinctly different responses to stimuli compared to primary macrophages matured *in vivo*. This difference might explain the unusual results in the co-culture group without stimulation, showing that macrophages grown in the lab react differently to those developed naturally in the body.

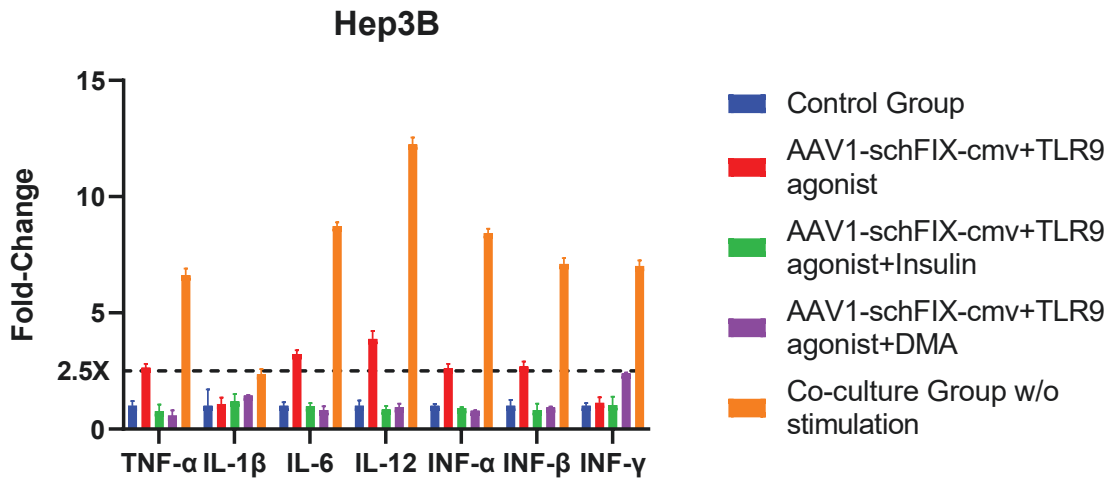

Figure 3.1 Gene expression change in Hep3B cell at 2h.

Overview of all cytokines and interferons expression. Groups were assigned with different colors. Fold-changes are expressed relative to the control group. A threshold line at 2.5-fold highlights significant alterations. The error bar represents standard error.

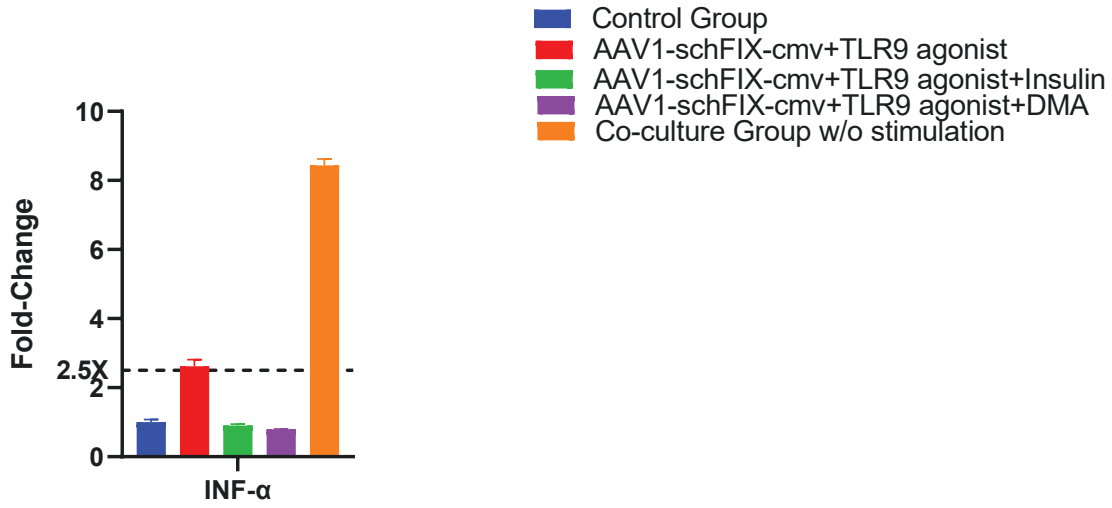

Figure 3.2 TNF-α expression in Hep3B cell at 2h.

Groups were assigned with different colors. Fold-changes are expressed relative to the control group. A threshold line at 2.5-fold highlights significant alterations. The error bar represents standard error.

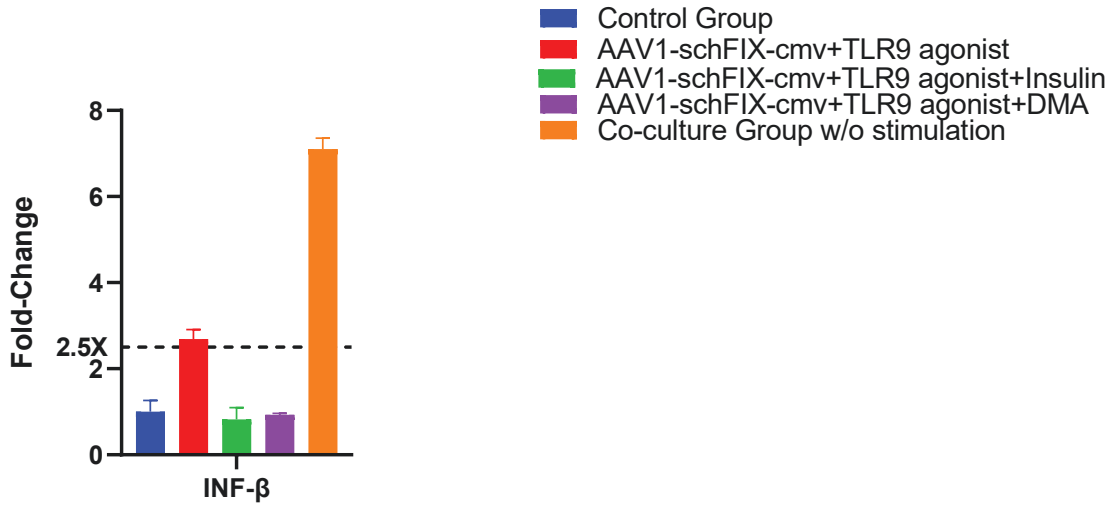

Figure 3.3 IL-1β expression in Hep3B cell at 2h.

Groups were assigned with different colors. Fold-changes are expressed relative to the control group. A threshold line at 2.5-fold highlights significant alterations. The error bar represents standard error.

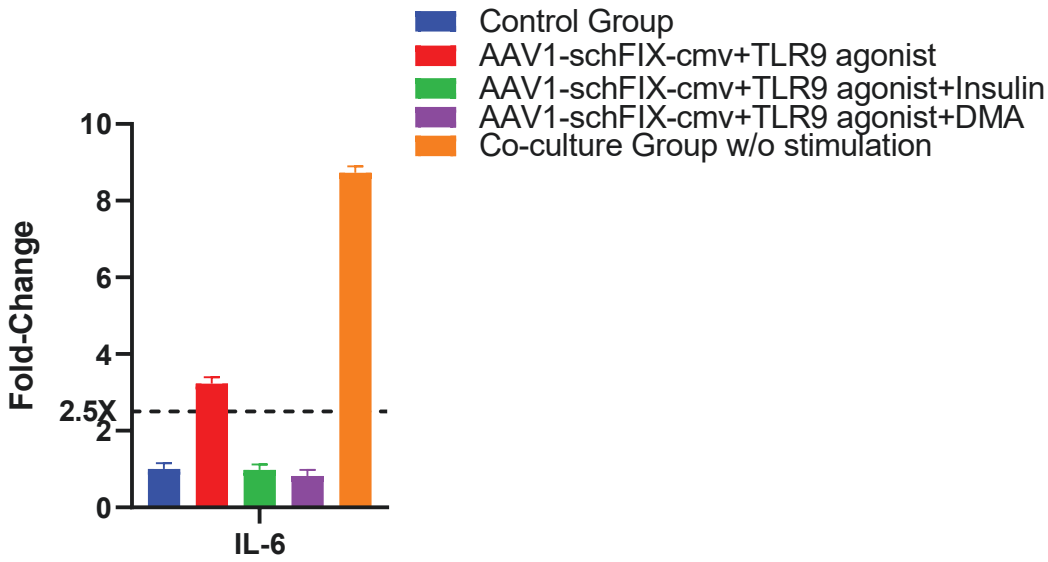

Figure 3.4 IL-6 expression in Hep3B cell at 2h.

Groups were assigned with different colors. Fold-changes are expressed relative to the control group. A threshold line at 2.5-fold highlights significant alterations. The error bar represents standard error.

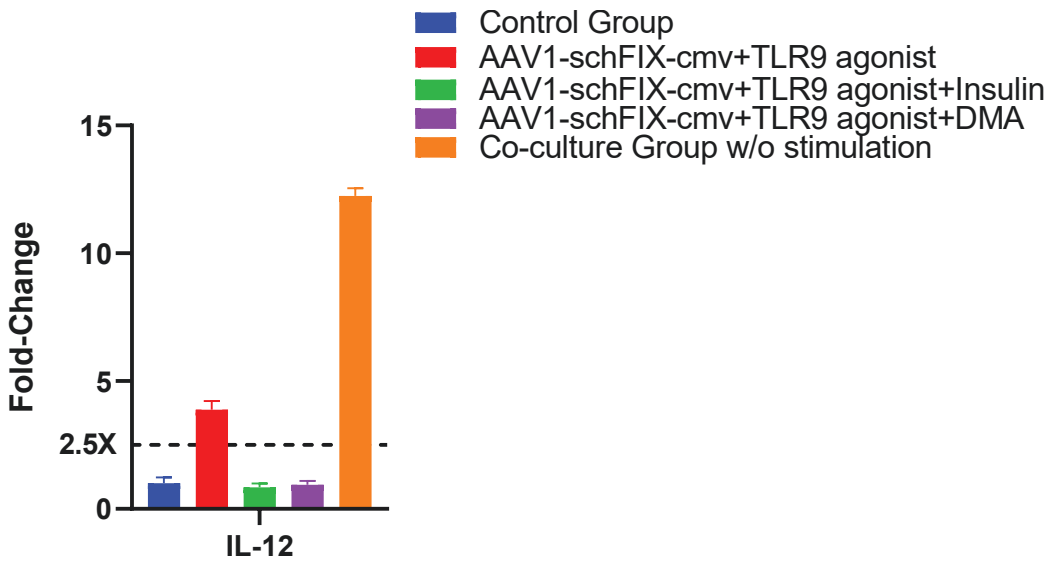

Figure 3.5 IL-12 expression in Hep3B cell at 2h.

Groups were assigned with different colors. Fold-changes are expressed relative to the control group. A threshold line at 2.5-fold highlights significant alterations. The error bar represents standard error.

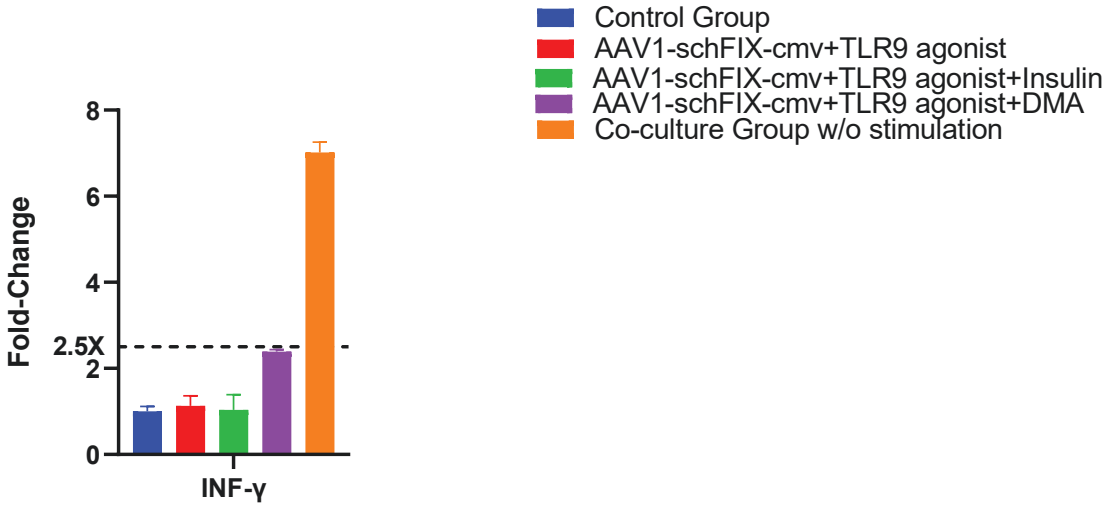

Figure 3.6 INF-γ expression in Hep3B cell at 2h.

Groups were assigned with different colors. Fold-changes are expressed relative to the control group. A threshold line at 2.5-fold highlights significant alterations. The error bar represents standard error.

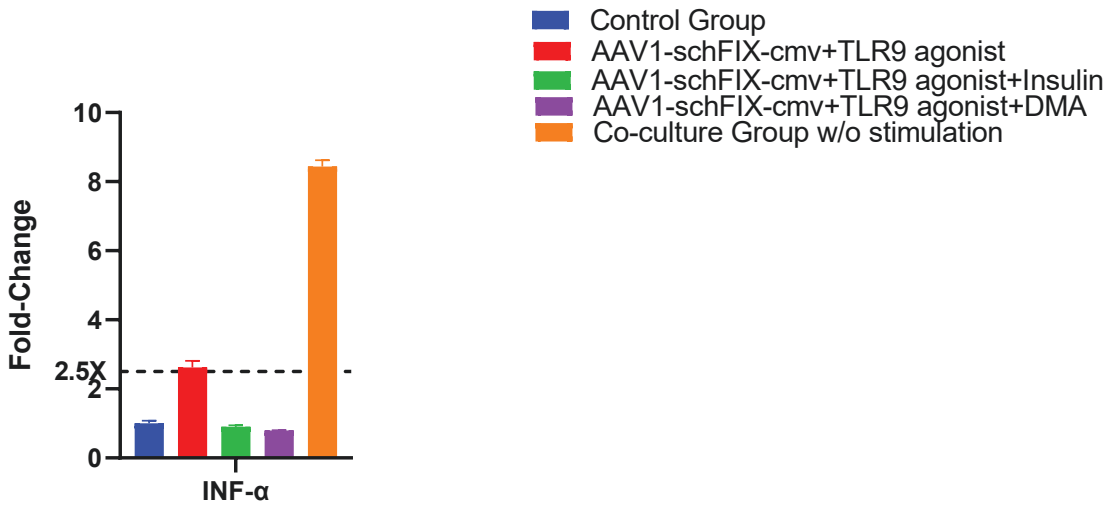

Figure 3.7 INF-α expression in Hep3B cell at 2h.

Groups were assigned with different colors. Fold-changes are expressed relative to the control group. A threshold line at 2.5-fold highlights significant alterations. The error bar represents standard error.

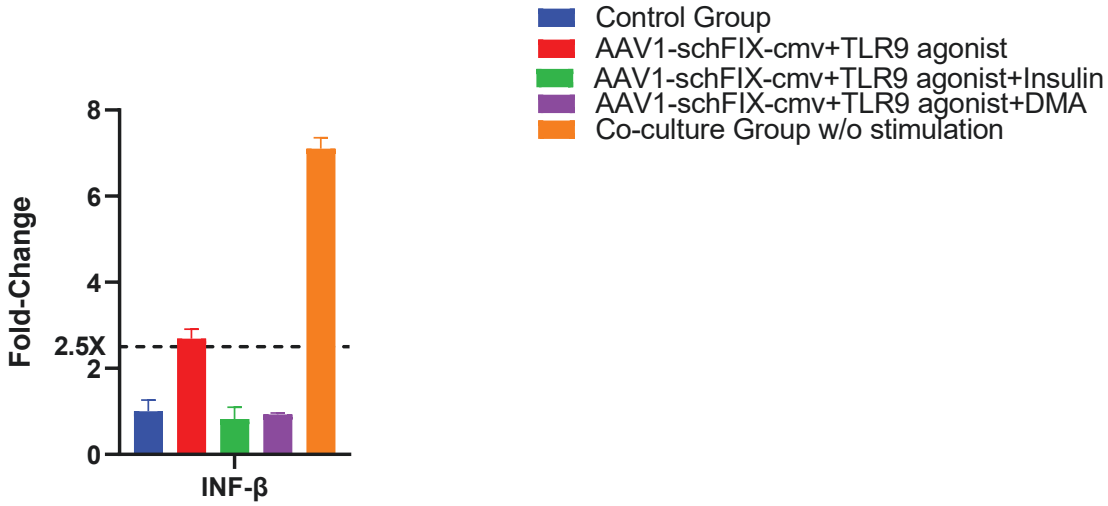

Figure 3.8 INF-β expression in Hep3B cell at 2h.

Groups were assigned with different colors. Fold-changes are expressed relative to the control group. A threshold line at 2.5-fold highlights significant alterations. The error bar represents standard error.

3.1.2 Gene Expression Change in U937 Cells

To determine the profile of cytokine responses to AAV1 and TLR9 agonist stimulation, cytokine expression was measured in U937 cells stimulated with the agonists alone or in combination with Insulin or DMA for 2 hr. The gene expression profile of the U937 cell line was depicted in Figure 3.9, with detailed cytokine and interferon data presented in Figures 3.10-3.16. A notable feature is the inclusion of a threshold line at a 2.5-fold increase, serving as a marker for significant alterations. In the U937 cell line, TNF-α levels did not show a notable elevation, and no group exhibited significant changes compared to the control group. IL-1β expression in the U937 cells increased by 6.54-fold. This increase was moderated by insulin, reducing it to 2.25-fold, and by DMA, which brought it down to 2.79-fold, both compared to the control group. IL-6 levels saw a 4.69-fold increase when stimulated with AAV and TLR9 agonist. While insulin partially suppressed this increase, the expression levels did not return to the baseline observed in the control group. In the DMA treatment group, IL-6 levels decreased compared to the AAV and TLR9 agonist group but were still elevated at 3.12-fold compared to the control group. IL-12 expression increased 4.9-fold upon stimulation. Neither insulin nor DMA were particularly effective in suppressing this increase, with the insulin group showing a 3.31-fold increase and the DMA group a 3.8-fold increase, both compared to the control group. INF-α levels did not increase in any of the groups compared to the control group. However, both DMA and insulin demonstrated a suppressive effect on INF-β. Upon stimulation, INF-β levels increased threefold, but DMA and insulin treatments reduced it to the normal levels observed in the control group. INF-γ increased 2.8-fold in the AAV+TLR9 group, but in the insulin and DMA groups, the levels returned to those seen

in the control group. Similar to Hep3B cells, the U937 cells also exhibited significant changes in the co-culture without stimulation group, particularly in IL-1, IL-6, IL-12, INF-β, and INF-γ. This could be attributed to the fact that the U937 cell is an in vitro induced macrophage, which may exhibit unusual and unexpected behavior. Overall, the U937 cells showed a more pronounced response to AAV and TLR9 stimulation compared to Hep3B cells, which is consistent with their macrophage nature. Insulin and DMA also demonstrated a suppressive effect on IL-1β, INF-β, and INF-γ.

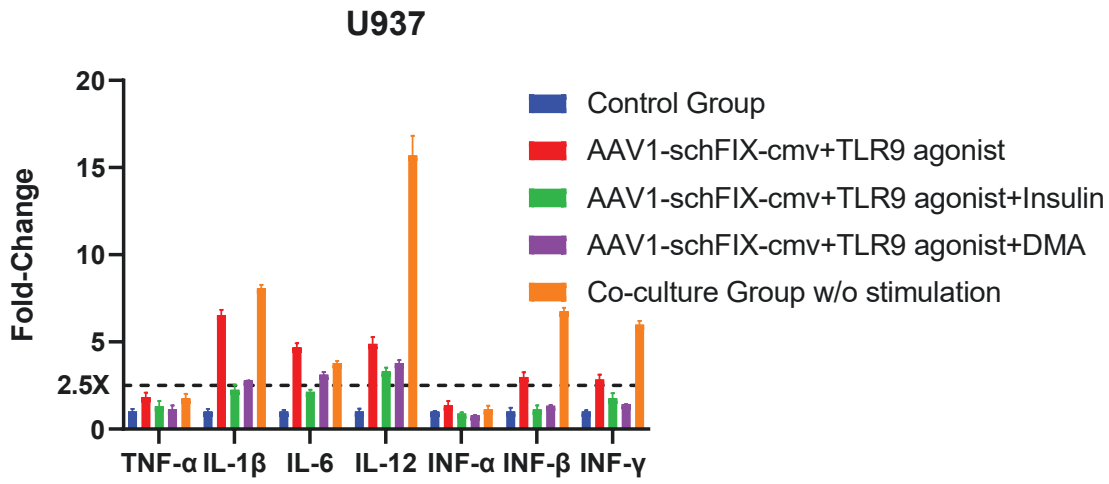

Figure 3.9 Gene expression change in U937 cell at 2h.

Overview of all cytokines and interferons expression. Groups were assigned with distinct colors. Fold-changes are expressed relative to the control group. A threshold line at 2.5-fold highlights significant alterations. The error bar represents standard error.

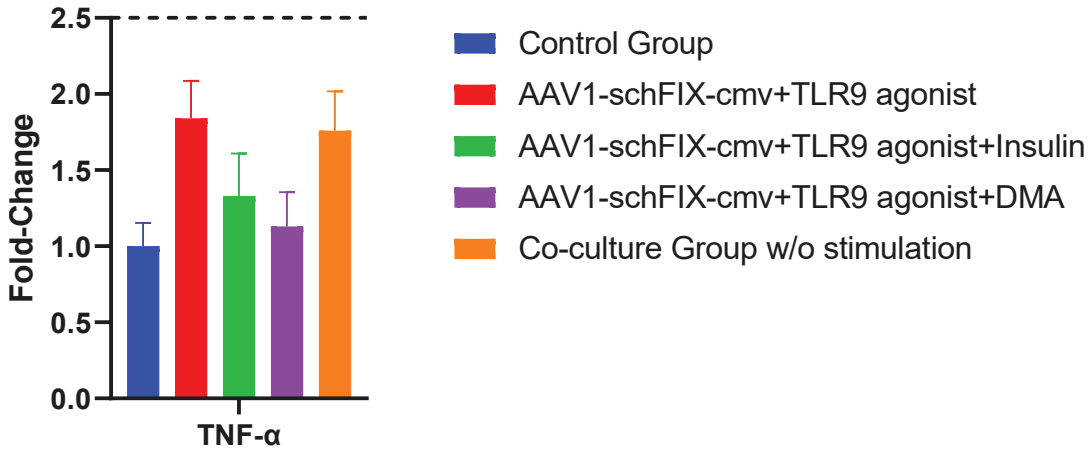

Figure 3.10 TNF-α expression in Hep3B cell at 2h.

Groups were assigned with different colors. Fold-changes are expressed relative to the control group. A threshold line at 2.5-fold highlights significant alterations. The error bar represents standard error.

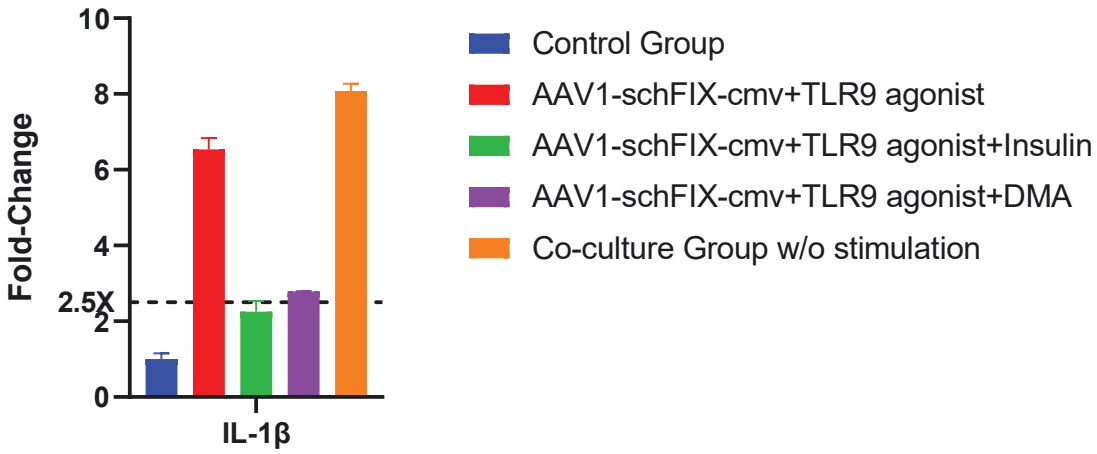

Figure 3.11 IL-1β expression in U937 cell at 2h.

Groups were assigned with different colors. Fold-changes are expressed relative to the control group. A threshold line at 2.5-fold highlights significant alterations. The error bar represents standard error.

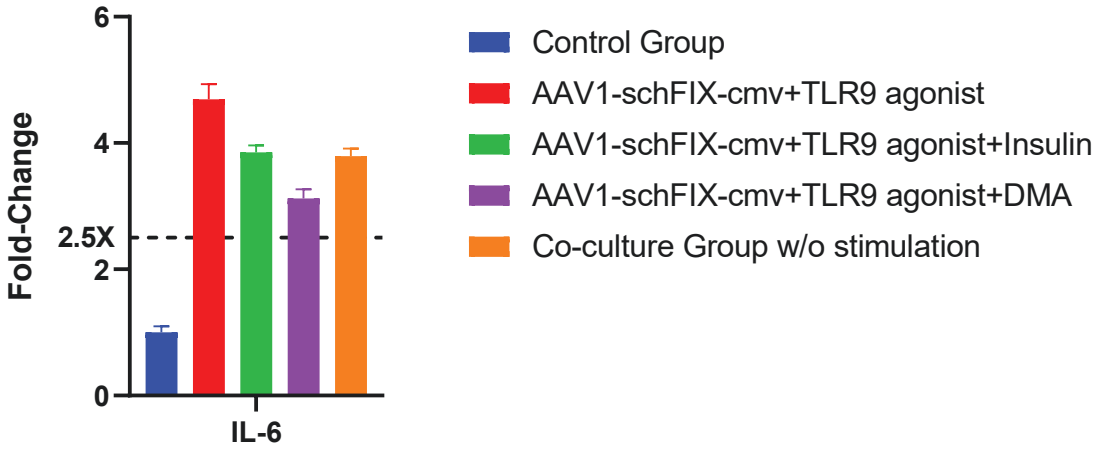

Figure 3.12 IL-6 expression in U937 cell at 2h.

Groups were assigned with different colors. Fold-changes are expressed relative to the control group. A threshold line at 2.5-fold highlights significant alterations. The error bar represents standard error.

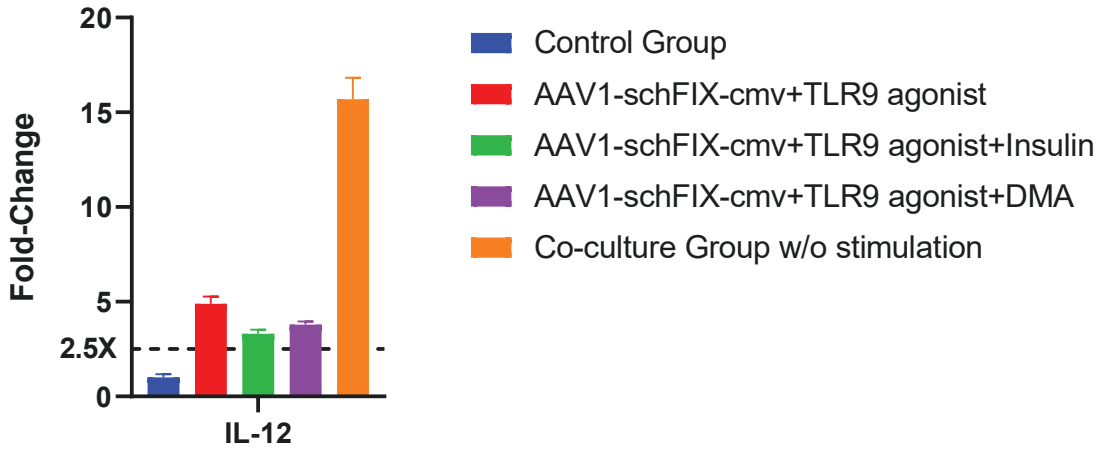

Figure 3.13 IL-12 expression in U937 cell at 2h.

Groups were assigned with different colors. Fold-changes are expressed relative to the control group. A threshold line at 2.5-fold highlights significant alterations. The error bar represents standard error.

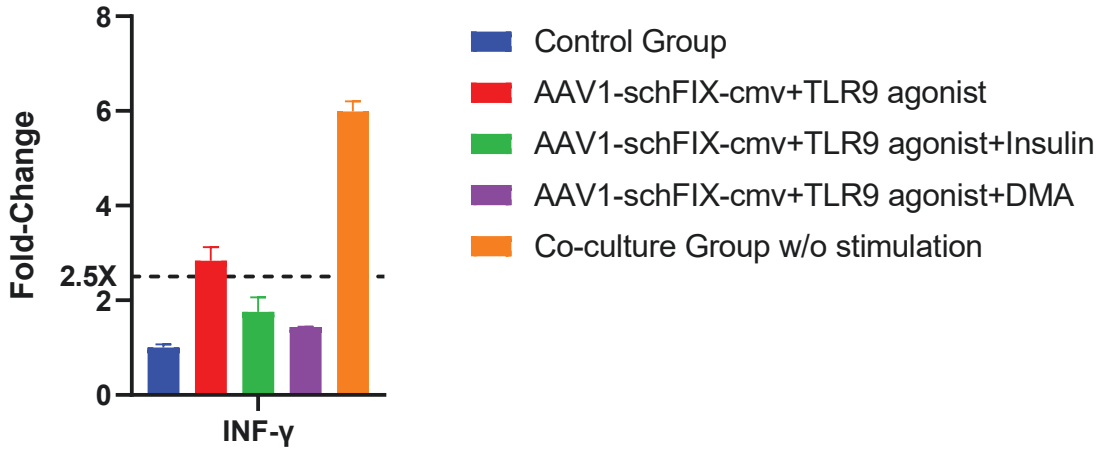

Figure 3.14 INF-γ expression in U937 cell at 2h.

Groups were assigned with different colors. Fold-changes are expressed relative to the control group. A threshold line at 2.5-fold highlights significant alterations. The error bar represents standard error.

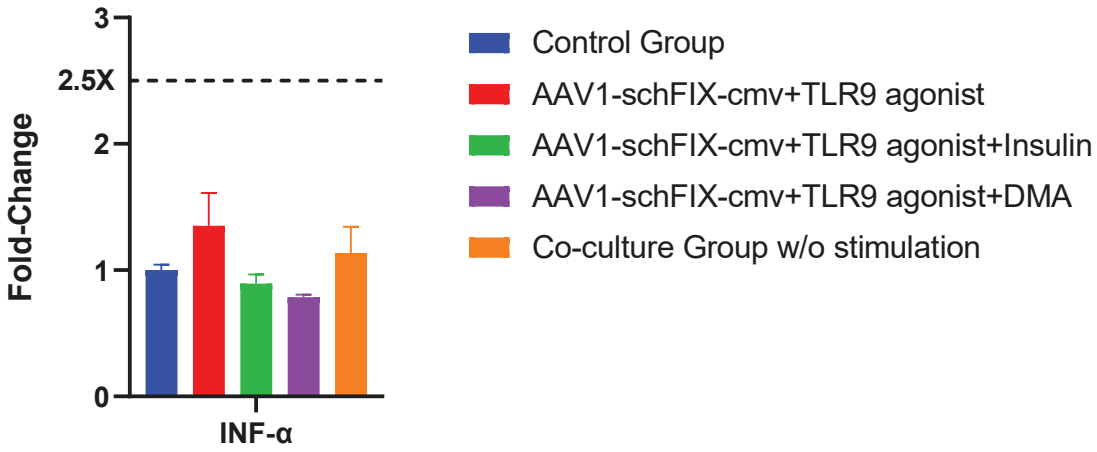

Figure 3.15 INF-α expression in U937 cell at 2h.

Groups were assigned with different colors. Fold-changes are expressed relative to the control group. A threshold line at 2.5-fold highlights significant alterations. The error bar represents standard error.

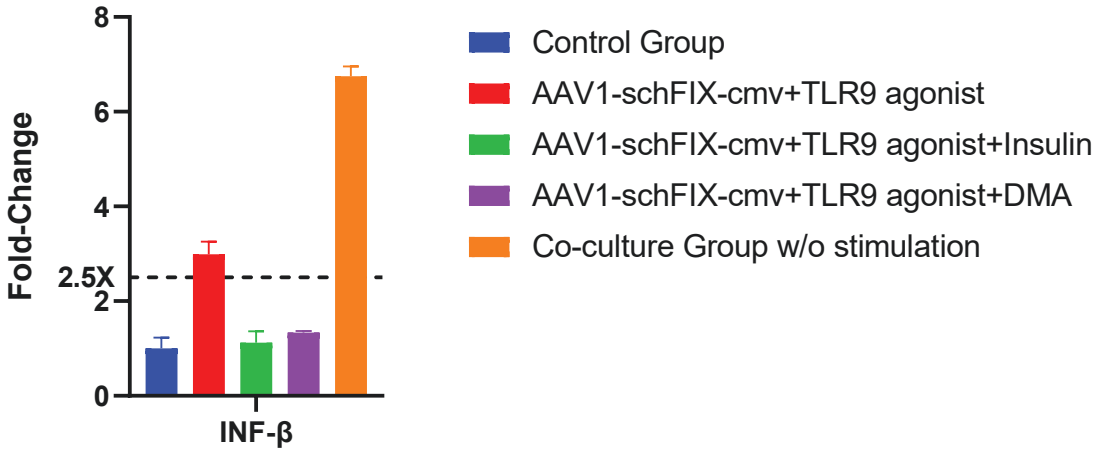

Figure 3.16 INF-β expression in U937 cell at 2h.

Groups were assigned with different colors. Fold-changes are expressed relative to the control group. A threshold line at 2.5-fold highlights significant alterations. The error bar represents standard error.

3.2 Gene Expression Change in Human Cell Line Upon Co-Culture for 6h

3.2.1 Gene Expression Change in Hep3B Cell

The gene expression profile of the Hep3B cell line is illustrated in Figure 3.17, where a threshold line at a 2.5-fold increase delineates significant alterations. Overall, neither any specific group nor gene surpassed this threshold. TNF-α levels across all groups remained close to those observed in the control group, indicating minimal variation. Intriguingly, IL-1β levels decreased significantly compared to the control group, suggesting a potential feedback effect following an initial increase at 2 hours, which warrants further investigation. For IL-6, IL-12, INF-α, INF-β, and INF-γ, the results were somewhat uniform: the groups treated with AAV and TLR9 agonists exhibited an increase in expression, but this was less than 2.5-fold. The groups treated with DMA and insulin showed expression levels comparable to the control group. These findings indicate that the cytokines and interferons triggered by AAV returned to normal levels at the 6-hour mark. This suggests a transient response to the AAV and TLR9 agonist stimulation, with the cell line reverting to baseline expression levels relatively quickly.

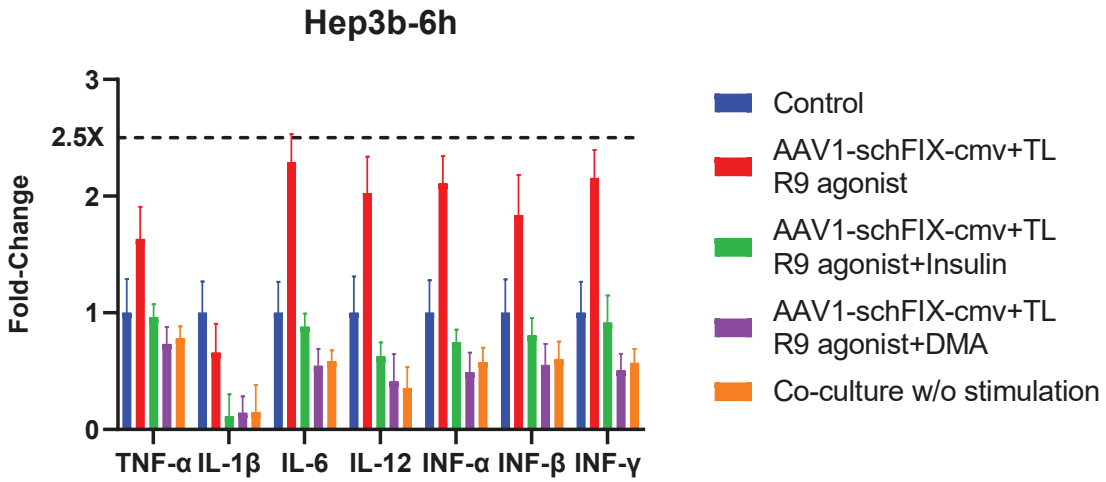

Figure 3.17 Gene expression change in Hep3B cell at 6h.

Groups were assigned with different colors. Overview of cytokines and interferons expression. Fold-changes are expressed relative to the control group. A threshold line at 2.5-fold highlights significant alterations. The error bar represents standard error.

3.2.2 Gene Expression Change in U937 Cells

The gene expression profile of the U937 cell line is depicted in Figure 3.18, where a threshold line at a 2.5-fold increase marks a significant alteration. Similar to the Hep3B cells at 6 hours, no specific group or gene in the U937 cell line exceeded this threshold. For TNF-α, IL-1β, and IL-6, the levels in all experimental groups remained comparable to those in the control group, indicating no significant changes. In the case of IL-12, all groups stimulated showed a decrease in expression compared to the control group. This decrease might be a feedback response to the stimulation, although the exact mechanism remains unclear. INF-α, INF-β, and INF-γ also exhibited decreases similar to IL-12, but the changes were less pronounced. Overall, mirroring the pattern observed in Hep3B cells, the levels of cytokines and interferons in U937 cells returned to normal at the 6-hour mark.

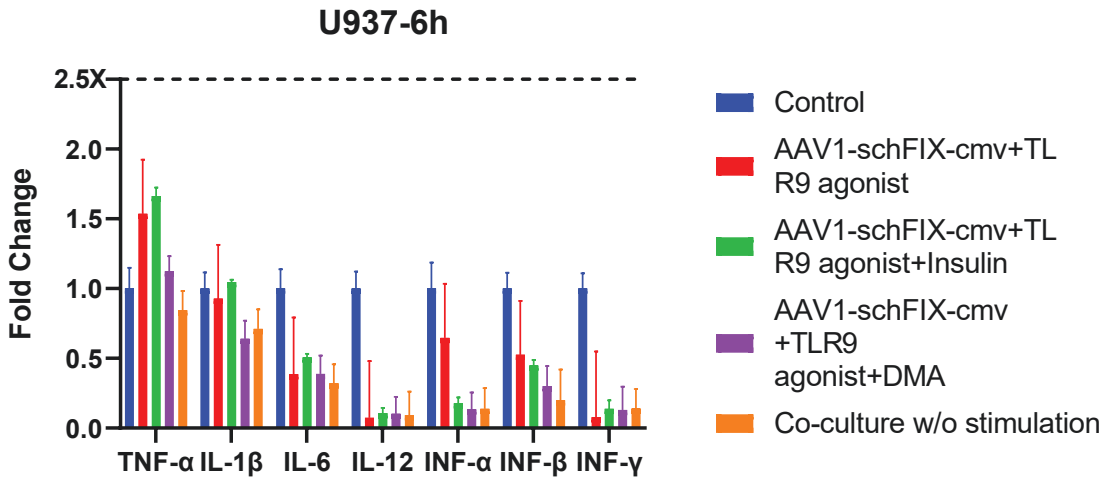

Figure 3.18 Gene expression change in U937 cell at 6h.

Overview of cytokines and interferons expression. Groups were assigned with different colors. Fold-changes are expressed relative to the control group. A threshold line at 2.5-fold highlights significant alterations. The error bar represents standard error.

3.3 Gene Expression Change in Human Cell Line Upon Co-Culture for 24h

Compared to the control group, neither any groups nor genes exhibited an increase. DMA and insulin did not demonstrate further suppressive effects. The innate immune response was confined to a short period, it was logical that by 24 hours, the expression of all cytokines and interferons had returned to normal levels.

3.3.1 Gene Expression Change in Hep3B Cells

The expression was shown in Figure 3.19.

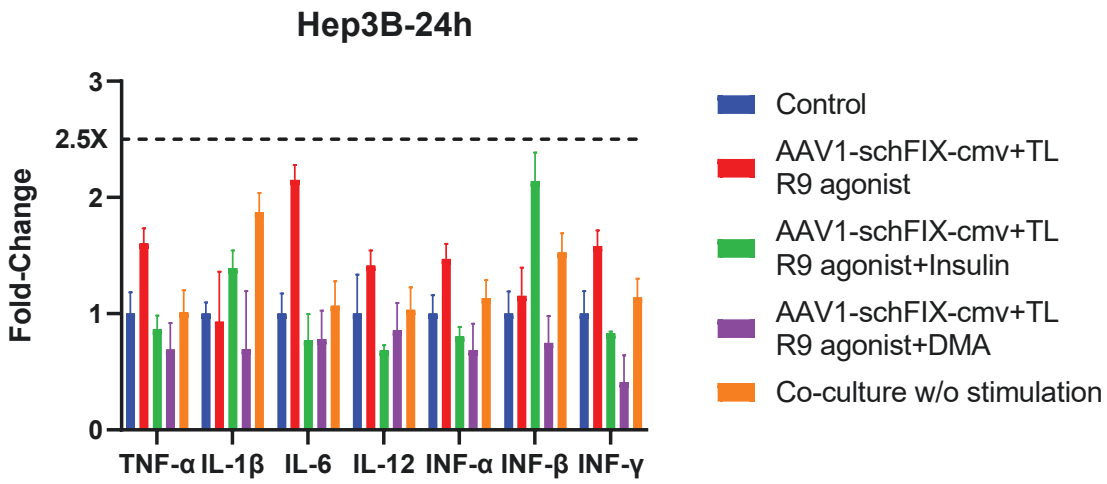

Figure 3.19 Gene expression change in Hep3B cell at 24h.

Overview of cytokines and interferons expression. Groups were assigned with different colors. Fold-changes are expressed relative to the control group. A threshold line at 2.5-fold highlights significant alterations. The error bar represents standard error.

3.3.2 Gene Expression Change in U937 Cells

The gene expression was shown in Figure 3.20.

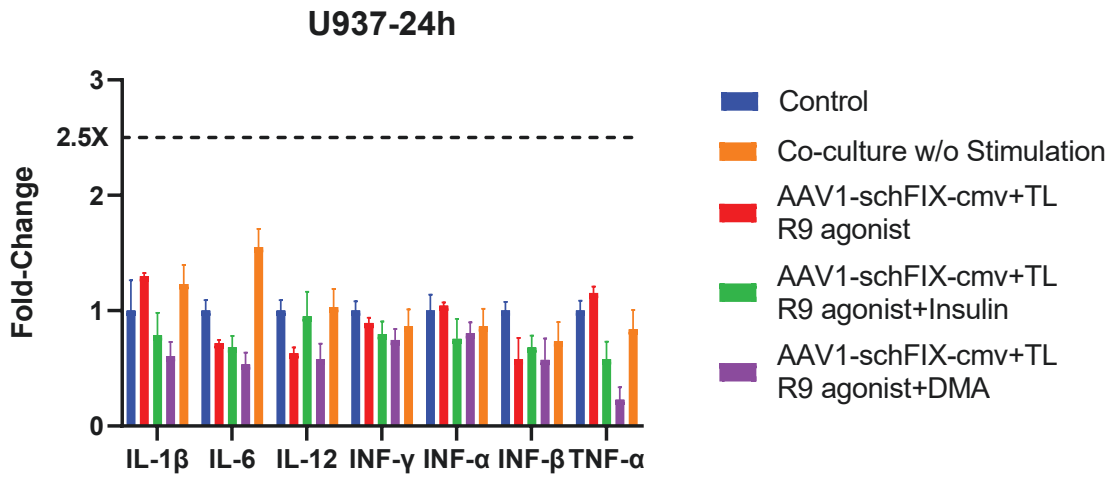

Figure 3.20 Gene expression change in U937 cell at 24h.

Overview of cytokines and interferons expression. Groups were assigned with different colors. Fold-changes are expressed relative to the control group. A threshold line at 2.5-fold highlights significant alterations. The error bar represents standard error.

3.4 Gene Expression Change in C57BL/6 Muscle Upon Insulin Stimulation

3.4.1 Gene Expression Change in C57BL/6 Muscle Upon Insulin Stimulation at 2h

The expressions of cytokines and interferons are depicted in Figure 3.21, with detailed information for each cytokine and interferon presented in Figures 3.22-3.28. A threshold line set at a 2.5-fold increase highlights significant changes, with all fold changes being compared to the control group. TNF-α expression levels remained unchanged across all groups. IL-1β exhibited a 2.7-fold increase in response to AAV and TLR9 stimulation, which was reversed by insulin. IL-6 displayed a 45-fold increase upon stimulation, but insulin reduced this to a 17-fold increase. IL-12 showed a 16-fold increase, which was suppressed by insulin to levels comparable to the control group. INF-α and INF-β increased by 2.8-fold and 3-fold, respectively; insulin suppressed these increases, although they did not return to normal levels. INF-γ did not exhibit any significant change.

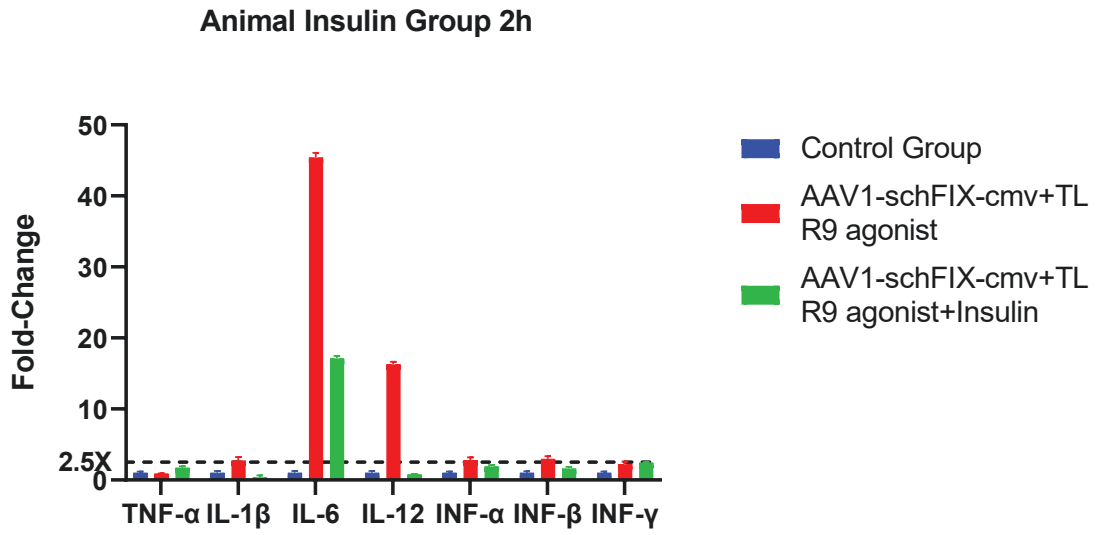

Figure 3.21 Gene expression change of muscle sample in insulin treatment group at 2h.

Overview of cytokines and interferons expression. Groups were assigned with different colors. Fold-changes are expressed relative to the control group. A threshold line at 2.5-fold highlights significant alterations. The error bar represents standard error.

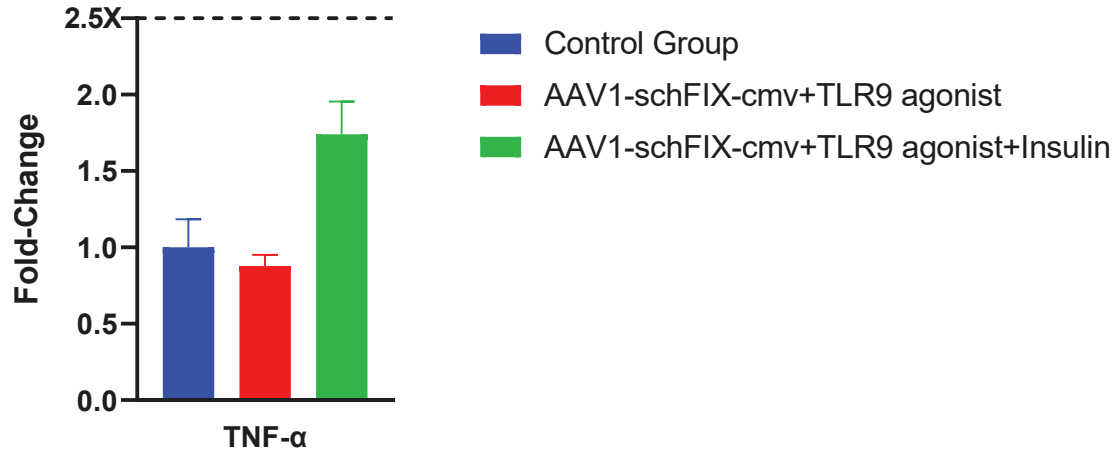

Figure 3.22 TNF-α expression of muscle sample in insulin treatment group at 2h.

Fold-changes are expressed relative to the control group. Groups were assigned with different colors. A threshold line at 2.5-fold highlights significant alterations. The error bar represents standard error.

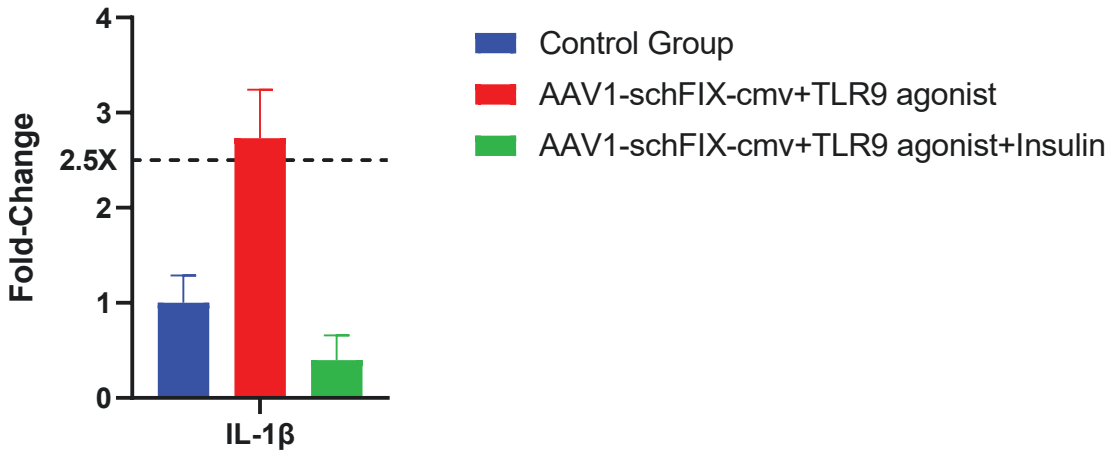

Figure 3.23 IL-1β expression of muscle sample in insulin treatment group at 2h.

Groups were assigned with different colors. Fold-changes are expressed relative to the control group. A threshold line at 2.5-fold highlights significant alterations. **T**he error bar represents standard error**.**

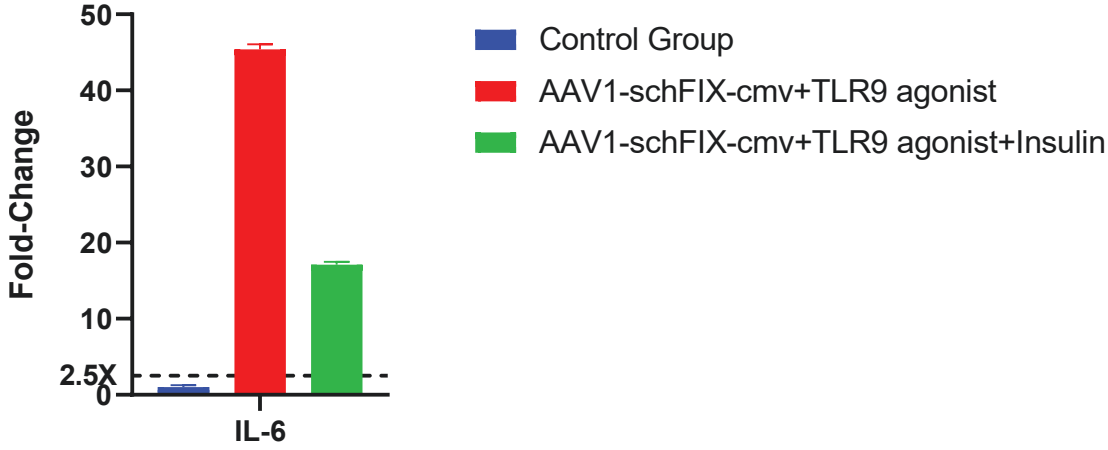

Figure 3.24 IL-6 expression of muscle sample in insulin treatment group at 2h.

Groups were assigned with different colors. Fold-changes are expressed relative to the control group. A threshold line at 2.5-fold highlights significant alterations. **T**he error bar represents standard error**.**

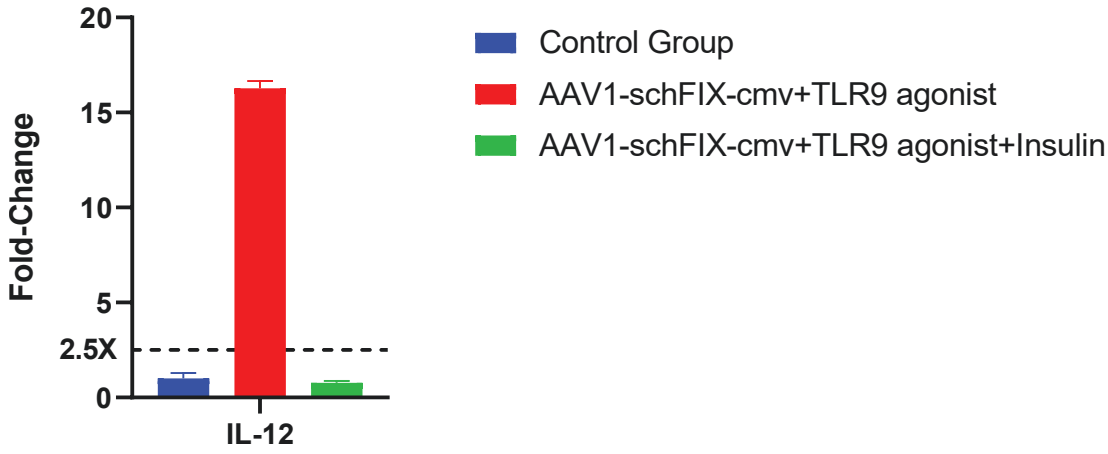

Figure 3.25 IL-12 expression of muscle sample in insulin treatment group at 2h.

Groups were assigned with different colors. Fold-changes are expressed relative to the control group. A threshold line at 2.5-fold highlights significant alterations. **T**he error bar represents standard error**.**

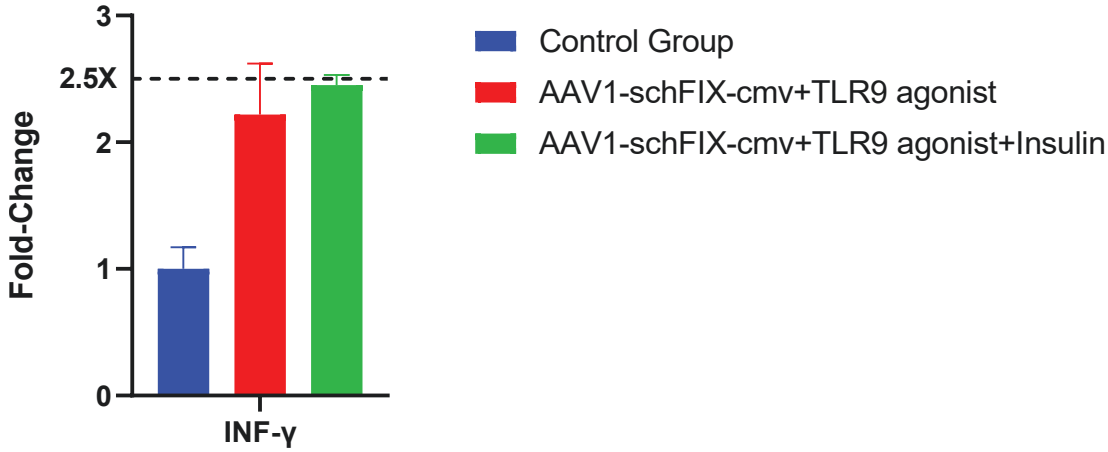

Figure 3.26 INF-γ expression of muscle sample in insulin treatment group at 2h.

Groups were assigned with different colors. Fold-changes are expressed relative to the control group. A threshold line at 2.5-fold highlights significant alterations. **T**he error bar represents standard error**.**

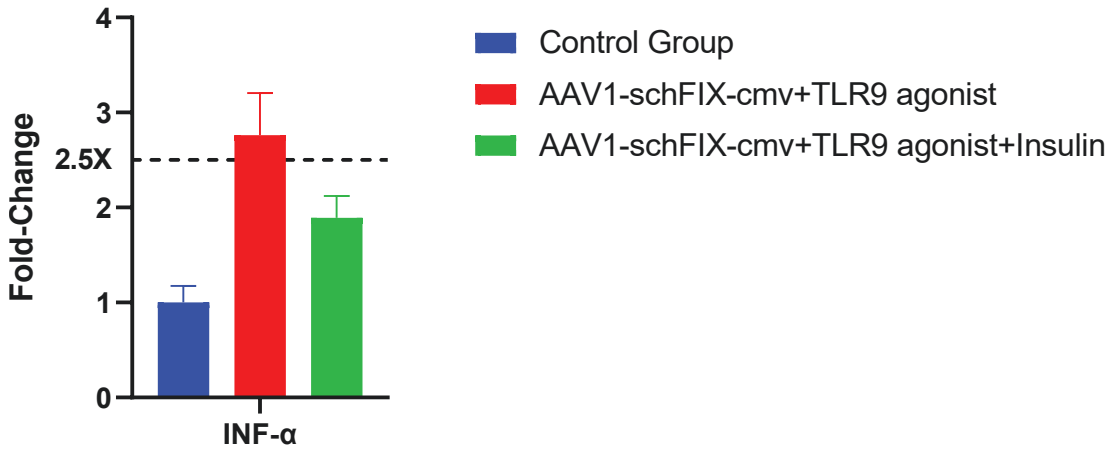

Figure 3.27 INF-α expression of muscle sample in insulin treatment group at 2h.

Groups were assigned with different colors. Fold-changes are expressed relative to the control group. A threshold line at 2.5-fold highlights significant alterations. **T**he error bar represents standard error**.**

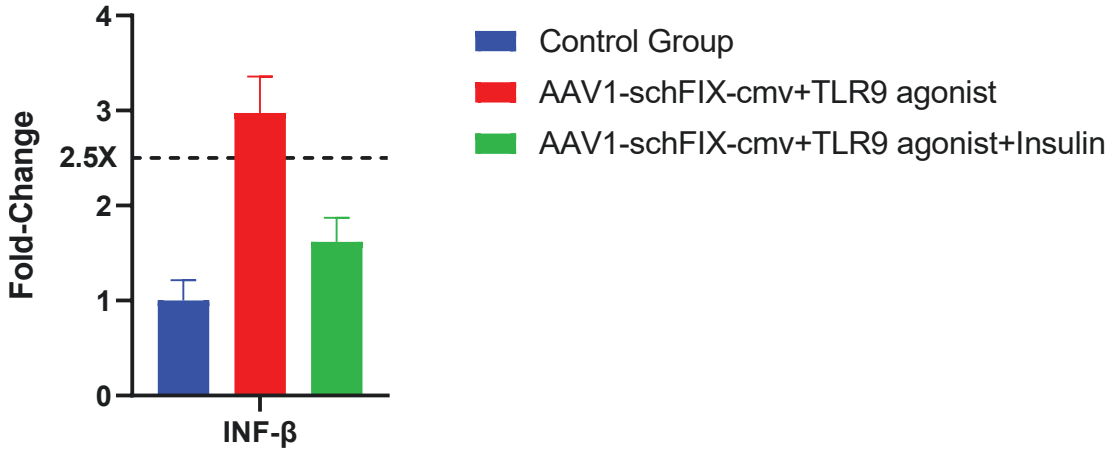

Figure 3.28 INF-β expression of muscle sample in insulin treatment group at 2h.

Groups were assigned with different colors. Fold-changes are expressed relative to the control group. A threshold line at 2.5-fold highlights significant alterations. **T**he error bar represents standard error**.**

3.4.2 Gene Expression Change in C57BL/6 Muscle Upon Insulin Stimulation at 6h

The expressions of cytokines and interferons are presented in Figure 3.28, with each cytokine and interferon detailed in Figure 3.29-3.35. A threshold line indicating a 2.5-fold increase was established to highlight significant changes, with all fold changes referenced against the control group. Notably, at the 6-hour mark, there were no significant changes in the levels of any cytokines or interferons. However, insulin demonstrated an additional suppressive effect on IL-1β and IL-12, with their expression levels reduced to 0.16-fold and 0.18-fold, respectively. This effect is likely attributable to the administration of insulin three times, commencing 45 minutes after the introduction of AAV and TLR9 agonists.

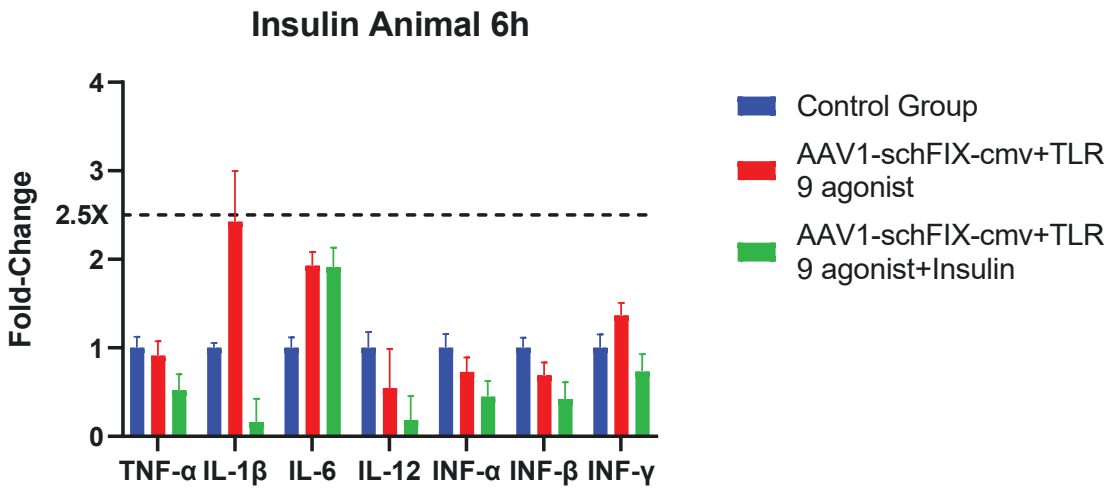

Figure 3.29 Gene expression change of muscle sample in insulin treatment group at 6h.

Overview of cytokines and interferons expression. Groups were assigned with different colors. Fold-changes are expressed relative to the control group. A threshold line at 2.5-fold highlights significant alterations. The error bar represents standard error.

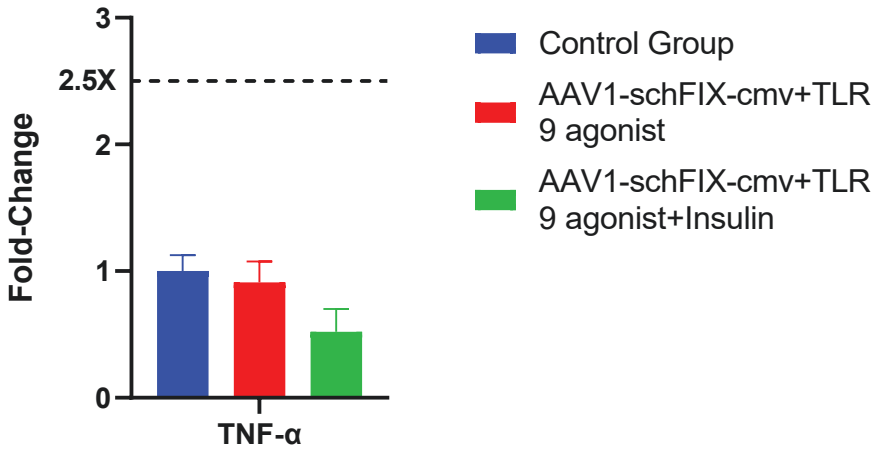

Figure 3.30 TNF-α expression of muscle sample in insulin treatment group at 6h.

Groups were assigned with different colors. Fold-changes are expressed relative to the control group. A threshold line at 2.5-fold highlights significant alterations. The error bar represents standard error.

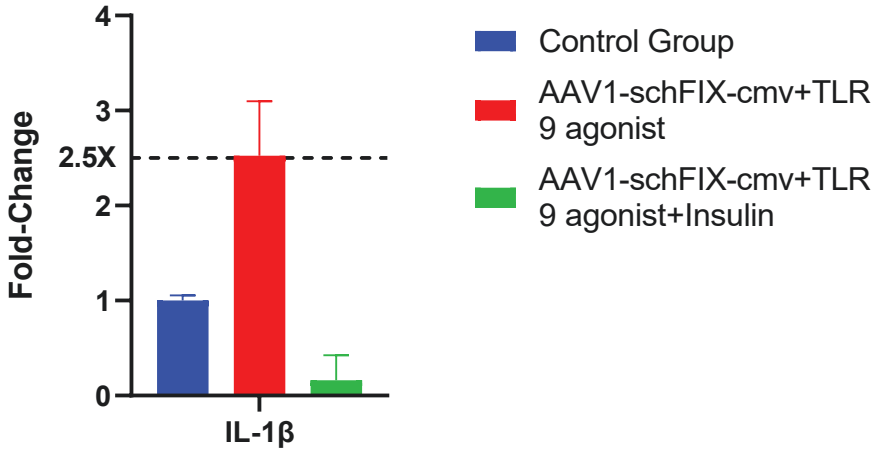

Figure 3.31 IL-1β expression of muscle sample in insulin treatment group at 6h.

Groups were assigned with different colors. Fold-changes are expressed relative to the control group. A threshold line at 2.5-fold highlights significant alterations. **T**he error bar represents standard error**.**

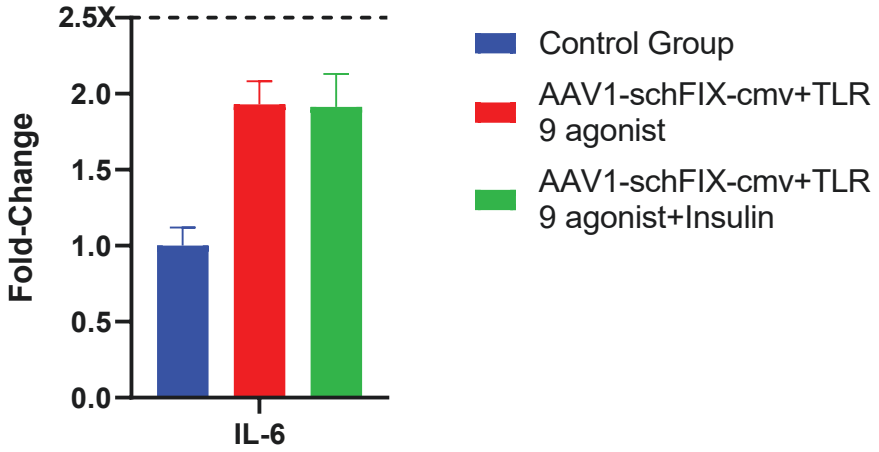

Figure 3.32 IL-6 expression of muscle sample in insulin treatment group at 6h.

Groups were assigned with different colors. Fold-changes are expressed relative to the control group. A threshold line at 2.5-fold highlights significant alterations. **T**he error bar represents standard error**.**

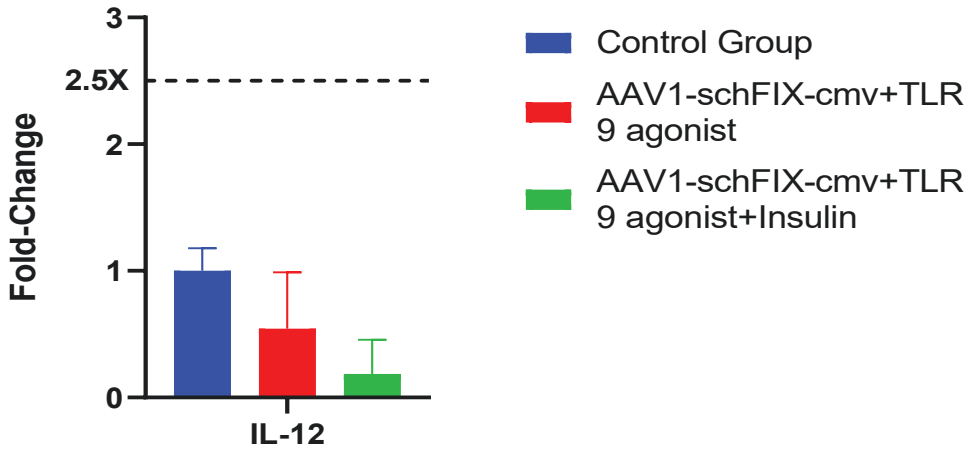

Figure 3.33 IL-12 expression of muscle sample in insulin treatment group at 6h.

Groups were assigned with different colors. Fold-changes are expressed relative to the control group. A threshold line at 2.5-fold highlights significant alterations. **T**he error bar represents standard error**.**

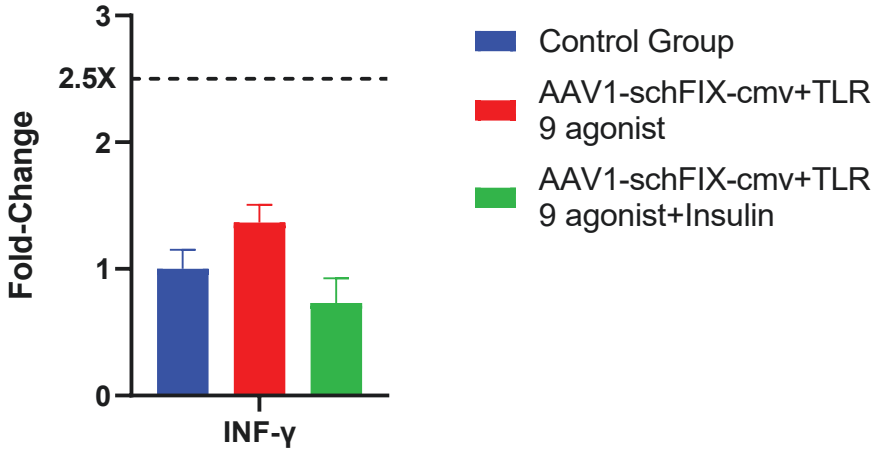

Figure 3.34 INF-γ expression of muscle sample in insulin treatment group at 6h.

Groups were assigned with different colors. Fold-changes are expressed relative to the control group. A threshold line at 2.5-fold highlights significant alterations. **T**he error bar represents standard error**.**

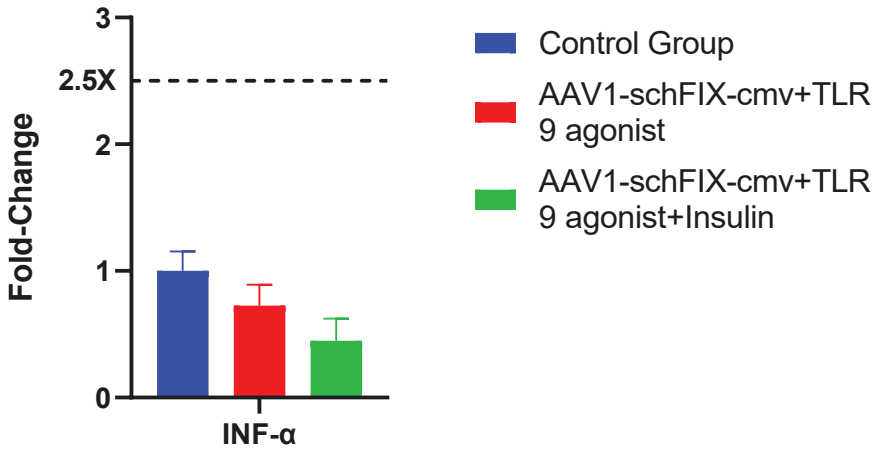

Figure 3.35 INF-α expression of muscle sample in insulin treatment group at 6h.

Groups were assigned with different colors. Fold-changes are expressed relative to the control group. A threshold line at 2.5-fold highlights significant alterations. **T**he error bar represents standard error**.**

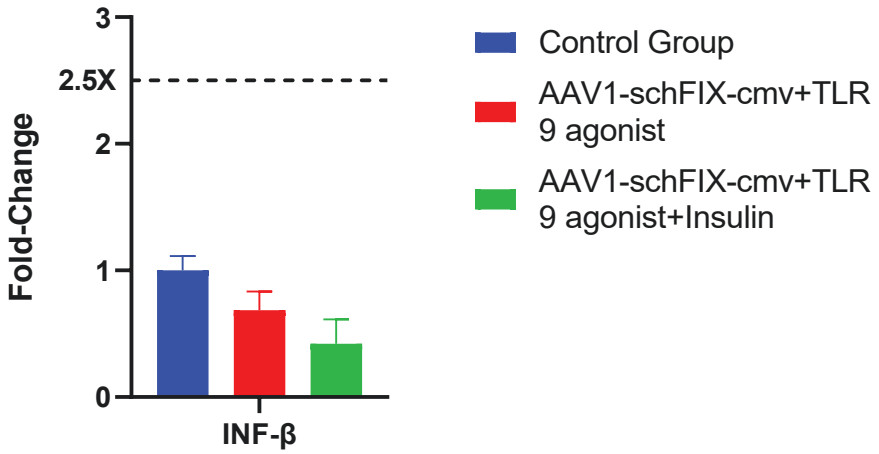

Figure 3.36 INF-β expression of muscle sample in insulin treatment group at 6h.

Groups were assigned with different colors. Fold-changes are expressed relative to the control group. A threshold line at 2.5-fold highlights significant alterations. **T**he error bar represents standard error**.**

3.5 Gene Expression Change in C57BL/6 Muscle Upon DMA Stimulation

3.5.1 Gene Expression Change in C57BL/6 Muscle Upon DMA Stimulation at 2h

Figure 3.5.1 illustrates the expressions of cytokines and interferons, with each cytokine and interferon further detailed in Figures 2-9. A designated threshold line at a 2.5-fold increase serves to emphasize significant alterations, and all fold changes are compared to those in the control group. TNF-α showed a 3.1-fold increase, which was reduced to 1.2-fold by DMA. IL-1β experienced a 2.8-fold increase, subsequently suppressed to 0.2-fold by DMA. IL-6 saw a substantial 52-fold increase, which DMA reduced to 19-fold. IL-12 increased by 2.9-fold, and DMA brought it down to 1.43-fold. Both INF-α and INF-β exhibited increases of 3.1-fold and 4.3-fold, respectively, and DMA effectively suppressed these to normal levels. INF-γ did not undergo any significant change, with all groups maintaining levels close to normal.

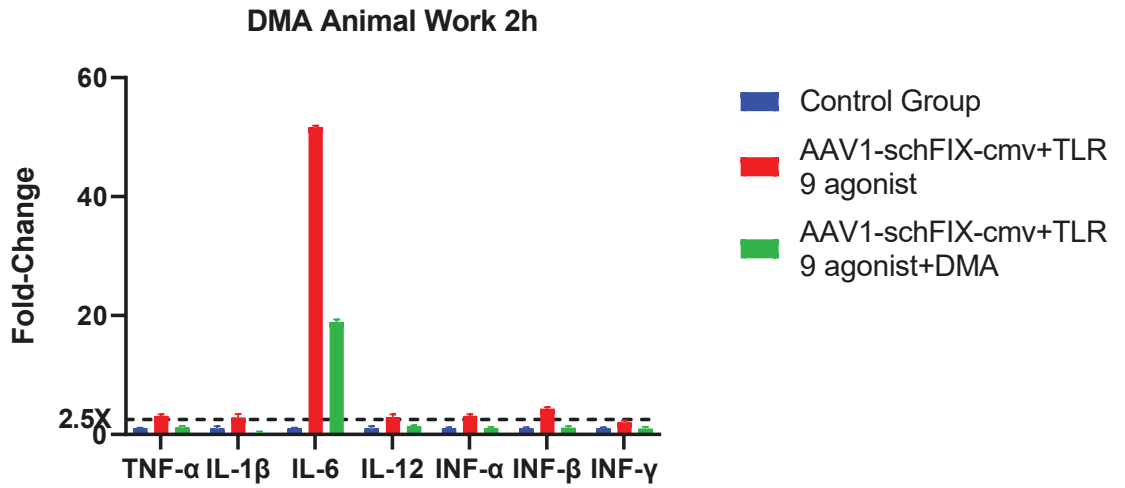

Figure 3.37 Gene expression change of muscle sample in DMA treatment group at 2h.

Overview of cytokines and interferons expression. Groups were assigned with different colors. Fold-changes are expressed relative to the control group. A threshold line at 2.5-fold highlights significant alterations. The error bar represents standard error.

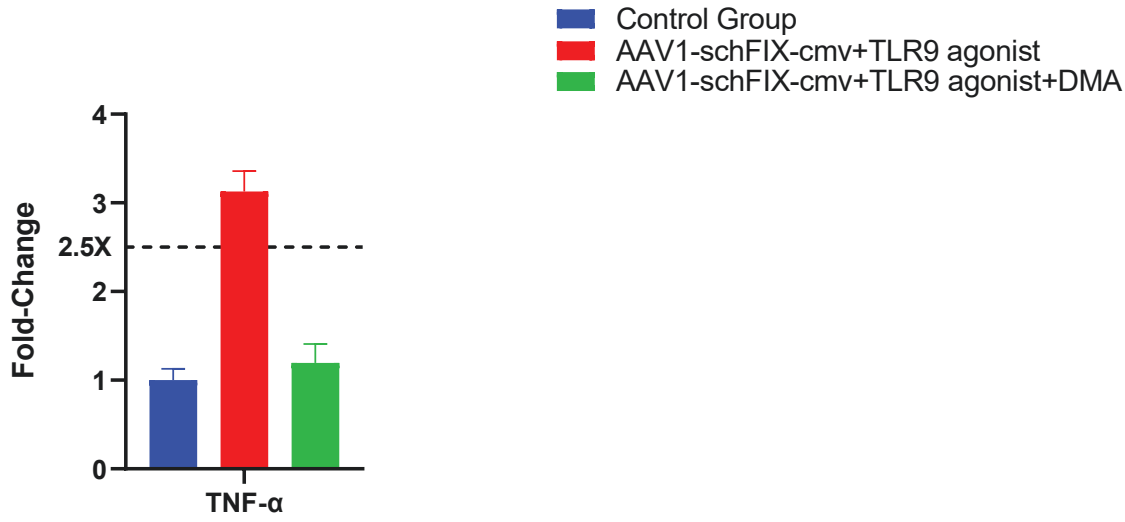

Figure 3.38 TNF-α expression of muscle sample in DMA treatment group at 2h.

Groups were assigned with different colors. Fold-changes are expressed relative to the control group. A threshold line at 2.5-fold highlights significant alterations. The error bar represents standard error.

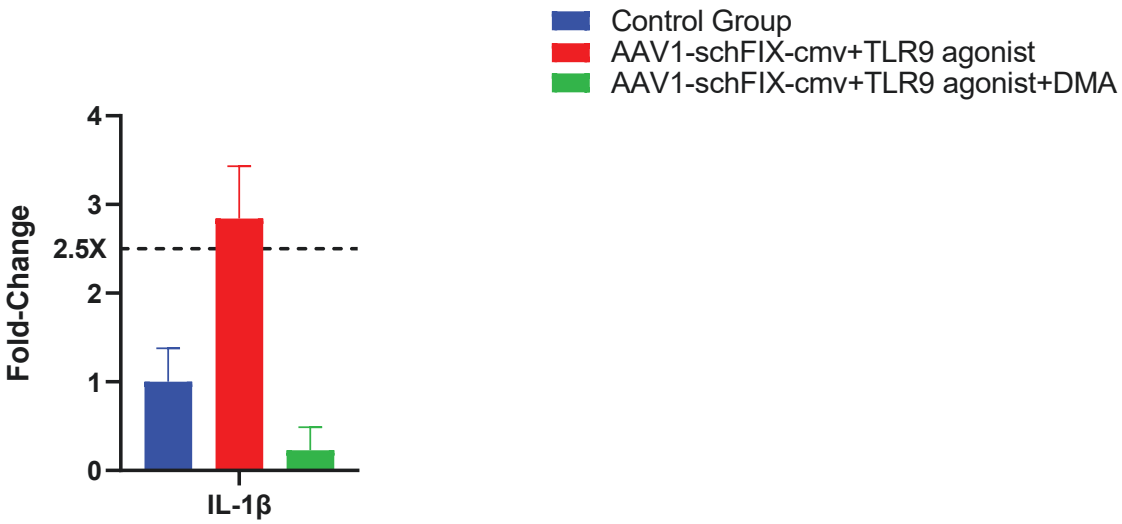

Figure 3.39 IL-1β expression of muscle sample in DMA treatment group at 2h.

Groups were assigned with different colors. Fold-changes are expressed relative to the control group. A threshold line at 2.5-fold highlights significant alterations. The error bar represents standard error.

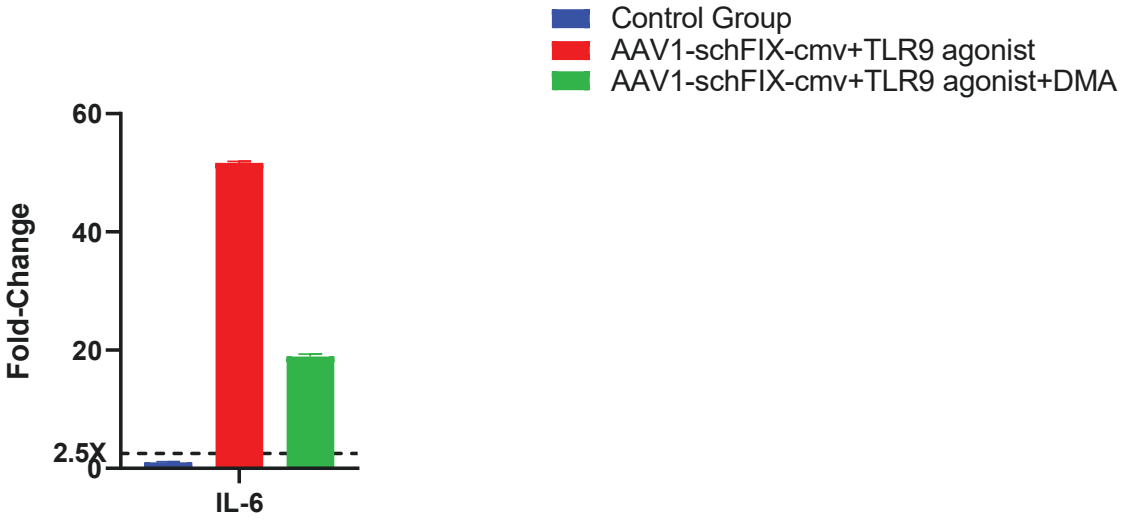

Figure 3.40 IL-6 expression of muscle sample in DMA treatment group at 2h.

Groups were assigned with different colors. Fold-changes are expressed relative to the control group. A threshold line at 2.5-fold highlights significant alterations. The error bar represents standard error.

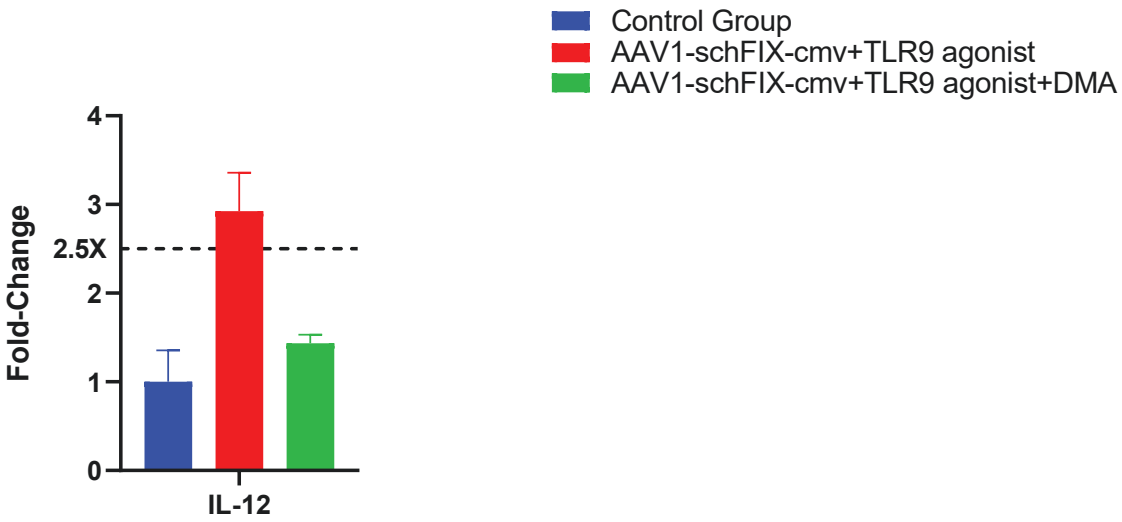

Figure 3.41 IL-12 expression of muscle sample in DMA treatment group at 2h.

Groups were assigned with different colors. Fold-changes are expressed relative to the control group. A threshold line at 2.5-fold highlights significant alterations. **T**he error bar represents standard error**.**

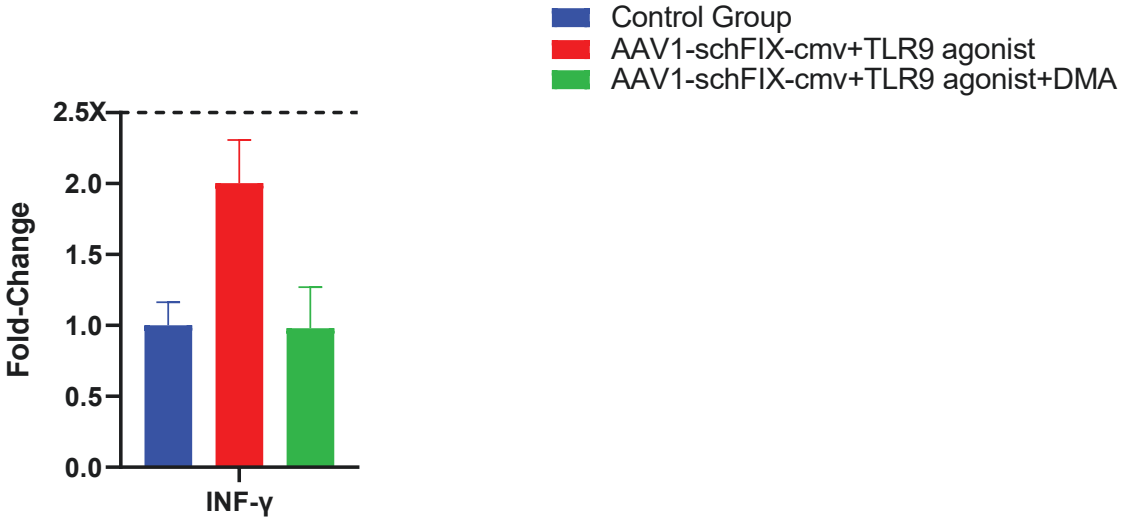

Figure 3.42 INF-γ expression of muscle sample in DMA treatment group at 2h.

Groups were assigned with different colors. Fold-changes are expressed relative to the control group. A threshold line at 2.5-fold highlights significant alterations. **T**he error bar represents standard error**.**

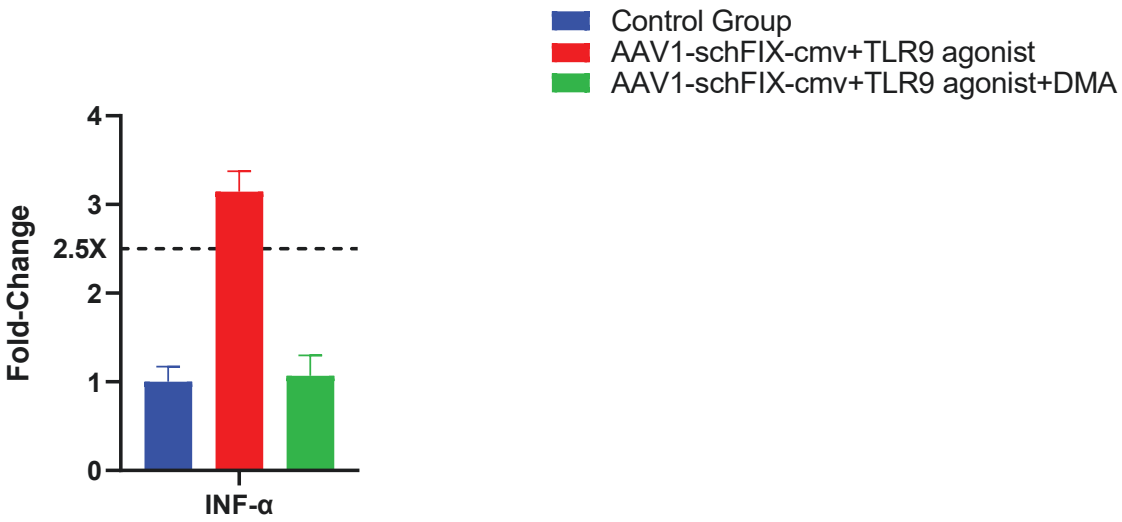

Figure 3.43 INF-α expression of muscle sample in DMA treatment group at 2h.

Groups were assigned with different colors. Fold-changes are expressed relative to the control group. A threshold line at 2.5-fold highlights significant alterations. **T**he error bar represents standard error**.**

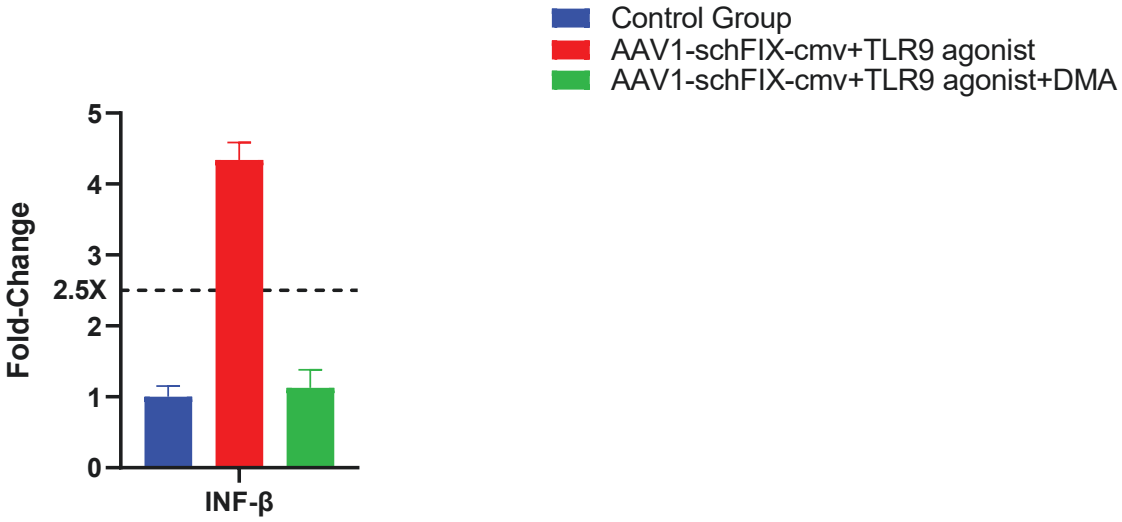

Figure 3.44 INF-β expression of muscle sample in DMA treatment group at 2h.

Groups were assigned with different colors. Fold-changes are expressed relative to the control group. A threshold line at 2.5-fold highlights significant alterations. **T**he error bar represents standard error**.**

3.5.2 Gene Expression Change in C57BL/6 Muscle Upon DMA Stimulation at 6h

Figure 3.4.2 displays the expressions of cytokines and interferons, with in-depth information on each provided in subsequent figures. A 2.5-fold increase threshold line is used to delineate significant changes, comparing all fold changes to the control group. At the 6-hour interval, it was observed that there were no substantial changes in the levels of any cytokines or interferons. Contrary to insulin, DMA did not exhibit additional suppressive effects on the levels of cytokines and interferons.

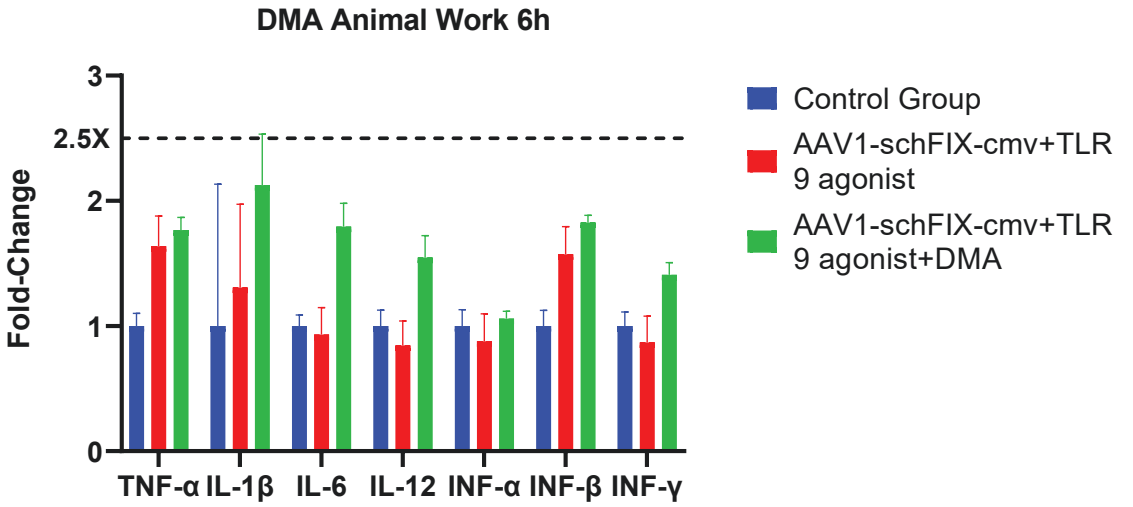

Figure 3.45 Gene expression change of muscle sample in DMA treatment group at 6h.

Overview of cytokines and interferons expression. Groups were assigned with different colors. Fold-changes are expressed relative to the control group. A threshold line at 2.5-fold highlights significant alterations. The error bar represents standard error.

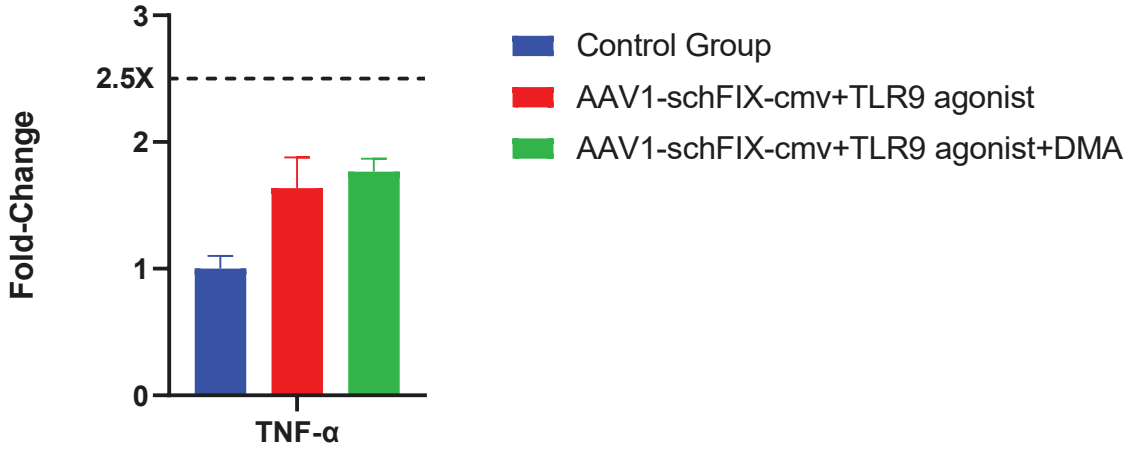

Figure 3.46 TNF-α expression of muscle sample in DMA treatment group at 6h.

Groups were assigned with different colors. Fold-changes are expressed relative to the control group. A threshold line at 2.5-fold highlights significant alterations. The error bar represents standard error.

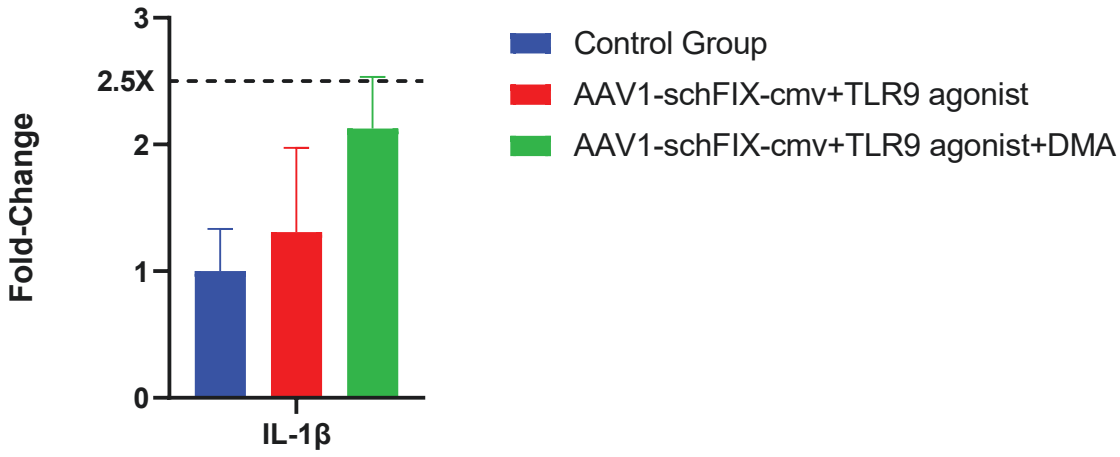

Figure 3.47 IL-1β expression of muscle sample in DMA treatment group at 6h.

Groups were assigned with different colors. Fold-changes are expressed relative to the control group. A threshold line at 2.5-fold highlights significant alterations. **T**he error bar represents standard error**.**

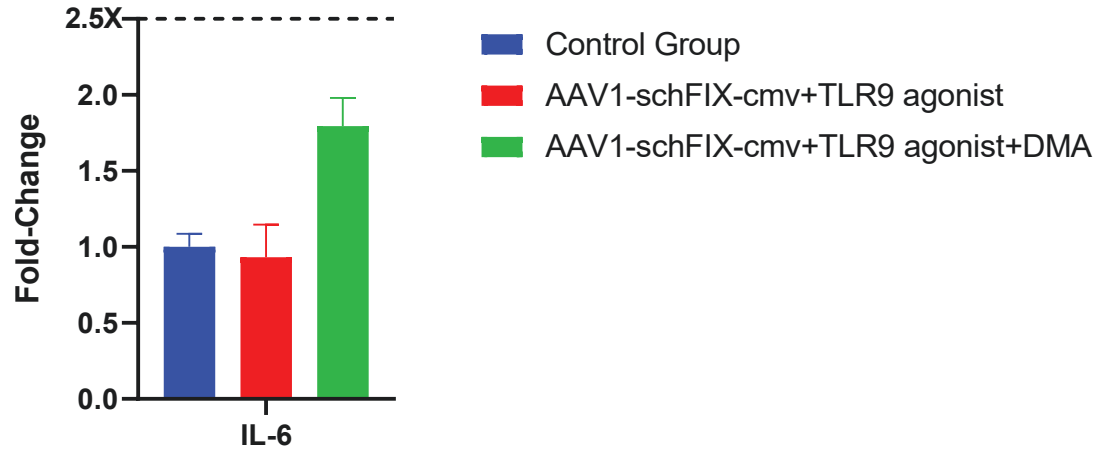

Figure 3.48 IL-6 expression of muscle sample in DMA treatment group at 6h.

Groups were assigned with different colors. Fold-changes are expressed relative to the control group. A threshold line at 2.5-fold highlights significant alterations. **T**he error bar represents standard error**.**

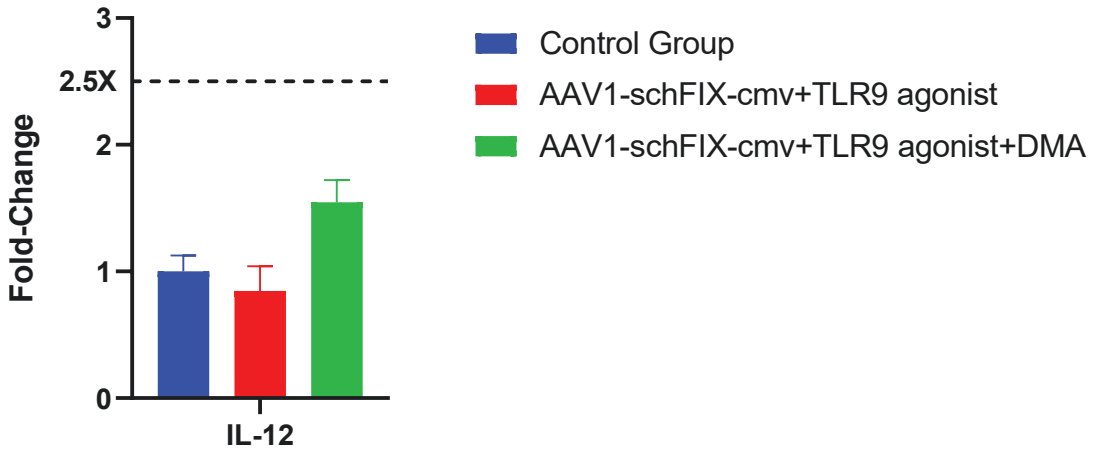

Figure 3.49 IL-12 expression of muscle sample in DMA treatment group at 6h.

Groups were assigned with different colors. Fold-changes are expressed relative to the control group. A threshold line at 2.5-fold highlights significant alterations. **T**he error bar represents standard error**.**

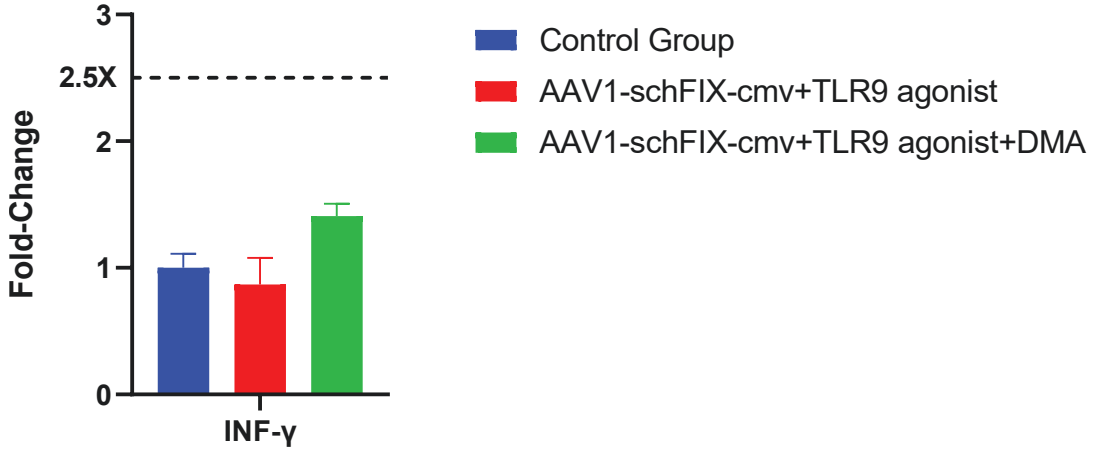

Figure 3.50 INF-γ expression of muscle sample in DMA treatment group at 6h.

Groups were assigned with different colors. Fold-changes are expressed relative to the control group. A threshold line at 2.5-fold highlights significant alterations. **T**he error bar represents standard error**.**

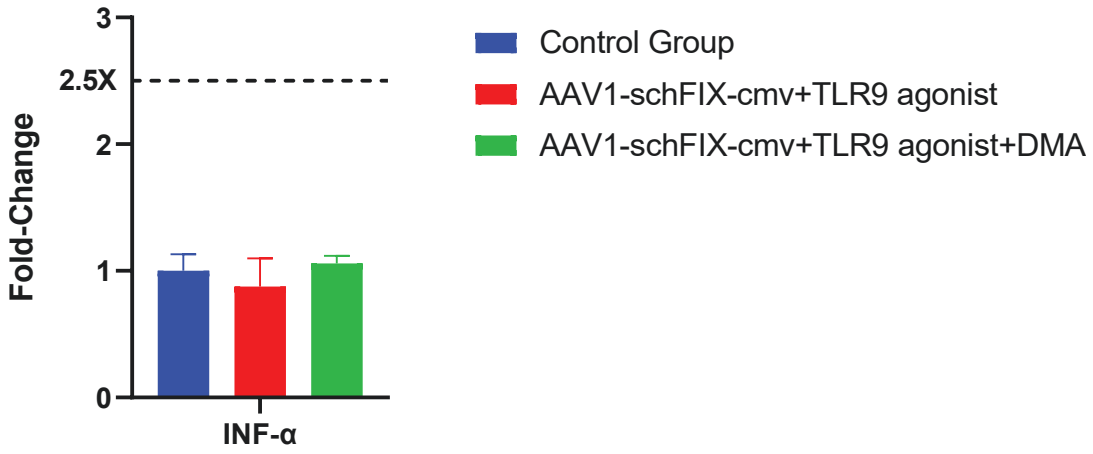

Figure 3.51 INF-α expression of muscle sample in DMA treatment group at 6h.

Groups were assigned with different colors. Fold-changes are expressed relative to the control group. A threshold line at 2.5-fold highlights significant alterations. **T**he error bar represents standard error**.**

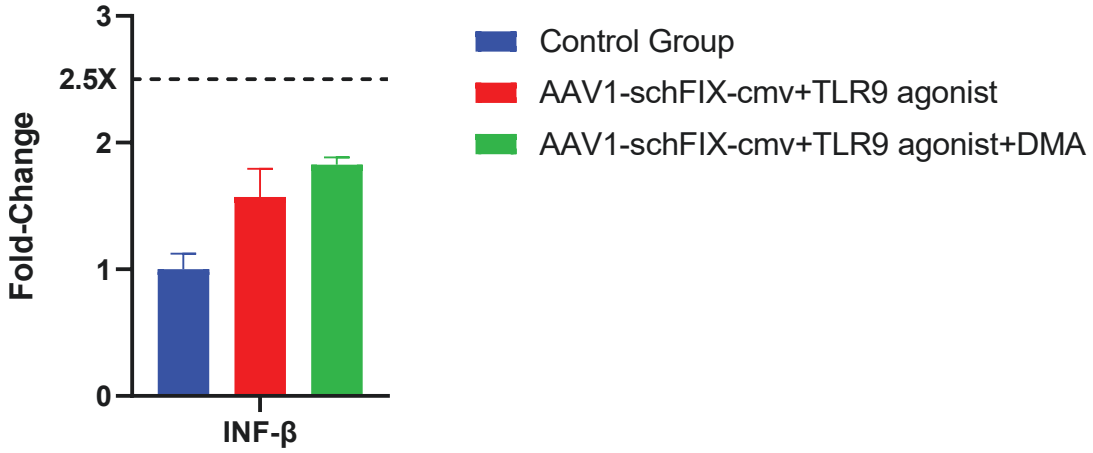

Figure 3.52 INF-β expression of muscle sample in DMA treatment group at 6h.

Groups were assigned with different colors. Fold-changes are expressed relative to the control group. A threshold line at 2.5-fold highlights significant alterations. **T**he error bar represents standard error**.**

3.6 Summary of Gene Expression in Animal Work

In both the insulin and DMA groups, IL-6 exhibited a markedly significant increase when treated with AAV and TLR9 agonists, with both DMA and insulin demonstrating their suppressive effects on IL-6 expression. Notably, IL-6 is an secreted cytokine, enabling the detection of its serum levels. While IL-12 showed significant changes in the insulin group, the DMA group did not exhibit similar alterations, possibly due to group-specific variations. Other cytokines and interferons either did not present a sufficient increase to be detectable in serum levels, or they are not excreted. Consequently, the serum level of IL-6 was chosen as the primary indicator for assessing the activation or inhibition of the innate immune response.

3.7 IL-6 Serum Level Change

The serum level of IL-6 was notably elevated 2 hours after stimulation with AAV and TLR9 agonists. In response, both the insulin and DMA treatment groups exhibited a reduction in IL-6 serum levels, albeit to varying extents. At the 6-hour mark, the IL-6 level in the group treated with AAV and TLR9 agonists alone did not demonstrate a significant change. However, the group treated with DMA displayed a statistically significant alteration, though the actual difference in values was relatively minor.

3.7.1 Insulin Treatment Group

The changes in IL-6 serum levels are depicted in the accompanying figure. At the 2-hour mark, there was a notable elevation in IL-6 serum levels within the group treated with AAV and TLR9 agonists. The insulin-treated group effectively suppressed this increase, bringing the levels in line with those of the control group. By the 6-hour point, the IL-6 serum levels had returned to baseline values.

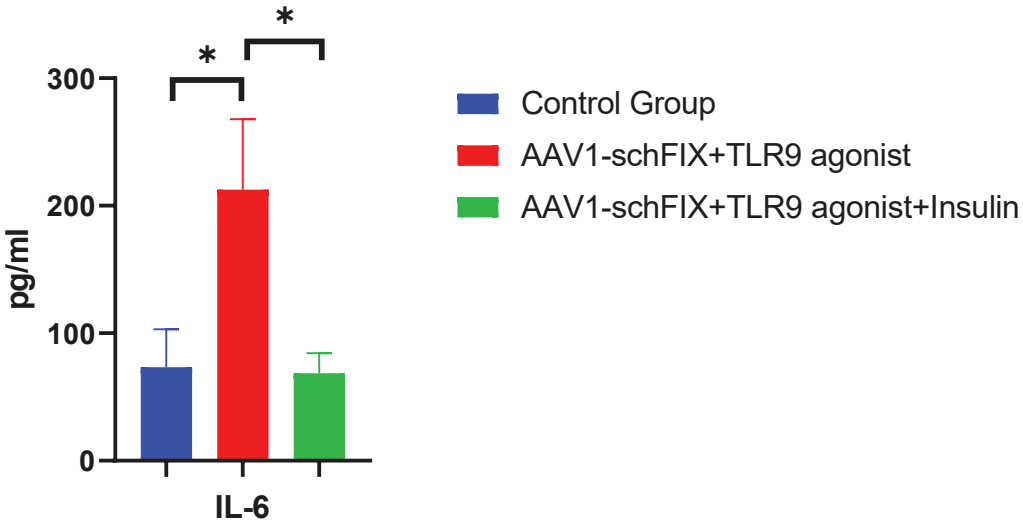

Figure 3.53 Serum IL-6 level of animal study insulin treatment group at 2h.

Groups were assigned with different colors. The error bar represents standard error. One way ANOVA was performed for statistically significant. * Indicated $p<0.05$.

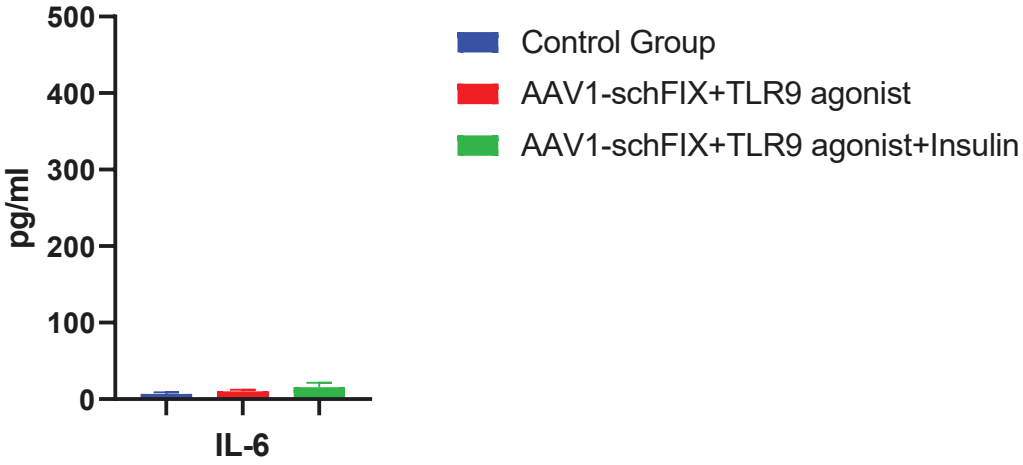

Figure 3.54 Serum IL-6 level of animal study insulin treatment group at 6h.

Groups were assigned with different colors. The error bar represents standard error. One way ANOVA was performed for statistically significant.

3.7.2 DMA treatment Group

The IL-6 serum level changes are illustrated in Figure 3.53 and Figure 3.54. Like the insulin groups, the IL-6 serum levels in the AAV and TLR9 agonist treatment group showed an increase at the 2-hour mark, which was notably blunted by DMA treatment. At the 6-hour interval, the DMA treatment group exhibited a significant increase from the control group, which needed additional investigation on the long-term DMA effect.

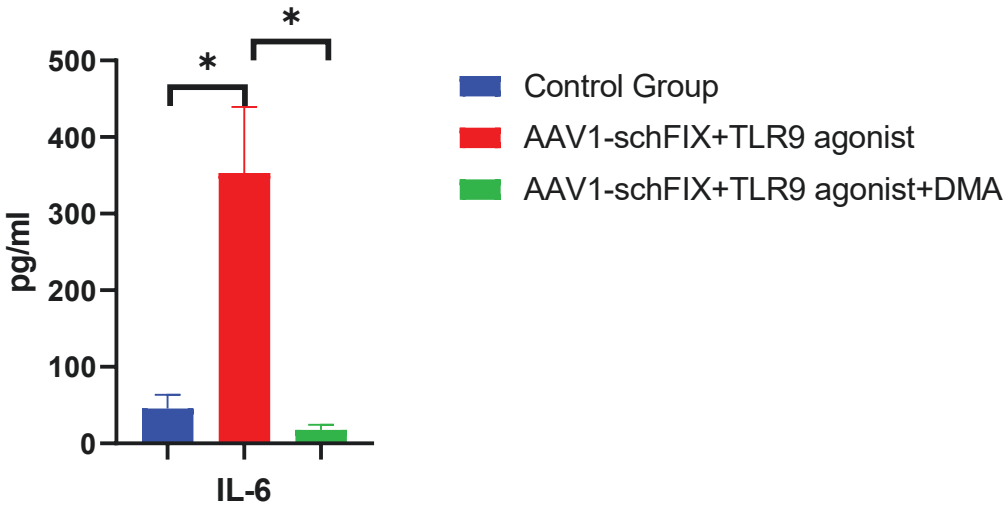

Figure 3.55 Serum IL-6 level of animal study DMA treatment group at 2h.

Groups were assigned with different colors. The error bar represents standard error. One way ANOVA was performed for statistically significant. * Indicated $p<0.05$.

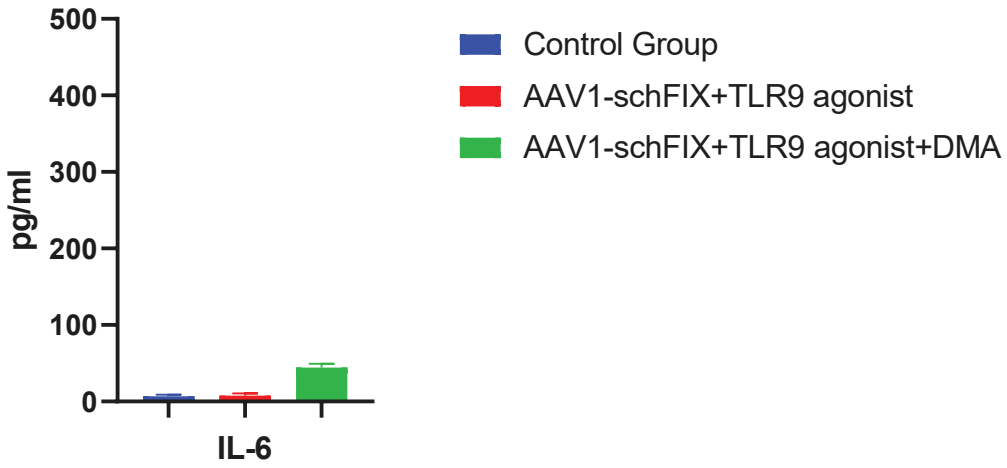

Figure 3.56 Serum IL-6 level of animal study DMA treatment group at 6h.

Groups were assigned with different colors. The error bar represents standard error. One way ANOVA was performed for statistically significant. ** Indicated $p<0.01$.

3.8 Immunohistochemistry

The immunohistochemistry results for the various groups were presented in Figures 3.55-3.66, corresponding to the insulin and DMA treatment groups, respectively. In each figure, Figure A was a 1:40 overview of tissue. B, C, D and E were 1:200 detail image. In these figures, the presence of M1/70 positive macrophages was indicated by brown-colored dots, while the nuclei were represented by blue or black dots. Notably, brown dots were observed only in the positive control groups and the group treated with AAV and TLR9 agonists. In contrast, the groups treated with DMA and insulin did not exhibit any brown dots. This absence suggested that both insulin and DMA might have effectively inhibited or delayed the recruitment of macrophages.

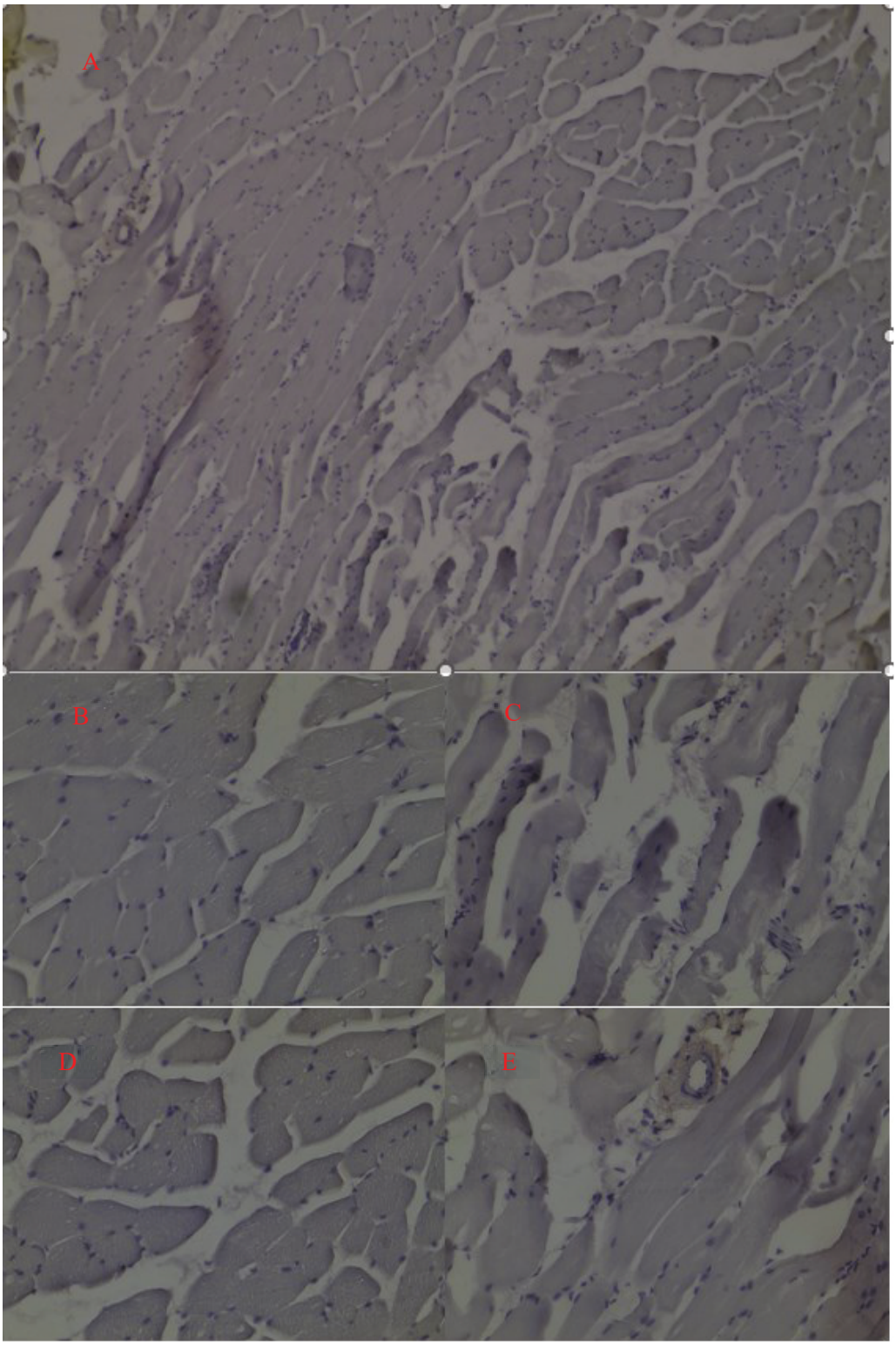

Figure 3.57 Immunohistochemistry staining of control group at 2h for insulin treatment groups.

A) Tissue at 10X. B) C) D) E) Different location on tissue at 40X.

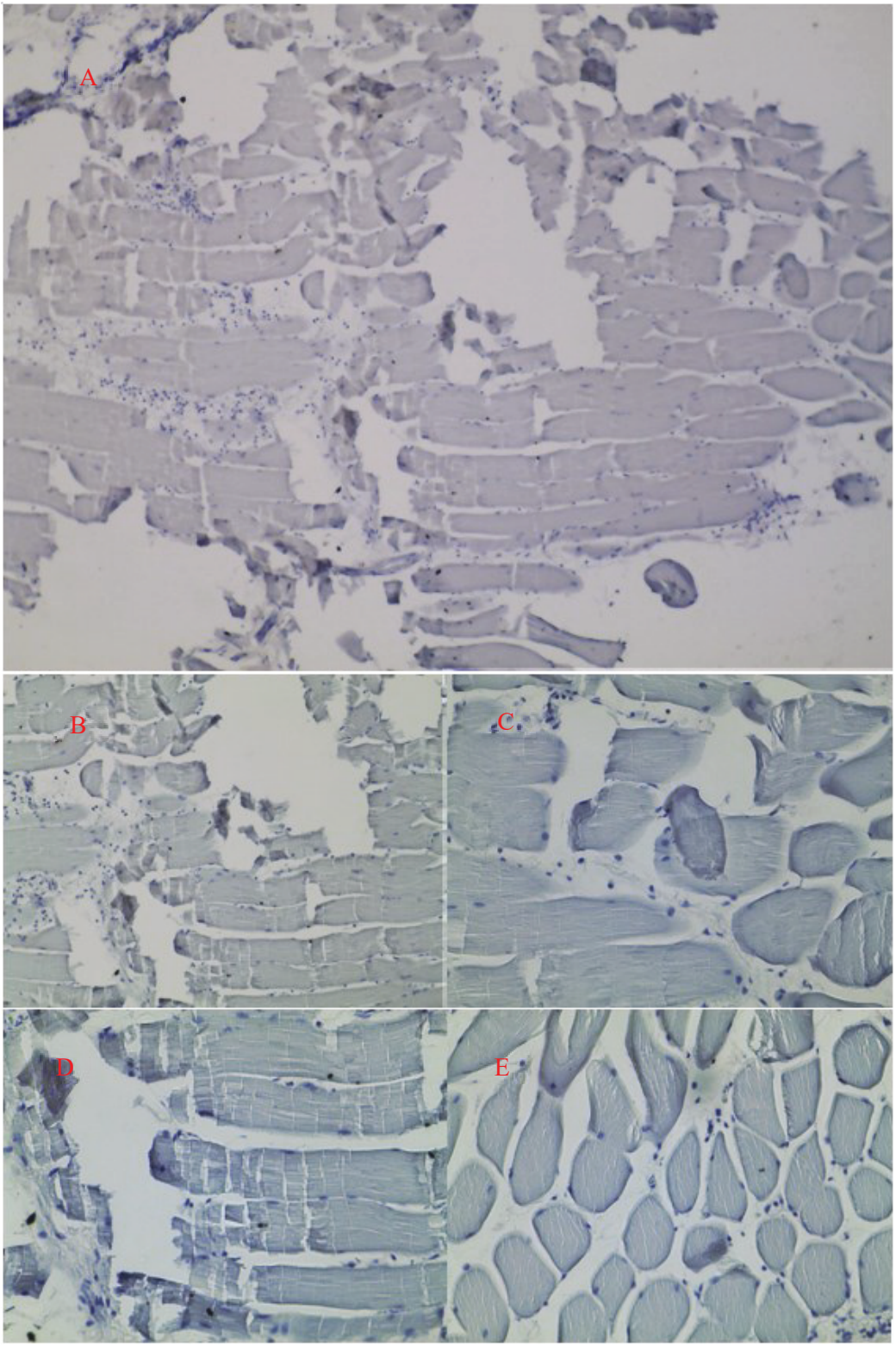

Figure 3.58 Immunohistochemistry staining of AAV1, TLR9 agonist group at 2h.

A) Tissue at 10X. B) C) D) E) Different location on tissue at 40X.

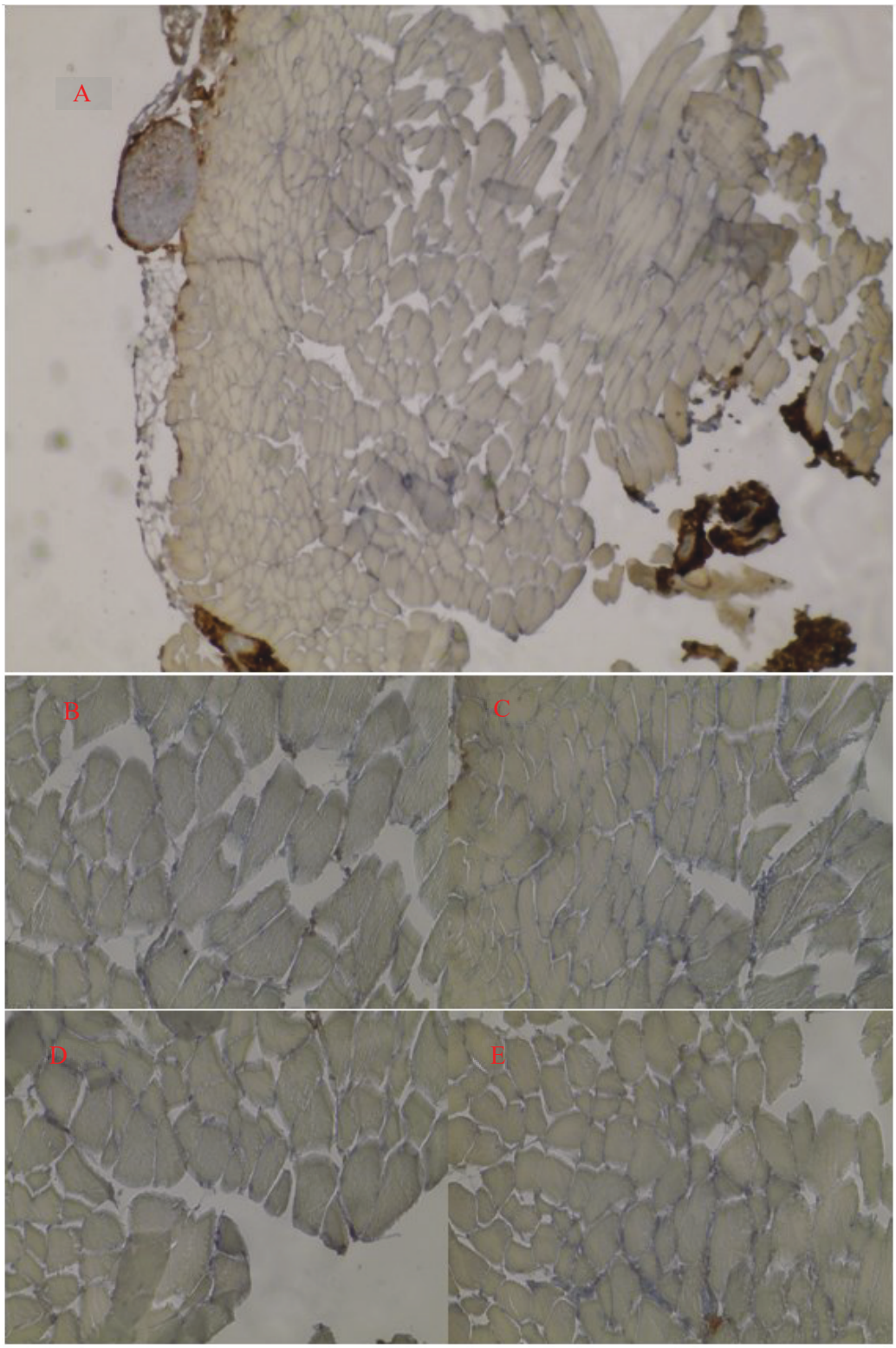

Figure 3.59 Immunohistochemistry staining of AAV1, TLR9 agonist and insulin group at 2h.

A) Tissue at 10X. B) C) D) E) Different location on tissue at 40X.

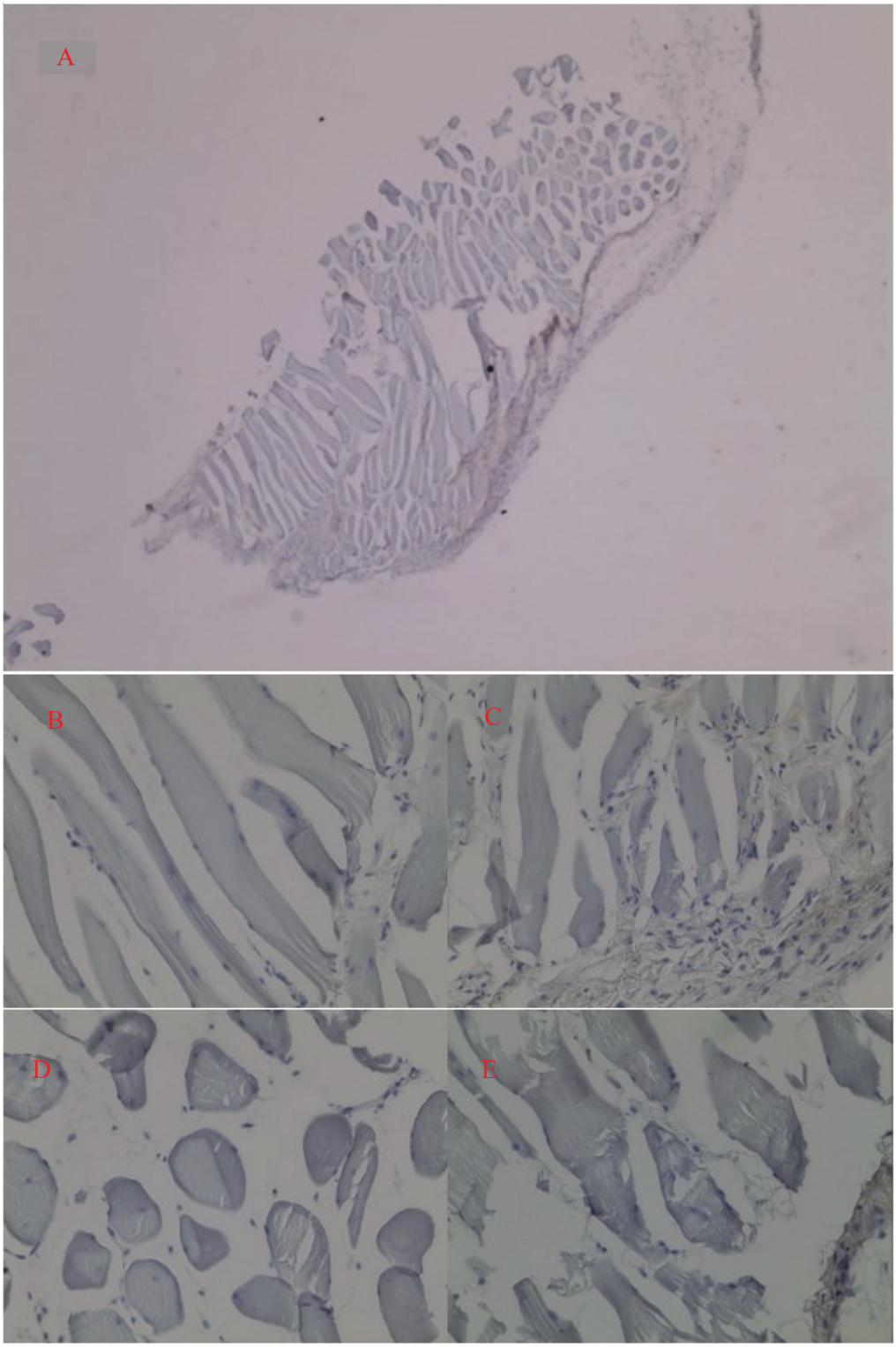

Figure 3.60 Immunohistochemistry staining of control group at 2h for DMA treatment.

A) Tissue at 10X. B) C) D) E) Different location on tissue at 40X.

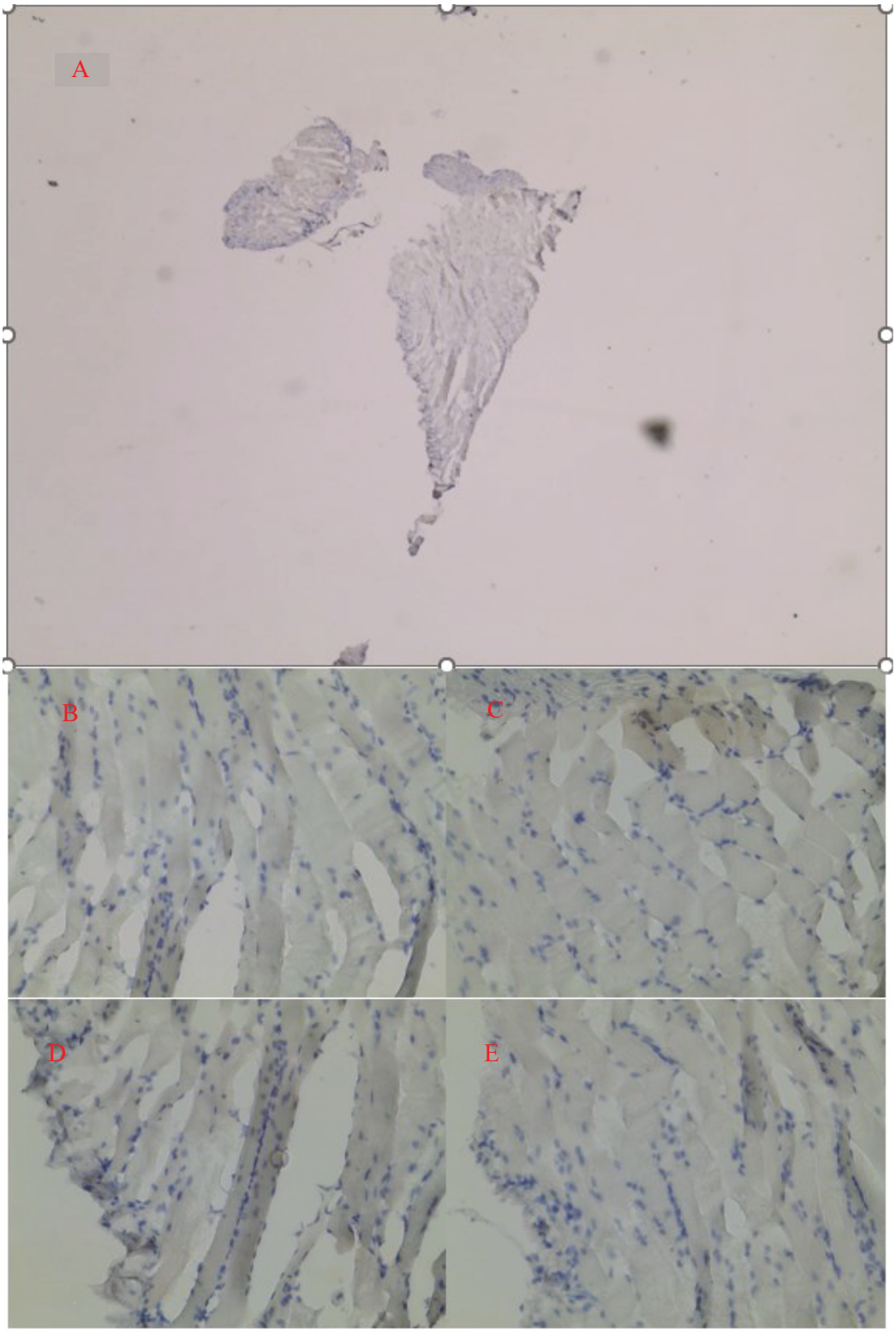

Figure 3.61 Immunohistochemistry staining of AAV1, TLR9 agonist group for DMA treatment at 2h.

A) Tissue at 10X. B) C) D) E) Different location on tissue at 40X**.**

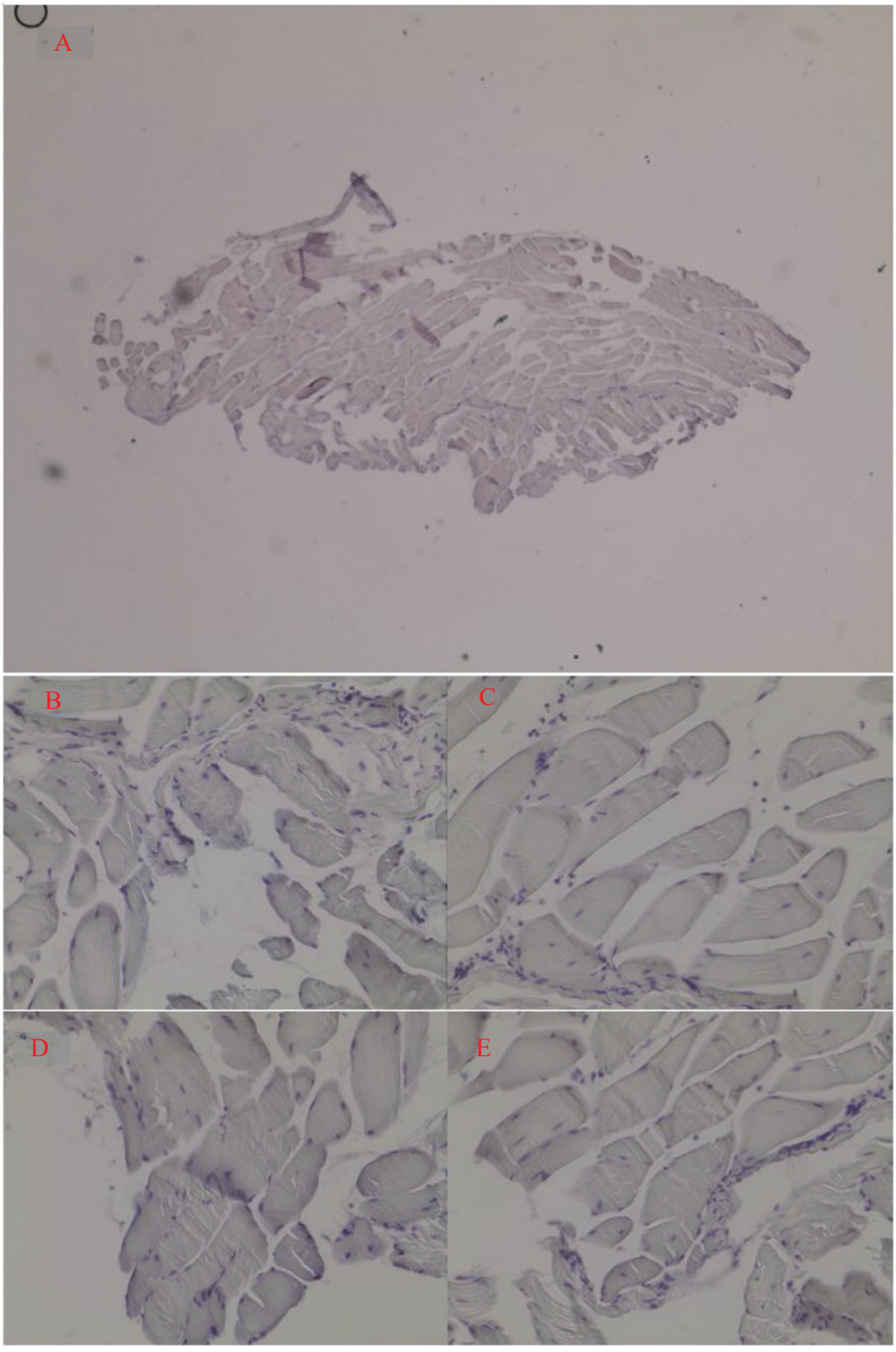

Figure 3.62 Immunohistochemistry staining of AAV1, TLR9 agonist and DMA group at 2h.

A) Tissue at 10X. B) C) D) E) Different location on tissue at 40X.

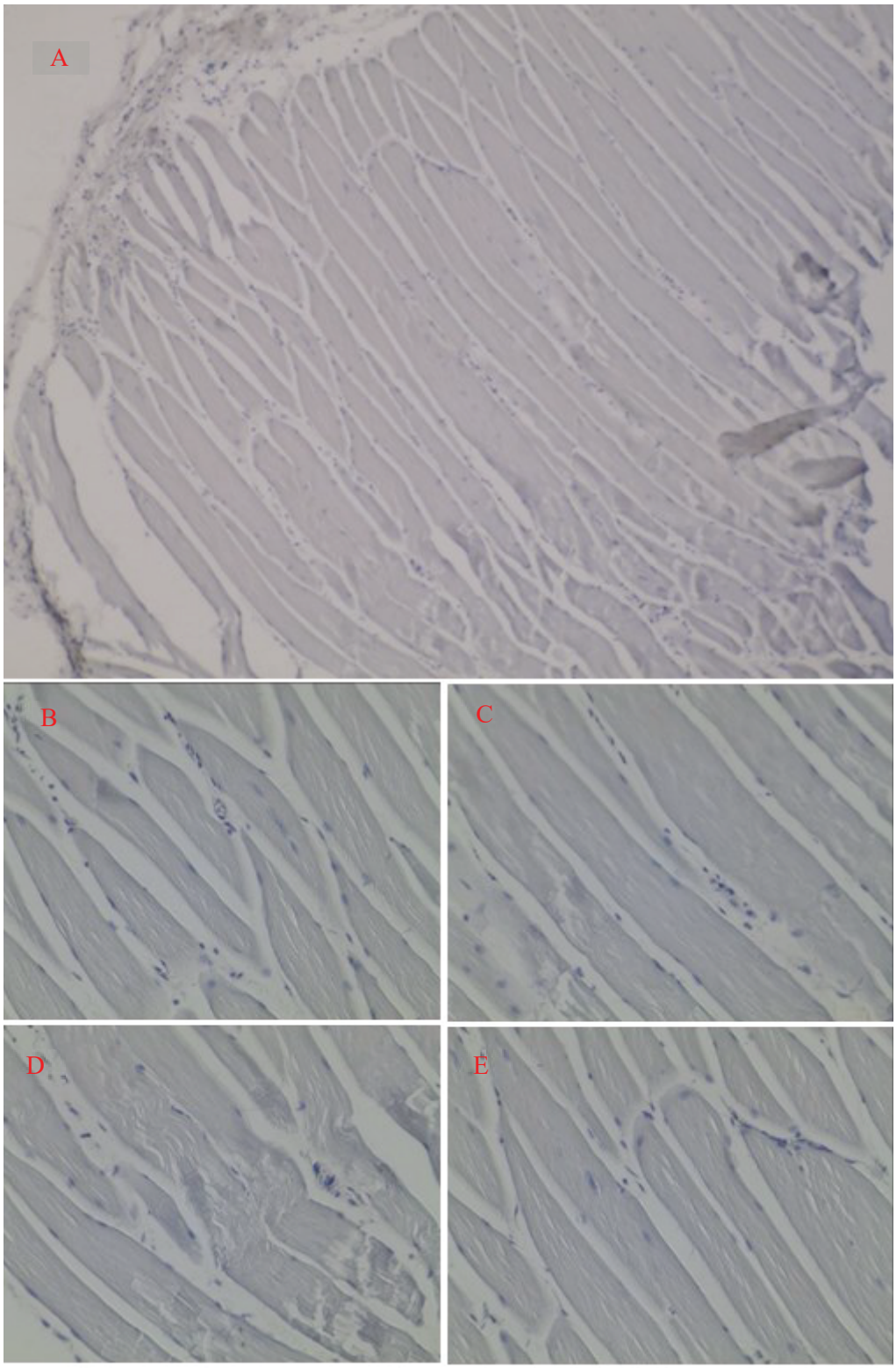

Figure 3.63 Immunohistochemistry staining of control group for insulin treatment at 6h.

A) Tissue at 10X. B) C) D) E) Different location on tissue at 40X.

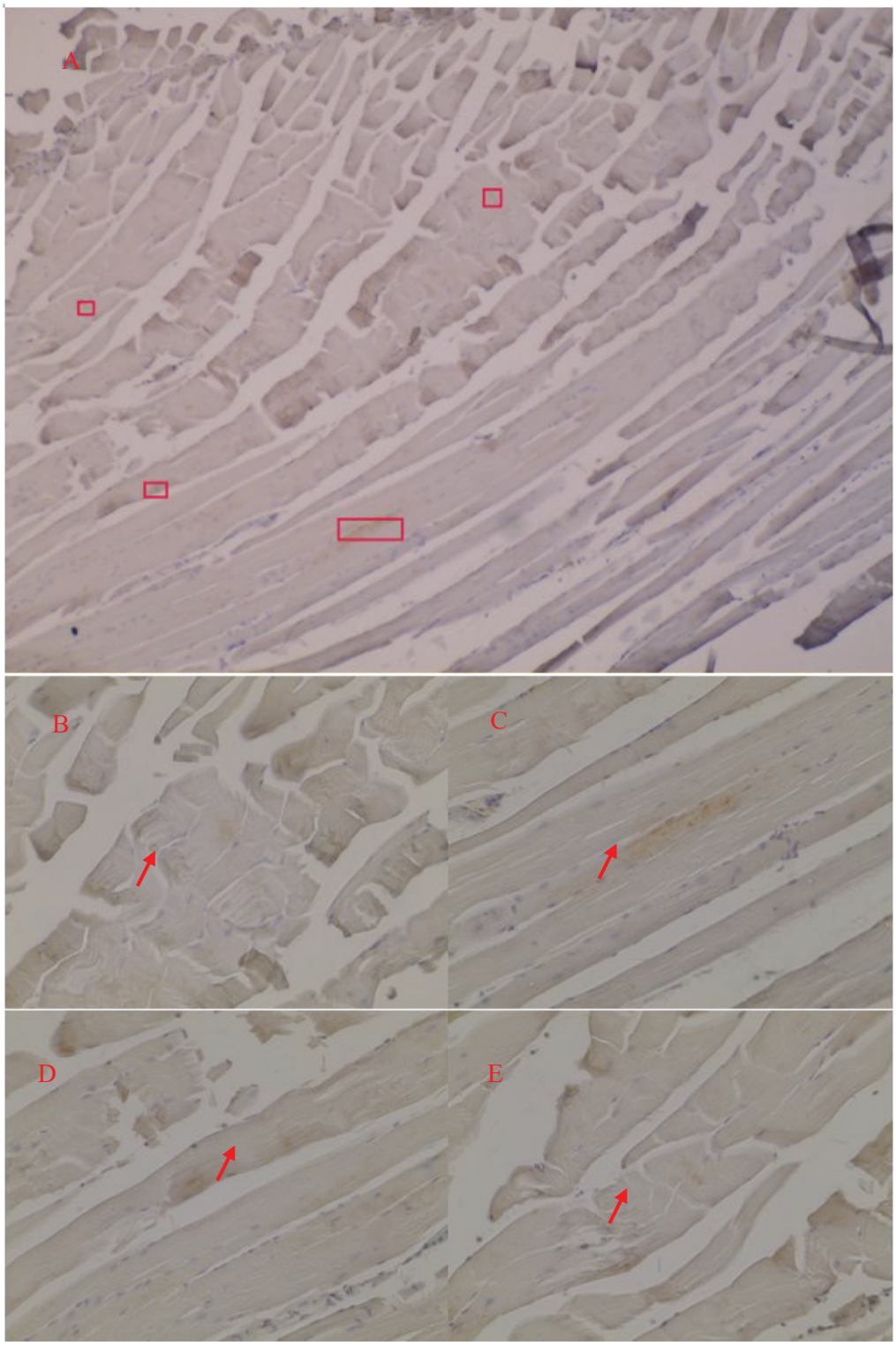

Figure 3.64 Immunohistochemistry staining of AAV1 and TLR9 agonist group for insulin treatment at 6h.

A) Tissue at 10X. Red block indicated B) C) D) E) location at 10X. B) C) D) E) Different location on tissue at 40X.

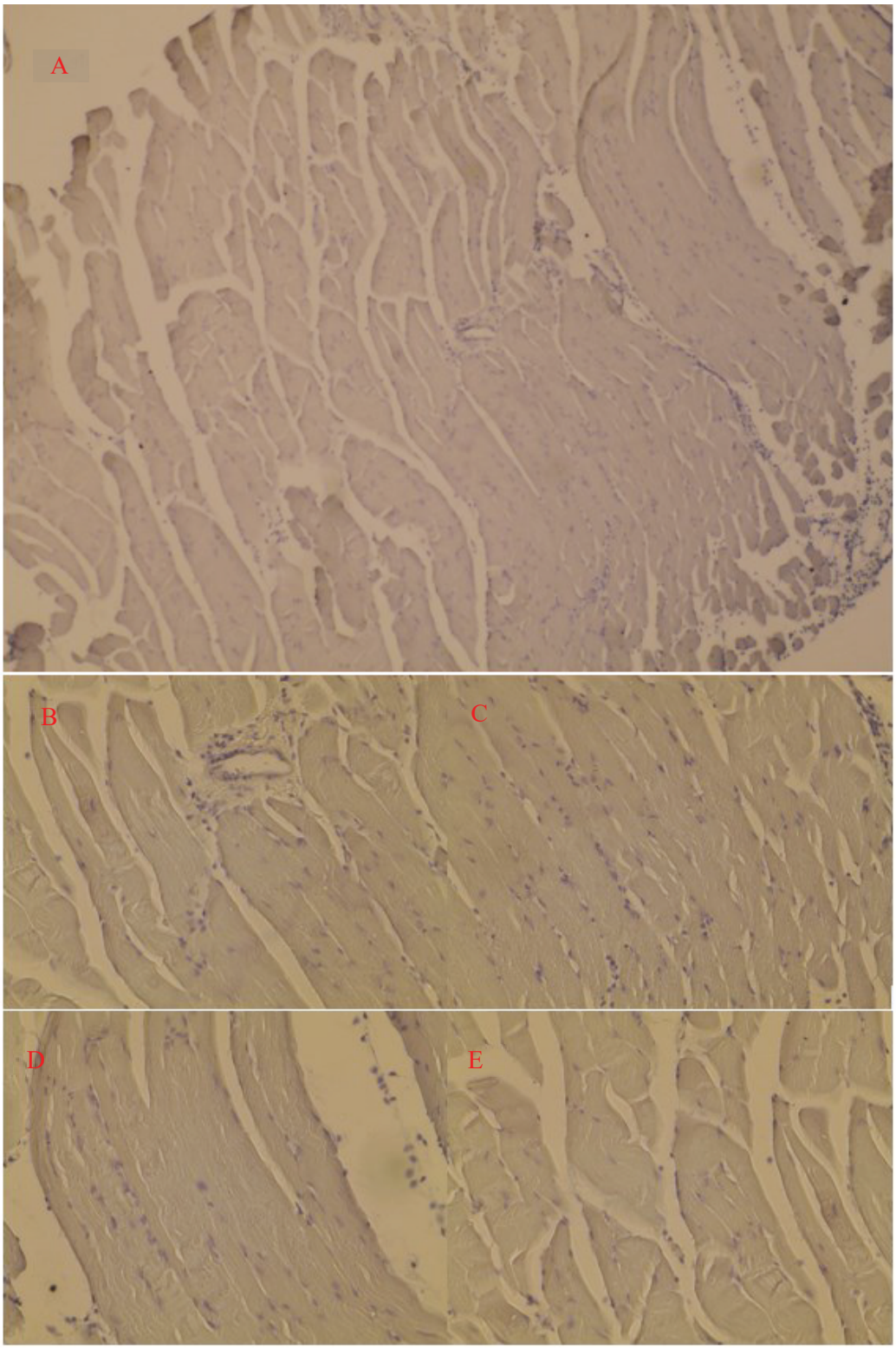

Figure 3.65 Immunohistochemistry staining of AAV1 TLR9 agonist and insulin group at 6h.

A) Tissue at 10X. B) C) D) E) Different location on tissue at 40X.

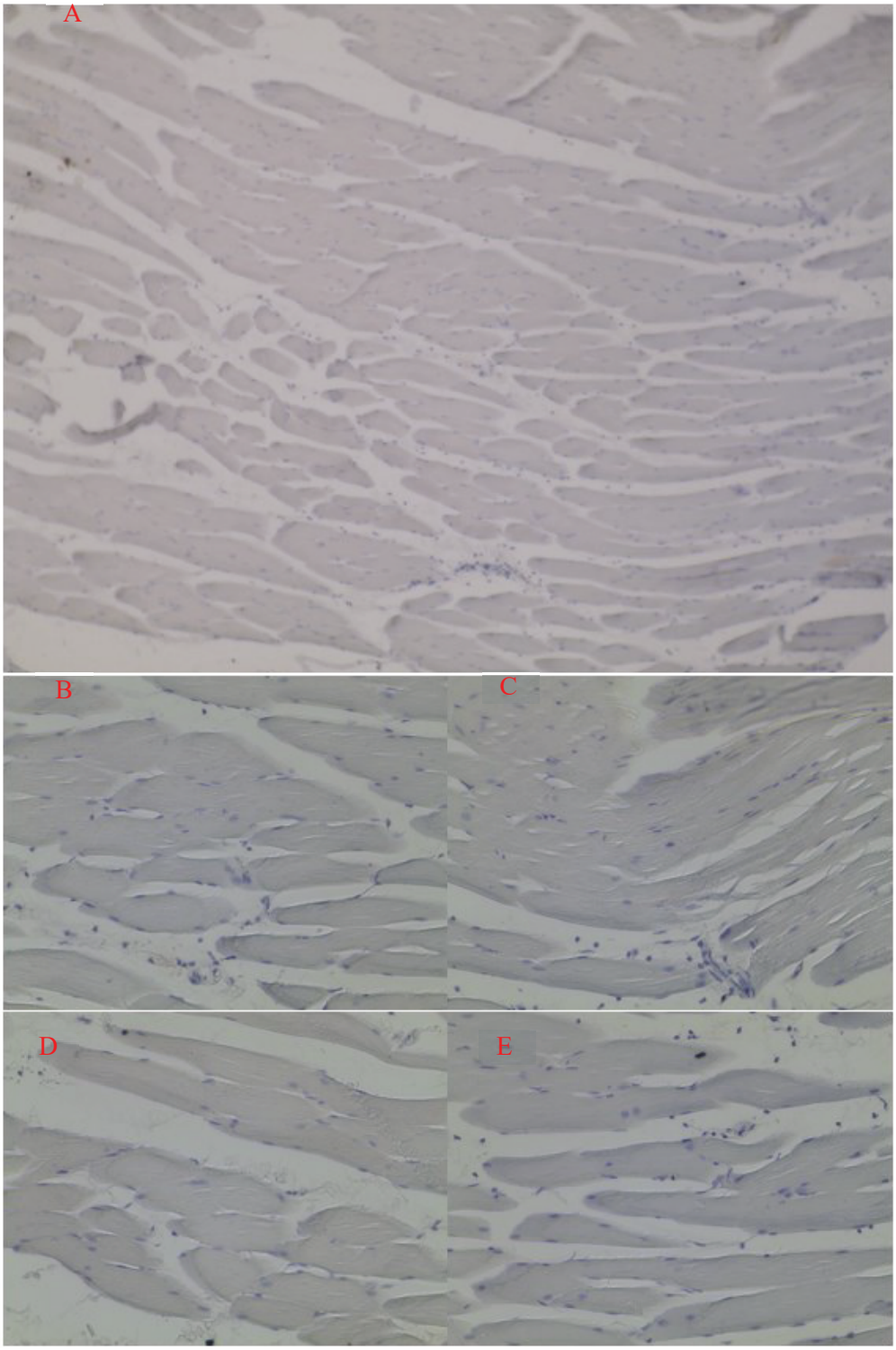

Figure 3.66 Immunohistochemistry staining of control group for DMA treatment at 6h.

A) Tissue at 10X. B) C) D) E) Different location on tissue at 40X.

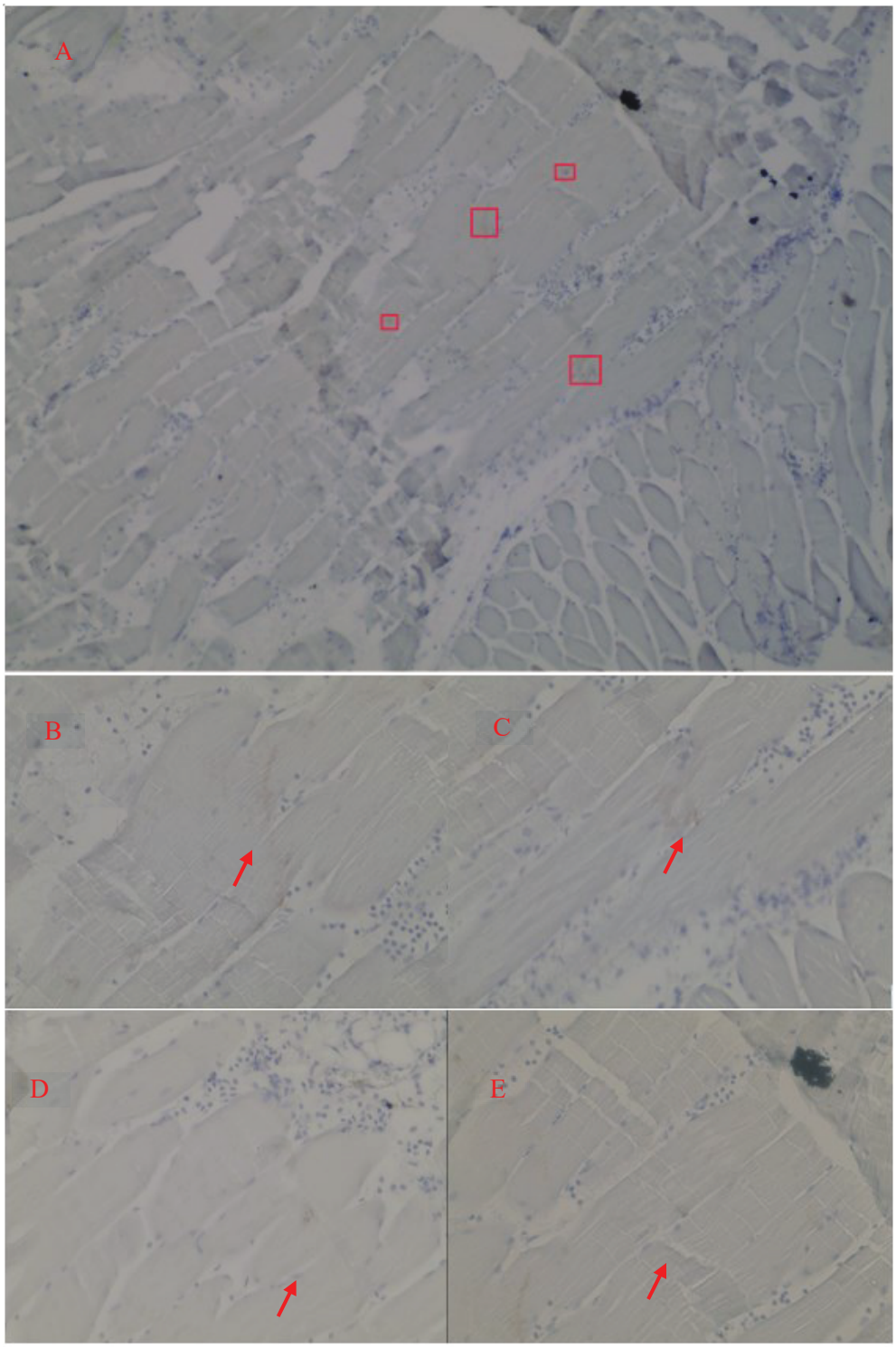

Figure 3.67 Immunohistochemistry staining of AAV1 and TLR9 agonist group for DMA treatment at 6h.

A) Tissue at 10X. Red block indicated B) C) D) E) location at 10X. B) C) D) E) Different location on tissue at 40X.

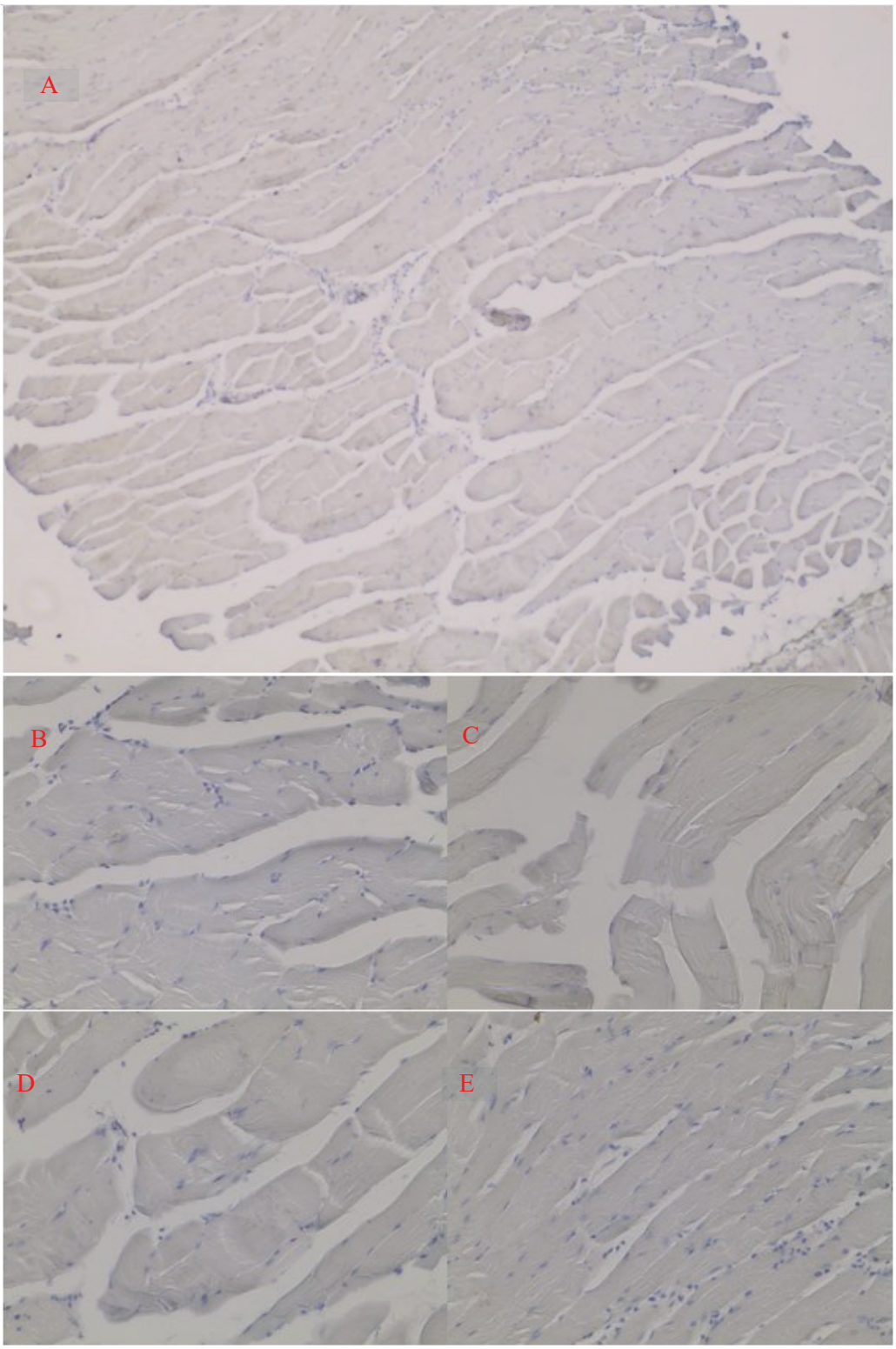

Figure 3.68 Immunohistochemistry staining of AAV1, TLR9 agonist and DMA group at 6h.

A) Tissue at 10X. B) C) D) E) Different location on tissue at 40X.

CHAPTER 4 DISCUSSIONS

4.1 Summary

Adeno-Associated Virus (AAV) is extensively utilized in various clinical trials and approved gene therapies.(Srivastava, 2023) Despite its widespread use, the immune response to AAV vectors remains a significant limitation. Extensive research has been conducted to mitigate adaptive immune challenges, such as pre-existing antibodies and inhibiting the adaptive immune response.(Calcedo et al., 2015) Our study, however, focused on the innate immune response elicited by AAV, exploring the modulatory effects of insulin and DMA.

We initially investigated the effects in vitro by employing a transwell-insert to co-culture normal and immune cells, simulating the innate immune response in vivo. Insulin and DMA demonstrated their capacity to attenuate the elevation in cytokine and interferon expression triggered by AAV. However, as the cell lines used were immortalized, their behavior and characteristics differed somewhat from typical cells.(Pan et al., 2009) Notably, unexpected results emerged in the co-culture group without stimulation. Following these in vitro studies, we progressed to in vivo experiments using C57BL/6 mice to validate the efficacy of insulin and DMA. At the 2-hour mark, both the IL-6 expression level and serum level showed significant increases in the AAV and TLR9 treatment group. In contrast, these increases were mitigated in the groups treated with DMA and insulin. By the 6-hour point, there were no significant changes in the expression or serum levels of cytokines and interferons. Additionally, we conducted immunohistochemical analysis on the muscle tissue at the injection site. In the group treated with AAV and TLR9 agonists at

6 hours, we observed recruitment of M1/70 positive macrophages. This recruitment was not evident in the DMA and insulin treatment groups.

4.2 Innate Immune Response Related Gene Expression against AAV *in vitro*

In our study, we employed a transwell system to co-culture liver and macrophage cell lines, aiming to simulate the immune system. However, this model was a simplified representation, lacking the full complexity of the immune response. The immune reaction to AAV infection involves various cell types beyond macrophages. For instance, natural killer cells, a key component of the innate immune system, can rapidly identify and eliminate virus-infected cells even before the activation of the adaptive immune system.(V. C. Lam & Lanier, 2017) Additionally, dendritic cells play a crucial role, migrating to lymph nodes to present antigens to T cells, thereby initiating the adaptive immune response.(Nikolic et al., 2011) Our research focused solely on the expression profile of macrophages, representing only a fraction of the innate immune cells.

Furthermore, the intercellular communication within the transwell setup remained unexplored. This interaction likely depended on precursor cytokines, challenging to detect due to the limited cell growth in the wells.

Another critical aspect to consider is that the cells used in our research were immortalized, essentially cancer cells. While these cells retain many characteristics of their original form, they may undergo unexpected genetic changes. Such variations could result in responses that differ from those of primary cells. Our study observed the most significant increase in the co-culture without stimulation compared to the control group, possibly came from differences between PMA-induced macrophages and primary macrophages.

Despite these limitations, our research provides a preliminary model that offers partial insight into the innate immune response *in vitro*. This model could be valuable for researching the immune response to AAV.

4.3 Innate Immune Response Related Response Against AAV *in vivo*

In our study, following in vitro experiments, we conducted in vivo research using C57BL/6 mice. We analyzed gene expression in muscle samples post-injection. IL-6, a marker of the acute phase response, upregulated following stimulation with AAV and TLR9 agonists, which was subsequently downregulated by DMA and insulin. Corresponding serum levels mirrored this pattern. Our findings suggest that insulin and DMA could be potential inhibitors of innate immunity, but some limitations should be acknowledged.

High Dosage of Insulin: The insulin dosage administered was above the safety threshold for mice. Throughout the study, we meticulously monitored the mice's blood glucose levels to prevent hypoglycemia. This high dosage poses limitations for application in primate models.

AAV's Immunogenicity in Mice: AAV alone does not elicit a strong immune response in mice. To amplify the immune response, we co-administered a TLR9 agonist with AAV. However, the immune response induced by this co-administration might differ from the innate immune response observed in humans.

Individual Variability in Gene Expression and Serum Levels: The gene expression and serum level profiles were generated from different individual animals. A more

convincing approach would be to establish a method for continuous real-time monitoring of gene expression and serum levels in a single mouse.

Overall, our research successfully demonstrated the suppressive effects of insulin and DMA on the innate immune response to AAV in vivo. However, the study's limitations highlight the need for further research to fully understand these dynamics and their implications for human applications.

4.4 Future Directions

Our study highlights the inhibitory effects of DMA and insulin on the innate immune response to Adeno-Associated Virus (AAV). While insulin's ability to enhance AAV transduction in both in vitro and in vivo settings is well-documented, the influence of DMA on AAV transduction remains largely uncharted territory. Notably, DMA, as a small molecule with a wide therapeutic range, presents a more feasible option for application compared to insulin.

In our in vitro studies, we employed a transwell co-culture system. The intercellular communication within this system was not fully investigated. A deeper analysis and understanding of this communication could significantly enhance our comprehension of the innate immune response triggered by AAV. Additionally, incorporating primary cells into these studies could provide a more accurate simulation of the in vivo immune system.

In our animal research, we observed that serum IL-6 levels returned to normal within 6 hours. Establishing a detailed curve to track the decline of IL-6 could offer greater insight into the mechanisms underlying the effects of DMA and insulin.

In clinical trials and gene therapy applications, a major challenge frequently encountered is the presence of pre-existing adaptive immunity, which frequently leads to the failure of AAV-based gene therapies. Our findings suggest that it's possible to mitigate the innate immune response to AAV. The future direction of this research could involve prolonging the duration of animal studies to assess whether the dampening effects of DMA or insulin on the innate immune response could subsequently reduce the activation of the adaptive immune system. This could be a pivotal step in enhancing the success rate of AAV gene therapies.

REFERENCES

Danaeifar, M. (2022). Recent advances in gene therapy: Genetic bullets to the root of the problem. *Clinical and Experimental Medicine*, *23*(4), 1107–1121. https://doi.org/10.1007/s10238-022-00925-x

Fischer, A., Asaad, W., Volos, P., Maksimov, D., Khavina, E., Deviatkin, A., Mityaeva, O., & Volchkov, P. (2023). AAV genome modification for efficient AAV production. *Heliyon*, *9*(4), e15071. https://doi.org/10.1016/j.heliyon.2023.e15071

B Koya, J., Shen, T., Lu, G., Gauthier, A., Mantell, L., R Ashby Jr, C., & E. Reznik, S. (2022). FDA-Approved Excipient N, N-Dimethylacetamide Attenuates Inflammatory Bowel Disease in In Vitro and In Vivo Models. *Fortune Journal of Health Sciences*, *05*(03). https://doi.org/10.26502/fjhs.076

Blanc, F., Bemelmans, A.-P., Affortit, C., Joséphine, C., Puel, J.-L., Mondain, M., & Wang, J. (2022). A Single Cisterna Magna Injection of AAV Leads to Binaural Transduction in Mice. *Frontiers in Cell and Developmental Biology*, *9*, 783504. https://doi.org/10.3389/fcell.2021.783504

Boutin, S., Monteilhet, V., Veron, P., Leborgne, C., Benveniste, O., Montus, M. F., & Masurier, C. (2010). Prevalence of Serum IgG and Neutralizing Factors Against Adeno-Associated Virus (AAV) Types 1, 2, 5, 6, 8, and 9 in the Healthy

Population: Implications for Gene Therapy Using AAV Vectors. *Human Gene Therapy*, *21*(6), 704–712. https://doi.org/10.1089/hum.2009.182

Calcedo, R., Franco, J., Qin, Q., Richardson, D. W., Mason, J. B., Boyd, S., & Wilson, J. M. (2015). Preexisting Neutralizing Antibodies to Adeno-Associated Virus Capsids in Large Animals Other Than Monkeys May Confound *In Vivo* Gene Therapy Studies. *Human Gene Therapy Methods*, *26*(3), 103–105. https://doi.org/10.1089/hgtb.2015.082

Carrig, S., Bijjiga, E., Wopat, M. J., & Martino, A. T. (2016). Insulin Therapy Improves Adeno-Associated Virus Transduction of Liver and Skeletal Muscle in Mice and Cultured Cells. *Human Gene Therapy*, *27*(11), 892–905. https://doi.org/10.1089/hum.2016.073

Carter, B. J. (2004). Adeno-associated virus and the development of adeno-associated virus vectors: A historical perspective. *Molecular Therapy*, *10*(6), 981–989. https://doi.org/10.1016/j.ymthe.2004.09.011

Chen, Z., Wang, W., Zhang, Y., Xue, X., & Hua, Y. (2023). Identification of four-gene signature to diagnose osteoarthritis through bioinformatics and machine learning methods. *Cytokine*, *169*, 156300. https://doi.org/10.1016/j.cyto.2023.156300

Dai, Y., Dong, H., Gleason, C., Mora, J., Kolaitis, G., Balasubramanian, N., Surapaneni, S., Kozhich, A., & Jawa, V. (2023). Comparison of Pre-existing Anti-AAV8 Total Antibody Screening and Confirmatory Assays with a Cell-Based Neutralizing

Assay in Normal Human Serum. *The AAPS Journal*, *25*(3), 35. https://doi.org/10.1208/s12248-023-00805-6

Dias, M. F., Joo, K., Kemp, J. A., Fialho, S. L., Da Silva Cunha, A., Woo, S. J., & Kwon, Y. J. (2018). Molecular genetics and emerging therapies for retinitis pigmentosa: Basic research and clinical perspectives. *Progress in Retinal and Eye Research*, *63*, 107–131. https://doi.org/10.1016/j.preteyeres.2017.10.004

Dougherty, J. A., & Dougherty, K. M. (2023). Valoctocogene Roxaparvovec and Etranacogene Dezaparavovec: Novel Gene Therapies for Hemophilia A and B. *Annals of Pharmacotherapy*, 10600280231202247. https://doi.org/10.1177/10600280231202247

Fischer, A., Hacein-Bey, S., & Cavazzana-Calvo, M. (2002). Gene therapy of severe combined immunodeficiencies. *Nature Reviews Immunology*, *2*(8), 615–621. https://doi.org/10.1038/nri859

Frew, J. W., Hawkes, J. E., & Krueger, J. G. (2018). A systematic review and critical evaluation of inflammatory cytokine associations in hidradenitis suppurativa. *F1000Research*, *7*, 1930. https://doi.org/10.12688/f1000research.17267.1

Gardin, A., & Ronzitti, G. (2023). Current limitations of gene therapy for rare pediatric diseases: Lessons learned from clinical experience with AAV vectors. *Archives de Pédiatrie*, *30*(8), 8S46-8S52. https://doi.org/10.1016/S0929-693X(23)00227-0

Gorasiya, S., Mushi, J., Pekson, R., Yoganathan, S., & Reznik, S. E. (2018). Repurposing N,N-Dimethylacetamide (DMA), a Pharmaceutical Excipient, as a Prototype

Novel Anti-inflammatory Agent for the Prevention and/or Treatment of Preterm Birth. *Current Pharmaceutical Design*, *24*(9), 989–992. https://doi.org/10.2174/1381612824666180130121706

Hadi, M., Qutaiba B. Allela, O., Jabari, M., Jasoor, A. M., Naderloo, O., Yasamineh, S., Gholizadeh, O., & Kalantari, L. (2024). Recent advances in various adeno-associated viruses (AAVs) as gene therapy agents in hepatocellular carcinoma. *Virology Journal*, *21*(1), 17. https://doi.org/10.1186/s12985-024-02286-1

Han, J. M., Patterson, S. J., Speck, M., Ehses, J. A., & Levings, M. K. (2014). Insulin Inhibits IL-10–Mediated Regulatory T Cell Function: Implications for Obesity. *The Journal of Immunology*, *192*(2), 623–629. https://doi.org/10.4049/jimmunol.1302181

Hermonat, P. L., & Muzyczka, N. (1984). Use of adeno-associated virus as a mammalian DNA cloning vector: Transduction of neomycin resistance into mammalian tissue culture cells. *Proceedings of the National Academy of Sciences*, *81*(20), 6466–6470. https://doi.org/10.1073/pnas.81.20.6466

Hoggan, M. D., Blacklow, N. R., & Rowe, W. P. (1966). Studies of small DNA viruses found in various adenovirus preparations: Physical, biological, and immunological characteristics. *Proceedings of the National Academy of Sciences*, *55*(6), 1467–1474. https://doi.org/10.1073/pnas.55.6.1467

Ji, X., Meng, W., Liu, Z., & Mu, X. (2022). Emerging Roles of lncRNAs Regulating RNA-Mediated Type-I Interferon Signaling Pathway. *Frontiers in Immunology*, *13*, 811122. https://doi.org/10.3389/fimmu.2022.811122

Jiang, F., Zhang, C., Liu, W., Liu, F., Huang, H., Tan, Y., & Qin, B. (2023). Bibliometric analysis of global research trends in adeno-associated virus vector for gene therapy (1991-2022). *Frontiers in Cellular and Infection Microbiology*, *13*, 1301915. https://doi.org/10.3389/fcimb.2023.1301915

Jin, J., Yang, Q. Q., & Zhou, Y. L. (2022). Non-Viral Delivery of Gene Therapy to the Tendon. *Polymers*, *14*(16), 3338. https://doi.org/10.3390/polym14163338

Kimura, T., Ferran, B., Tsukahara, Y., Shang, Q., Desai, S., Fedoce, A., Pimentel, D. R., Luptak, I., Adachi, T., Ido, Y., Matsui, R., & Bachschmid, M. M. (2019). Production of adeno-associated virus vectors for in vitro and in vivo applications. *Scientific Reports*, *9*(1), 13601. https://doi.org/10.1038/s41598-019-49624-w

Kumagai, Y., Takeuchi, O., & Akira, S. (2008). TLR9 as a key receptor for the recognition of DNA☆. *Advanced Drug Delivery Reviews*, *60*(7), 795–804. https://doi.org/10.1016/j.addr.2007.12.004

Lam, A. K., Mulcrone, P. L., Frabutt, D., Zhang, J., Chrzanowski, M., Arisa, S., Munoz, M., Li, X., Biswas, M., Markusic, D., Herzog, R. W., & Xiao, W. (2023). Comprehensive Comparison of AAV Purification Methods: Iodixanol Gradient Centrifugation vs. Immuno-Affinity Chromatography. *Advances in Cell and Gene Therapy*, *2023*, 1–12. https://doi.org/10.1155/2023/2339702

Lam, V. C., & Lanier, L. L. (2017). NK cells in host responses to viral infections. *Current Opinion in Immunology*, *44*, 43–51. https://doi.org/10.1016/j.coi.2016.11.003

Leebeek, F. W. G., & Miesbach, W. (2021). Gene therapy for hemophilia: A review on clinical benefit, limitations, and remaining issues. *Blood*, *138*(11), 923–931. https://doi.org/10.1182/blood.2019003777

Lendeckel, U., Venz, S., & Wolke, C. (2022). Macrophages: Shapes and functions. *ChemTexts*, *8*(2), 12. https://doi.org/10.1007/s40828-022-00163-4

Li, X., Le, Y., Zhang, Z., Nian, X., Liu, B., & Yang, X. (2023). Viral Vector-Based Gene Therapy. *International Journal of Molecular Sciences*, *24*(9), 7736. https://doi.org/10.3390/ijms24097736

Lu, H., Huang, D., Yao, K., Li, C., Chang, S., Dai, Y., Sun, A., Zou, Y., Qian, J., & Ge, J. (2015). Insulin enhances dendritic cell maturation and scavenger receptor-mediated uptake of oxidised low-density lipoprotein. *Journal of Diabetes and Its Complications*, *29*(4), 465–471. https://doi.org/10.1016/j.jdiacomp.2015.03.005

Makhijani, P., Basso, P. J., Chan, Y. T., Chen, N., Baechle, J., Khan, S., Furman, D., Tsai, S., & Winer, D. A. (2023). Regulation of the immune system by the insulin receptor in health and disease. *Frontiers in Endocrinology*, *14*, 1128622. https://doi.org/10.3389/fendo.2023.1128622

Manno, C. S., Chew, A. J., Hutchison, S., Larson, P. J., Herzog, R. W., Arruda, V. R., Tai, S. J., Ragni, M. V., Thompson, A., Ozelo, M., Couto, L. B., Leonard, D. G. B., Johnson, F. A., McClelland, A., Scallan, C., Skarsgard, E., Flake, A. W., Kay, M.

A., High, K. A., & Glader, B. (2003). AAV-mediated factor IX gene transfer to skeletal muscle in patients with severe hemophilia B. *Blood*, *101*(8), 2963–2972. https://doi.org/10.1182/blood-2002-10-3296

Martino, A. T., & Markusic, D. M. (2020). Immune Response Mechanisms against AAV Vectors in Animal Models. *Molecular Therapy - Methods & Clinical Development*, *17*, 198–208. https://doi.org/10.1016/j.omtm.2019.12.008

McNeill, A. (2023). The complex genomics of single gene disorders. *European Journal of Human Genetics*, *31*(6), 609–610. https://doi.org/10.1038/s41431-023-01386-w

Mosser, D. M., & Edwards, J. P. (2008). Exploring the full spectrum of macrophage activation. *Nature Reviews Immunology*, *8*(12), 958–969. https://doi.org/10.1038/nri2448

Naso, M. F., Tomkowicz, B., Perry, W. L., & Strohl, W. R. (2017). Adeno-Associated Virus (AAV) as a Vector for Gene Therapy. *BioDrugs*, *31*(4), 317–334. https://doi.org/10.1007/s40259-017-0234-5

Nathwani, A. C., Tuddenham, E. G. D., Rangarajan, S., Rosales, C., McIntosh, J., Linch, D. C., Chowdary, P., Riddell, A., Pie, A. J., Harrington, C., O'Beirne, J., Smith, K., Pasi, J., Glader, B., Rustagi, P., Ng, C. Y. C., Kay, M. A., Zhou, J., Spence, Y., … Davidoff, A. M. (2011). Adenovirus-Associated Virus Vector–Mediated Gene Transfer in Hemophilia B. *New England Journal of Medicine*, *365*(25), 2357–2365. https://doi.org/10.1056/NEJMoa1108046

Nikolic, D. S., Lehmann, M., Felts, R., Garcia, E., Blanchet, F. P., Subramaniam, S., & Piguet, V. (2011). HIV-1 activates Cdc42 and induces membrane extensions in immature dendritic cells to facilitate cell-to-cell virus propagation. *Blood*, *118*(18), 4841–4852. https://doi.org/10.1182/blood-2010-09-305417

Ohi, S., Dixit, M., Tillery, M. K., & Plonk, S. G. (1990). Construction and replication of an adeno-associated virus expression vector that contains human β-globin cDNA. *Gene*, *89*(2), 279–282. https://doi.org/10.1016/0378-1119(90)90018-M

Oliveira, A. (2010). Herpes Simplex Virus Type 1/Adeno-Associated Virus Hybrid Vectors. *The Open Virology Journal*, *4*(1), 109–122. https://doi.org/10.2174/1874357901004010109

Ovchinnikov, D. A. (2008). Macrophages in the embryo and beyond: Much more than just giant phagocytes. *Genesis*, *46*(9), 447–462. https://doi.org/10.1002/dvg.20417

Pan, C., Kumar, C., Bohl, S., Klingmueller, U., & Mann, M. (2009). Comparative Proteomic Phenotyping of Cell Lines and Primary Cells to Assess Preservation of Cell Type-specific Functions. *Molecular & Cellular Proteomics*, *8*(3), 443–450. https://doi.org/10.1074/mcp.M800258-MCP200

Perry, C., & Rayat, A. C. M. E. (2021). Lentiviral Vector Bioprocessing. *Viruses*, *13*(2), 268. https://doi.org/10.3390/v13020268

Petersen, M. C., & Shulman, G. I. (2018). Mechanisms of Insulin Action and Insulin Resistance. *Physiological Reviews*, *98*(4), 2133–2223. https://doi.org/10.1152/physrev.00063.2017

Qudus, M. S., Tian, M., Sirajuddin, S., Liu, S., Afaq, U., Wali, M., Liu, J., Pan, P., Luo, Z., Zhang, Q., Yang, G., Wan, P., Li, Y., & Wu, J. (2023). The roles of critical pro-inflammatory cytokines in the drive of cytokine storm during SARS-CoV-2 infection. *Journal of Medical Virology*, *95*(4), e28751. https://doi.org/10.1002/jmv.28751

Rodrigues, G. A., Shalaev, E., Karami, T. K., Cunningham, J., Slater, N. K. H., & Rivers, H. M. (2019). Pharmaceutical Development of AAV-Based Gene Therapy Products for the Eye. *Pharmaceutical Research*, *36*(2), 29. https://doi.org/10.1007/s11095-018-2554-7

Rogers, G. L., Martino, A. T., Aslanidi, G. V., Jayandharan, G. R., Srivastava, A., & Herzog, R. W. (2011). Innate Immune Responses to AAV Vectors. *Frontiers in Microbiology*, *2*. https://doi.org/10.3389/fmicb.2011.00194

Rogers, G. L., Suzuki, M., Zolotukhin, I., Markusic, D. M., Morel, L. M., Lee, B., Ertl, H. C. J., & Herzog, R. W. (2015). Unique Roles of TLR9- and MyD88-Dependent and -Independent Pathways in Adaptive Immune Responses to AAV-Mediated Gene Transfer. *Journal of Innate Immunity*, *7*(3), 302–314. https://doi.org/10.1159/000369273

Rolling, F., & Samulski, R. J. (1995). AAV as a viral vector for human gene therapy: Generation of recombinant virus. *Molecular Biotechnology*, *3*(1), 9–15. https://doi.org/10.1007/BF02821330

Sant'Anna, T. B., & Araujo, N. M. (2022). Adeno-associated virus infection and its impact in human health: An overview. *Virology Journal*, *19*(1), 173. https://doi.org/10.1186/s12985-022-01900-4

Schultz, U. (2004). The interferon system of non-mammalian vertebrates. *Developmental & Comparative Immunology*, *28*(5), 499–508. https://doi.org/10.1016/j.dci.2003.09.009

Sonksen, P., & Sonksen, J. (2000). Insulin: Understanding its action in health and disease. *British Journal of Anaesthesia*, *85*(1), 69–79. https://doi.org/10.1093/bja/85.1.69

Srivastava, A. (2023). Rationale and strategies for the development of safe and effective optimized AAV vectors for human gene therapy. *Molecular Therapy - Nucleic Acids*, *32*, 949–959. https://doi.org/10.1016/j.omtn.2023.05.014

Tang, Q., Keeler, A. M., Zhang, S., Su, Q., Lyu, Z., Cheng, Y., Gao, G., & Flotte, T. R. (2020). Two-Plasmid Packaging System for Recombinant Adeno-Associated Virus. *BioResearch Open Access*, *9*(1), 219–228. https://doi.org/10.1089/biores.2020.0031

Taylor-Cousar, J. L., Boyd, A. C., Alton, E. W. F. W., & Polineni, D. (2023). Genetic therapies in cystic fibrosis. *Current Opinion in Pulmonary Medicine*, *29*(6), 615–620. https://doi.org/10.1097/MCP.0000000000001019

Tessaro, F. H. G., Ayala, T. S., Nolasco, E. L., Bella, L. M., & Martins, J. O. (2017). Insulin Influences LPS-Induced TNF-α and IL-6 Release Through Distinct Pathways in Mouse Macrophages from Different Compartments. *Cellular*

Physiology and Biochemistry, *42*(5), 2093–2104. https://doi.org/10.1159/000479904

Trivedi, P. D., Byrne, B. J., & Corti, M. (2023). Evolving Horizons: Adenovirus Vectors' Timeless Influence on Cancer, Gene Therapy and Vaccines. *Viruses*, *15*(12), 2378. https://doi.org/10.3390/v15122378

Wang, D., Tai, P. W. L., & Gao, G. (2019). Adeno-associated virus vector as a platform for gene therapy delivery. *Nature Reviews Drug Discovery*, *18*(5), 358–378. https://doi.org/10.1038/s41573-019-0012-9

Wang, J., & Chen, G. (2020). Dimethylacetamide-induced toxic hepatitis in spandex workers: Clinical presentation and treatment outcomes. *QJM: An International Journal of Medicine*, *113*(5), 324–329. https://doi.org/10.1093/qjmed/hcz282

Ward, C. W., & Lawrence, M. C. (2009). Ligand-induced activation of the insulin receptor: A multi-step process involving structural changes in both the ligand and the receptor. *BioEssays*, *31*(4), 422–434. https://doi.org/10.1002/bies.200800210

Wei, Z.-H., Koya, J., Acharekar, N., Trejos, J., Dong, X.-D., Schanne, F. A., Ashby, C. R., & Reznik, S. E. (2023). N,N-dimethylacetamide targets neuroinflammation in Alzheimer's disease in in-vitro and ex-vivo models. *Scientific Reports*, *13*(1), 7077. https://doi.org/10.1038/s41598-023-34355-w

Wu, Z., Asokan, A., & Samulski, R. J. (2006). Adeno-associated Virus Serotypes: Vector Toolkit for Human Gene Therapy. *Molecular Therapy*, *14*(3), 316–327. https://doi.org/10.1016/j.ymthe.2006.05.009

Ye, J., Coulouris, G., Zaretskaya, I., Cutcutache, I., Rozen, S., & Madden, T. L. (2012). Primer-BLAST: A tool to design target-specific primers for polymerase chain reaction. *BMC Bioinformatics*, *13*(1), 134. https://doi.org/10.1186/1471-2105-13-134

Yuan, C., Mo, Y., Yang, J., Zhang, M., & Xie, X. (2020). Influences of advanced glycosylation end products on the inner blood–retinal barrier in a co-culture cell model in vitro. *Open Life Sciences*, *15*(1), 619–628. https://doi.org/10.1515/biol-2020-0067

Zhu, J., Huang, X., & Yang, Y. (2009). The TLR9-MyD88 pathway is critical for adaptive immune responses to adeno-associated virus gene therapy vectors in mice. *Journal of Clinical Investigation*, *119*(8), 2388–2398. https://doi.org/10.1172/JCI37607

Zlotnik, A., & Yoshie, O. (2012). The Chemokine Superfamily Revisited. *Immunity*, *36*(5), 705–716. https://doi.org/10.1016/j.immuni.2012.05.008

Hacein-Bey, S., & Cavazzana-Calvo, M. (2002). Gene therapy of severe combined immunodeficiencies. *Nature Reviews Immunology*, *2*(8), 615–621. https://doi.org/10.1038/nri859

Grilley, B. J., & Gee, A. P. (2003). Gene transfer: Regulatory issues and their impact on the clinical investigator and the good manufacturing production facility. *Cytotherapy*, *5*(3), 197–207. https://doi.org/10.1080/14653240310001271

Jackson, M., Marks, L., May, G. H. W., & Wilson, J. B. (2018). The genetic basis of disease. *Essays in Biochemistry*, *62*(5), 643–723. https://doi.org/10.1042/EBC20170053

Mulligan, R. C. (1993). The Basic Science of Gene Therapy. *Science*, *260*(5110), 926–932. https://doi.org/10.1126/science.8493530

Zhang, W.-W., Li, L., Li, D., Liu, J., Li, X., Li, W., Xu, X., Zhang, M. J., Chandler, L. A., Lin, H., Hu, A., Xu, W., & Lam, D. M.-K. (2018). The First Approved Gene Therapy Product for Cancer Ad- *p53* (Gendicine): 12 Years in the Clinic. *Human Gene Therapy*, *29*(2), 160–179. https://doi.org/10.1089/hum.2017.218

Vita

Name	*Tianxiang Qi*
Baccalaureate Degree	*Bachelor of engineering,* *Beijing University of Science and Technology, Beijing* *Major: Pharmaceutical engineering*
Date Graduated	*June,2011*
Other Degrees and Certificates	*Master of Science,* *St. John's University, New York,* *Major: Pharmacology*
Date Graduated	*May,2018*